A STUDY OF THE VARIATIONAL THEORY OF REACTION RATES COMPARED TO CLASSICAL TRAJECTORY RESULTS AND STUDIES OF THE COMBINED PHASE-SPACE/TRAJECTORY PROCEDURE FOR THE (H, H_2) AND (H, I_2) SYSTEMS

By

DAVID LINVILLE MARTIN

Bachelor of Science

Cameron University

1973

Submitted to the Faculty of the Graduate College
of the Oklahoma State University
in partial fulfillment of the requirements
for the Degree of
DOCTOR OF PHILOSOPHY
December, 1979

A STUDY OF THE VARIATIONAL THEORY OF REACTION RATES COMPARED TO CLASSICAL TRAJECTORY RESULTS AND STUDIES OF THE COMBINED PHASE-SPACE/TRAJECTORY PROCEDURE FOR THE (H, H_2 AND (H, I_2) SYSTEMS

Thesis Approved:

Leonid M. Raff
Thesis Adviser

Paul Westhaus.

J Paul Dorchi

Norman N Durham
Dean of the Graduate College

To Janey

ACKNOWLEDGMENTS

I would like to express my thanks to the following people who served as members of my advisory committee: Drs. L. M. Raff, P. A. Westhaus, J. P. Devlin, and G. J. Mains. In particular, Dr. Raff my committee chairman and research adviser who initially suggested the problem. In the early stages the problem was not clearly defined. Dr. Raff's diligence in helping to reduce the problem to a workable research problem, and his helpful guidance in the form of careful discussion of the problem in various stages of development is extremely appreciated. I would also like to thank Dr. Westhaus who was always willing to discuss difficulties associated with the problem.

I sincerely appreciate financial support from the Chemistry Department and Graduate College in the form of teaching assistantship, awards, and fellowships. I would also like to acknowledge a summer fellowship from CONOCO, and the National Science Foundation for providing financial support during the later part of this study through a research fellowship from NSF CHE 78-25563.

I would like to extend thanks to the Oklahoma State University computer and library staff for providing much valuable assistance during my graduate school years.

I would like to extend thanks to my friends during my stay in graduate school who provided fellowship and encouragement. In particular, my thanks go to Gary Ritzhaupt, Charles Smith, Raji Viswanathan,

Drs. Courtney Stroud, and N. Sathyamurthy who always made discussions of life, science and ideas a pleasant experience.

I would like to extend my thanks to Dolores Behrens for carefully typing the final copy of this thesis.

I would like to express my thanks to my family particularly my parents Mr. and Mrs. David Martin who taught me many things and provided much love and encouragement throughout my life.

In conclusion, I would like to express thanks to my wife, Janey, for her continuous love, encouragement, support, understanding, and assistance during the preparation of this manuscript. For these reasons, I sincerely dedicate this thesis and the work it embodies to Janey.

TABLE OF CONTENTS

LIST OF TABLES

LIST OF FIGURES

Figures

CHAPTER I

SUMMARY OF PHASE SPACE THEORIES OF REACTION RATES

Introduction

Formulation of reaction-rate theories has been a subject of intense interest to scientists for several years. Many ingenious methods have been devised and applied with reasonable success to calculate reaction rate coefficients, reaction cross sections and product energy distributions. One theory that has received substantial attention is the statistical phase-space theory and an extension of phase-space theory, the variational theory of reaction rates (1).

As with most other theories of reaction rates, the interaction potential is considered to be adiabatic. In essence this means the potential energy of the system is described by a "single" surface that is a function of the nuclear configuration. In some instances the adiabatic assumption may not be valid. For example two potential-surfaces may be separated by a narrow energy gap for given nuclear configurations (2) (3). In cases such as this, it becomes very difficult to assess the appropriate nature of the potential.

Phase-Space Theories

Phase-space models which involve the computation of a flux across a surface dividing the phase space of the products from that of the

reactants, contain other theories as special cases. If the dividing surface is in the reactant region of phase space, the method is termed a collision theory. If the surface is placed through or near the phase space of the saddle point, it then becomes "absolute rate" theory, as pointed out by Johnston (4).

One of the earliest calculations of this nature was by Eyring and coworkers (5) in which they calculated a probability for recombination of three hydrogen atoms to form the diatomic molecule and a separated hydrogen atom. Using transition-state theory, they were able to calculate a rate for this process with the crossing probability replacing the usual transmission coefficient.

Keck (6) proposed a general statistical theory of reaction rates applied to the recombination of two atoms under the influence of a third in a "strong coupling" approximation. The recombination rate was given by the rate of flow of phase points from a free state through the collision complex where the dividing surface was located into the phase space of the products. He was able to show that his theory encompassed three-body collision theories of recombination, available energy theories of dissociation, and the variational theory of atomic recombination (7) (8) (9) (10). This flow of points is actually the equilibrium flow of points crossing the surface defining the collision complex in one direction. The reaction rate obtained should always be an upper bound to the true reaction rate because some of the phase points recross the surface many times before they go into the product or reactant phase space. Consequently some nonreactive trajectories contribute to the flux across the dividing surface. These trajectories

cross the surface toward the product phase space and then backtrack to the reactant phase space.

Alternately an "available phase-space" theory has been formulated for systems without activation energy (11). The hypothesis was posed as follows: The probability of formation of any given product in a "strong coupling" collision is proportional to the ratio of phase space available to that product divided by the total phase space available to the system within the constraints imposed by conservation of total energy and total angular momentum. In this form, application of the theory has led to the computation of reaction cross sections for model ion-molecule systems.

The available phase-space theory later proved to be unsatisfactory because it failed to satisfy the principle of detailed balancing (12). Consequently, a new formalism was developed in the spirit of the strong coupling assumption which satisfied this criterion for both classical and quantum mechanical treatments (13). In addition, this formalism retained the geometric interpretation, that the probability of formation of a given product is proportional to the phase space available to that product. It was applied with some success to biomolecular exchange ion-molecule reactions without activation energy, bimolecular atom-diatomic molecule processes without activation energy, ion-molecular systems with and without activation energy and neutral atom-diatomic molecule systems with activation energy (14) (15) (16) (17).

Eu and Ross (18) applied Wigner's (19) R-matrix theory to the molecular scattering problem. In the R-matrix theory approach, the configuration space of the system is divided into two regions, an

internal region in which the collision complex is well defined and bounded by a surface that separates it from the external region. In the external region it is assumed that the interaction between particles is small or in the event of large interaction, the forces are known. The appropriate wave equations are then solved subject to the boundary conditions on the surface separating the two regions. Upon application of this formalism they were able to obtain rate expressions for the activated complex theory of Eyring (20), Keck's statistical theory (6), and the available phase-space theory of Light and coworkers (11) (13).

Miller (21) has given an account of a unified statistical phase-space theory model for "complex" and "direct" reaction mechanisms. The model employs the calculation of fluxes through surfaces dividing the phase-space of the system into reactant and product regions in which the variational procedure of Keck (22) is applied to locate the dividing surfaces such that the flux is either maximized or minimized. The "direct" mechanism refers to a single surface crossing. In this case, the flux through the dividing surface is minimized and the model reduces to transition state theory (20). However, for the long lived "complex" mechanisms, such as orbiting and non-adiabatic trapping collisions, many surface crossings are completed, maximizing the flux through the dividing surface, and transition state theory is no longer valid. In this limit, the model takes on the character of the statistical theories of Light (23) and Nikitin (24).

A rather unique application of phase-space theory, the "information theoretic approach" has recently been proposed (25) (26). The

method concerns itself with the analysis of branching ratios in chemical reactions from a thermodynamic viewpoint. The argument being that the fractional yield or rate for a given reaction pathway is proportional to the volume of phase-space accessible to that product (27). The information theoretic approach proceeds as follows: First, one computes the most probable way to distribute the molecules among all available quantum states, or maximize the entropy for a given reaction path. This is the basis of the equilibrium phase-space assumption in that all available quantum states have equal "a prior" probability from which the entropy of the equilibrium phase-space is evaluated. The actual entropies are then obtained from any information available on the molecular system. From this an entropy difference is computed, termed the "surprisal". The basic postulate of the theory is that the system will behave in such a manner as to maximize the system's entropy or minimize the surprisal. From this analysis branching ratios may be computed for competing reaction pathways by analysis in terms of the surprisal for each product (28). Some applications of the information theoretic approach have been investigation of branching ratios in reactive H or D atom collisions with hydrogen halides and interhalogens, internal and translational energy distributions for reactive collisions, the effect of vibrational and rotational excitation of the reactants on reaction rates, the energy distributions of reaction products for atom-diatomic molecule reactions and the isotopic branching ratio for the reaction F + HD, and vibrational energy transfer in inelastic and reactive atom-diatomic molecule collisions (29) (26) (30) (31) (32). The results for the most part, give reasonable agreement with experiment and trajectory calculations. However, in the reactions F + H_2,

D_2 the results must be regarded with caution since the rotational energy distributions agree with trajectory calculations but, disagree with infrared chemiluminescence results (31).

Variational Theories

Variational rate theories are a branch of phase-space theories in that they still involve a dividing surface but they also investigate the possibility of minimizing the rate by varying the location of the dividing surface. The rate evaluated in this manner is the equilibrium flux crossing the dividing surface, which should be an upper bound to the rate as described earlier.

One of the earliest variational calculations was applied to elementary association reactions (10). In its application to recombination reactions, the dividing surface was located where the energy of the diatomic system would be zero and the number of points crossing the surface per unit time would be an upper bound to the rate. It was noted that this upper bound could probably be lowered somewhat by choosing a more appropriate dividing surface. When the formalism was applied to the association of iodine atoms under the influence of a third body, the calculated rates were lower than the experimental results. This was attributed possibly to errors in the Morse potential employed and the number of electronic states contributing to products.

Horiuti (34) formulated an expression for the rate in which the variation of the rate with respect to a coordinate normal to the surface was required to be zero. This constraint led to the requirement that for a minimum flow through the surface in the configuration

space of the system the coordinate normal to the surface was related to the principal radii of curvature of the other coordinates as parameters on which the rate was dependent. In comparison of this rate with the transition-state theory rate, it was found to have a small difference at room temperature. However, at higher temperatures transition-state theory gave a much larger rate.

Keck (35), following the variational approach of Wigner (10), applied the method to the calculation of a rigorous upper bound for the rate of three-body recombinations. This calculated rate was found to be lower than experimental rates obtained for these systems. However, the experimental error was large enough that the calculated rate might still have been an upper bound to the true reaction rate.

An important extension of the variational approach was realized when the variational method was coupled with Monte Carlo techniques for a trajectory analysis of dissociation cross sections for diatomic molecules (40). The initial conditions were selected from a dividing surface located tangent to the top of the rotational barrier. The time evolution of a trajectory was determined by forward and backward integration of the equations of motion for the phase point from the dividing surface to see if it would originate as reactants and terminate as products. One observation was that a large fraction of trajectories examined were reactive and a reduction of computational effort as compared with conventional trajectory methods seemed likely.

The variational theory was realized to be very general in nature in the sense that it contained many other reaction rate theories as special cases (22). By incorporating the constraints pertinent to a given theory as conditions on the dividing surface, Keck (22) was

able to derive rate expressions for: unimolecular decay theory, the available energy theory, absolute rate theory, and statistical theories (37) (38) (20) (6) (13) (18). In the statistical theory, with arguments dealing with conservation of density in phase space, Keck (22) pointed out that the arbitrary measure used by Pechukas and Light (13) in their quantum formulation of phase space available to a product channel was analogous to his rate of flow of phase fluid into the various channels from a classical viewpoint. A discussion of conservation of density in phase space may be found in various texts on statistical mechanics (36). From this he noted that the omission of the flow velocity of phase points was what made Light's (11) original theory fail to satisfy the principle of detailed balancing.

Another application of the variational procedure coupled with Monte Carlo trajectory methods was used to evaluate rates of atomic excitation and ionization by thermal electrons (39). Mansbach and Keck (39) obtained rates for these processes by evaluating the equilibrium surface crossing rate by the solution of the master equation for the system. The procedure then called for forming the product of the equilibrium crossing rate with a statistically weighted ratio of successful deexcitation trajectories to the total number to obtain the deexcitation rate. They concluded that the corrected surface crossing rate was in accord with the available experimental data at the time.

Equilibrium Assumption

For the most part the theories discussed so far have included some sort of equilibrium condition for formation of a collision complex.

This assumption is also inherent in transition-state theory and the combined phase-space-trajectory or combined variational theory-trajectory procedures (41) (42). This assumption has been treated in some detail for collinear and three dimensional studies. Karplus and coworkers (43) cast transition-state theory into a form that permitted evaluation of the reaction probabilities as a function of energy for collinear reactions. In the low-energy domain, transition-state theory gave a reasonable account of the reaction probability with the potential-energy surface used. However, in the high-energy domain the reaction probability became greater than unity. It was concluded from this that transition-state theory included certain regions of phase space that were inaccessible to the system.

In an extension of prior work, Morokuma and Karplus (43) (44) used classical trajectory analysis to check the validity of an equilibrium distribution assumption at the transition state and investigated the possibility of the transmission coefficient being less than unity. These assumptions were tested to see how they behaved with respect to the nature of the potential-energy surface. They determined that the shape of the potential-energy surface in regions other than the transition region does affect the reaction probability and the distribution at the transition state. Also the location of the barrier displaced toward the exit or entrance channels can produce a nonequilibrium distribution in the transition region. More investigations of this nature for a complete three dimensional treatment on an extended LEPS surface with a barrier in the exit valley proved nonequilibrium distributions in the transition region could occur (45).

The Combined Phase-Space Theory and Combined Variational Theory Procedures

Anderson (41) (42) has developed a combined phase-space theory wherein he combined variational theory and trajectory methods. It is referred to collectively as the (CPST) method following the procedures outlined by Keck (6) (22) (40). The tests used to establish the CPST procedure have been comparisons with standard quasiclassical trajectory methods (SQCT) currently acknowledged as being the most useful theoretical method for investigating molecular scattering events (46). Anderson's motivation for the CPST procedure is that it could reduce computation time substantially for processes in which the SQCT method would be inefficient.

The rationale of the CPST procedure is to first select a dividing surface $\underset{\sim}{S}$ without "wrinkles" or "holes" in the phase space of the interaction region such that it separates the phase space of the reactants from that of the products. The thermal equilibrium flux $K'(T)$ of phase points crossing $\underset{\sim}{S}$ in one direction is then evaluated in the classical approximation. This should be an upper bound to the reaction rate, and it should be possible to lower this upper bound by varying $\underset{\sim}{S}$ in the interaction region. This is the variational aspect of the problem. However, the CPST procedure calls for selecting initial conditions for the trajectories from a Boltzmann distribution on $\underset{\sim}{S}$. The next step in the procedure is to integrate the classical equations of motion both forward and backward in time to determine if they originate in the reactant phase space and terminate in the product phase space. The

fraction $\xi(T)$ of reactive trajectories is then evaluated, and the expression for the thermal rate coefficient is

$$K(T) = \xi(T)\ K'(T). \qquad (1\text{-}1)$$

There are two assumptions inherent in this procedure:

1. the thermal rate coefficient is independent of the location of $\underset{\sim}{S}$
2. the initial phase points may be selected from a Boltzmann distribution of $\underset{\sim}{S}$ (47).

Anderson has suggested that any non-Boltzmann character on $\underset{\sim}{S}$ is corrected by the conversion factor $\xi(T)$ and that the true distribution is the equilibrium distribution with trajectories from products missing. This assumption has been questioned (47) (48).

The CPST procedure has been subjected to a number of tests and comparisons with the SQCT method. Some of its applications so far have been a study of vibrational population inversion in HI, the molecular dynamics of the system (H_2, I_2) as compared to the SQCT results obtained by Raff and coworkers (52) using the same potential-energy surface and other SQCT results obtained by Anderson et al. (49) (50) (51) (53). Several collinear model systems have been investigated by Anderson (41) (54) on a variety of potential-energy surfaces intersecting rectangular channels of different elevation, smooth curves of parabolic cross section and the potential-energy surface for the reaction $H_2 + I \rightarrow H + HI$. It was applied to both forward and reverse reactions for the system $F + H_2 \rightarrow HF + H$ and compared to the previous SQCT result (42) (55) obtained with the same potential-energy surface. The CPST

procedure was applied to the (H, I_2) and (H, Br_2) systems and compared with SQCT results in the same study (47). Also a model system A + BB → AB + B closely related to the H + F_2 → HF + H system was investigated to assess the validity of the thermal rate coefficient being independent of the location of the dividing surface (56).

Conclusions regarding the CPST procedure are that for some systems the thermal rate coefficient may be obtained nearly within the statistical error of the SQCT results (41) (47) (56). Claims of large reduction in computational time have been made but, they are not believed to be general (40) (41) (47). The validity of the method should increase as the accuracy of classical mechanics increases in describing the nuclear motion (42). The initial assumption of a Boltzmann distribution on the surface $\underset{\sim}{S}$ when it is located in the interaction region may induce nonequilibrium distributions in the reactants (47). The CPST procedure is not reliable for accurate determinations of reaction cross sections and is not applicable to nonthermal systems (47) (42).

Statement of Research Problem

The present research problem is twofold in character. The first part being to apply Keck's (22) variational procedure to minimize the variational rate coefficient by systematic variation of $\underset{\sim}{S}$ over a given potential-energy surface. One in particular will be the potential-energy surface obtained by Porter and Karplus (57) for the (H, H_2) system. Once the minimum variational rate coefficient has been found for a given temperature for the minimum crossing surface $\underset{\sim}{S}_0$, a number of variational rate coefficients will be computed at other temperatures

for the surface $\underset{\sim}{S}_0$. In addition to this, rate coefficients will be computed from classical trajectories at various temperatures to allow comparison of the classical trajectory and variational rate coefficient's temperature dependence.

In the second part of the problem, once the minimum variational rate coefficient has been found, the surface, $\underset{\sim}{S}_0$, will be used to select initial conditions for the classical trajectories required to compute the thermal rate coefficient from Eq. (1-1). These results will then be compared with the corresponding SQCT results on the (H, H_2) system (58). It is realized that this is one of the most severe tests of the CPST procedure. There is a significant amount of zero-point energy in the (H, H_2) system which is entirely neglected in the CPST approach. Also, there is a large barrier to reaction which could introduce significant error if the zero-point energy is ignored. In addition to this, the CPST rate coefficient, differential scattering cross sections and energy distributions will be compared with the classical trajectory results. It is hoped that from these detailed comparisons a quantitative assessment may be made of the CPST procedure.

CHAPTER II

FORMULATION OF THE PROBLEM

Description of the Problem

The initial part of the problem is to compute classical trajectories for the (H, H_2) system using two different methods to select the initial conditions for the internal coordinates and momenta for the BC molecule. Method I involves selection of the initial BC relative momenta from randomly chosen classical vibrational and rotational action variables with the BC radial distance randomly chosen from a Morse oscillator distribution. Method II calls for randomly choosing the initial conditions for the internal dynamical variables of BC from Boltzman weighting of the classical internal BC Hamiltonian.

The formulation of the variational rate coefficient involves a linear transformation from the relative configuration space of the A-B-C system (r, θ, ϕ, R, Θ, Φ) to a (W, V, θ, ϕ, Θ, Φ) configuration space. The variational rate coefficient depends upon the location of the dividing surface, which may be varied to find a local minimum. A minimization of the variational rate coefficients is carried out for both the (H, H_2) and (H, I_2) systems.

Once a minimum crossing surface, S_0, has been found for the variational rate coefficient for the (H, H_2) system at one temperature, it

will be used to compute variational rate coefficients at a number of other temperatures. In addition, rate coefficients from classical trajectory procedures will be evaluated at these temperatures and compared with the minimum variational rate coefficients. To evaluate the CPST rate coefficient at these temperatures, the phase points are assumed to have Boltzmann weighting on S_0 and initial conditions for the CPST trajectories will be chosen for the eleven degrees of freedom on S_0 from the appropriate distribution functions according to Anderson's (41) (42) (49) prescription.

After the CPST rate coefficients have been evaluated at the various temperatures mentioned above, they will be compared to both the CT rate coefficients and the minimum variational rate coefficients. The various statistical distributions obtained in the CPST procedure will be compared with those obtained from the CT results. Indeed, the reactant distributions obtained from the CPST procedure should provide some insight into the question as to whether both procedures sample the same set of trajectories. The CT procedure requires that atom A and molecule BC be separated by a large enough distance such that the intermolecular potential is negligible. So, for thermal systems, a Boltzmann distribution is assured in the CT procedure. That is, all trajectories originating in the reactant valley should be in thermal Boltzmann equilibrium.

Classical Trajectories-Method I

The procedure for random selection of initial states for classical trajectories has been well described previously (46) (58) so only

pertinent equations will be given here. If the dynamical variables of the system are assumed to be separable, the Monte Carlo random number for the variable x is defined by

$$\xi(x) = \int_{x_o}^{x} w(x')dx' \Big/ \int_{x_o}^{\bar{x}} w(x')dx', \qquad (2\text{-}1)$$

where $0 \leq \xi(x) \leq 1$. In the equation given above $w(x)dx$ is the weight associated with the variable x. x_o is the lower limit of integration and $\bar{x}$ is the upper limit of integration. The solutions of Eq. (2-1) for x provides the randomly chosen initial condition for the dynamical variable x.

The rotational action (46) in the rigid rotor approximation for method I is assumed to be continuous in J with Boltzmann weight factor

$$w(J)dJ = (2J + 1)\, e^{-J(J+1)\hbar^2/2IkT} dJ, \qquad (2\text{-}2)$$

where I is the equilibrium moment of inertia. When $w(J)dJ$ is substituted into Eq. (2-1), the integral in the denominator becomes the rotational partition function

$$Q_r = 2IkT/\hbar^2 . \qquad (2\text{-}3)$$

The solution to Eq. (2-1) for the continuous rotational action variable becomes

$$J = \tfrac{1}{2}(-1 + (1 - 8IkT\ln(1-\xi(J))/\hbar^2)^{\frac{1}{2}}). \qquad (2\text{-}4)$$

The random selection of the initial vibrational action variable (46) for BC in the harmonic oscillator approximation proceeds by substituting the Boltzmann weight factor

$$w(v)dv = e^{-v\hbar\omega_o/kT} dv \ . \tag{2-5}$$

Substituting Eq. (2-5) into (2-1) with $v_o = 0$ and $\bar{v} = \infty$, then solving for the upper limit of the numerator integral one obtains

$$v = -kT \ln(1-\xi(v))/\hbar\omega_o \ . \tag{2-6}$$

The initial BC radial separation is obtained by setting a random number R equal to the radial distribution function D(r) (59) so that,

$$R = \tfrac{1}{2} - \frac{1}{\pi} \arcsin\left(\frac{b\xi + 2a}{\xi\sqrt{b^2-4ac}}\right) , \tag{2-7}$$

where $a = E - D$, $b = 2D$, $c = -D$, E is the energy of the Morse oscillator, and

$$\xi = e^{-\alpha(r-r_e)} \ . \tag{2-8}$$

Solving Eq. (2-7) for r one obtains

$$r = r_e - \frac{1}{\alpha} \ln((-2a)/(b-\sqrt{b^2-4ac}\ \cos\pi R)). \tag{2-9}$$

If the argument of $\cos(\pi R)$ is replaced with $2\pi R + \pi/2$, which retains the same weighting as the argument R, Eq. (2-9) becomes

$$r = r_e - \frac{1}{\alpha} \ln((-2a)/(b+\sqrt{b^2-4ac}\ \sin(2\pi R))), \tag{2-10}$$

this is the equation obtained by Porter, Raff and Miller (59).

Initially, the radial vector of BC is aligned along the z-axis with its angular momentum vector pointing in the positive x direction. This gives the following relative cartesian coordinates and mementa for BC (46)

$$\begin{aligned} Q_1^o &= 0 \\ Q_2^o &= 0 \\ Q_3^o &= r \\ P_1^o &= 0 \\ P_2^o &= (J(J+1)^{\frac{1}{2}}\hbar/r \\ P_3^o &= \pm(2\mu\ (E - V(r)))^{\frac{1}{2}}, \end{aligned} \tag{2-11}$$

In the above equations, μ is the BC reduced mass, E is the vibrational energy in the harmonic oscillator approximation for the given vibrational action v and V(r) is the Morse potential (46).

To accomplish the random orientation of the BC relative coordinates and momenta, rotation matrices are employed. Written out in operator form the equations for the rotations are

$$\begin{pmatrix} Q_1 \\ Q_2 \\ Q_3 \end{pmatrix} = R_z(\phi)\ R_y(\theta)\ R_z(\eta) \begin{pmatrix} Q_1^o \\ Q_2^o \\ Q_3^o \end{pmatrix}$$

$$\begin{pmatrix} P_1 \\ P_2 \\ P_3 \end{pmatrix} = R_z(\phi)\ R_y(\theta)\ R_z(\eta) \begin{pmatrix} P_1^o \\ P_2^o \\ P_3^o \end{pmatrix}. \tag{2-12}$$

The rotation matrices $R_z(\phi)$ and $R_y(\phi)$ (46) (52) are given by

$$R_z(\phi) = \begin{pmatrix} \cos\phi & \sin\phi & 0 \\ -\sin\phi & \cos\phi & 0 \\ 0 & 0 & 1 \end{pmatrix} \tag{2-13}$$

$$R_y(\phi) = \begin{pmatrix} \cos\phi & 0 & -\sin\phi \\ 0 & 1 & 0 \\ \sin\phi & 0 & \cos\phi \end{pmatrix}. \tag{2-14}$$

The orientation angles ϕ, θ, and η expressed in terms of the appropriate random numbers are

$$\begin{aligned} \phi &= 2\pi\xi(\phi) \\ \eta &= 2\pi\xi(\eta) \\ \theta &= \arccos(1 - 2\,\xi(\theta)). \end{aligned} \tag{2-15}$$

The initial separation between A and the BC center of mass is fixed at R_o at the beginning of each trajectory, where R_o is a distance such that the intermolecular interaction between A and BC is neglible. The initial cartesian coordinates and conjugate momenta of A relative to the BC center of mass are given by (58)

$$\begin{aligned} Q_4 &= 0 \\ Q_5 &= b \\ Q_6 &= -(R_o^2 - b^2)^{\frac{1}{2}} \\ P_4 &= 0 \\ P_5 &= 0 \\ P_6 &= \mu_{A,BC} V_r, \end{aligned} \tag{2-16}$$

where $\mu_{A,BC}$ is the A, BC reduced mass, V_r is the relative velocity of A with respect to the BC center of mass and b is the impact parameter. The initial impact parameter is chosen from (46)

$$b = b_M \xi(b) \tag{2-17}$$

The reaction probability obtained from a set of N trajectories containing N_r reactive trajectories is defined by

$$P(V_r,b) = \begin{cases} N_r/N, & b \leq b_M \\ 0, & b > b_M \end{cases}, \tag{2-18}$$

where b_M is the maximum impact parameter. To obtain b_M, one computes trajectories at fixed values of b and relative velocities above the threshold velocity, whenever $P(V_r, b) \to 0$, one chooses that value of b as b_m.

After all the steps above have been completed, the initial conditions for an A + BC collision have been completely specified. The trajectories are time integrated from the initial reactant state to the final state by a fourth order Runge-Kutta method (60). Initially, non-statistical trajectories are computed to find the maximum impact parameter according to Eq. (2-18). Trajectories are then computed at low relative velocities until it is possible to approximate the reaction threshold V_o, the relative velocity below which no reactions occur. If b is defined by Eq. (2-17), the reaction cross section is given by

$$S(V_r) = \begin{cases} 0, & V_r \leq V_o \\ 2\pi b_M^2 \frac{1}{N} \sum_{i=1}^{N_r} \xi(b_i), & V_r > V_o \end{cases}, \tag{2-19}$$

where $\xi(b_i)$ is the random number associated with the impact parameter for a given reactive trajectory i, N_r is the total number of reactive trajectories, and N is the total number of trajectories examined for a given relative velocity (46). To obtain V_o, trajectories are computed at fixed relative velocities until a relative velocity is found for which $S(V_r)$ vanishes, this relative velocity is then chosen as V_o.

Cross sections averaged over rotation and vibration are computed for several relative velocities via Eq. (2-19). The statistical error is given by

$$\sigma = \left(\sum_{i=1}^{N_r} (\xi(b_i))^2 - \frac{1}{N}\left(\sum_{i=1}^{N_r} \xi(b_i)\right)^2\right)^{1/2} \Big/ \sum_{i=1}^{N_r} \xi(b_i) \quad . \tag{2-20}$$

Once the cross sections have been computed, the rate coefficient may be obtained from (58)

$$K(T) = C\,(2/\pi)^{1/2}(\mu_{A,BC}/kT)^{3/2} \int_{V_o}^{\infty} S(V_r)\, e^{-\mu_{A,BC} V_r^2/2kT}\, V_r^3 dV_r \quad , \tag{2-21}$$

where C is a conversion factor converting the rate coefficient into cm^3/mole-sec. The upper limit of infinity for the relative velocity may be replaced by a finite upper limit V_r' above which the value of the integrand makes small contribution to the integral.

Molecular units (52) are used throughout the body of the text unless otherwise specified.

Classical Trajectories-Method II

To select the initial internal momenta and coordinates of BC for

method II, let A be a distance R_o away from the center of mass of BC, so that there is little interaction between A and BC. The BC Hamiltonian in spherical polar coordinates is approximately

$$H = \frac{1}{2\mu} (p_r^2 + p_\theta^2/r^2 + p_\phi^2/r^2 \sin^2\theta) + V(r) , \tag{2-22}$$

where V(r) is the Morse potential

$$V(r) = D_1 (1 - e^{-\alpha(r-r_e)})^2. \tag{2-23}$$

One begins the selection of initial conditions by substituting the appropriate Boltzmann weight factor for a particular degree of freedom into Eq. (2-1). The Boltzmann weight factors for the momenta all fall into the same category

$$w(p)dp = e^{-a\,p^2}\, dp \tag{2-24}$$

for p_r $a = \beta/2\mu$, where $\beta = 1/kT$. Substituting this into Eq. (2-1) with appropriate limits one obtains

$$\xi(p) = \int_{-p}^{p} e^{-ap'^2}\, dp' \Big/ \int_{-\infty}^{\infty} e^{-ap^2}\, dp. \tag{2-25}$$

The denominator integral is $\sqrt{\pi/a}$ taking $a = 1/2\sigma^2$ it becomes $\sqrt{2\pi}\,\sigma$. Changing variables from p' to $y' = p'/(\sqrt{2}\,\sigma)$ Eq. (2-25) becomes

$$\xi(y) = \frac{2}{\sqrt{\pi}} \int_0^y e^{-y'^2}\, dy' = \mathrm{erf}(y) \tag{2-26}$$

the error function (36). To find p that is the solution to Eq. (2-26) one solves

$$\xi(y) - \mathrm{erf}(y) = 0 \ , \tag{2-27}$$

and

$$p = \pm \sqrt{2}\ \sigma\ y \tag{2-28}$$

with the plus or minus sign chosen randomly. The spherical polar momenta for BC may be determined by Eq. (2-28) and the appropriate y for each momentum for the solution to Eq. (2-27). It has already been noted for p_r, that $a = 1/2\mu kT$, $\sigma = 1/\sqrt{2a} = \sqrt{\mu kT}$ so

$$p_r = \pm \sqrt{2\mu kT}\ y_r . \tag{2-29}$$

Similarly, by appropriate substitution, one has for p_θ and p_ϕ

$$p_\theta = \pm\ r\ \sqrt{2\mu kT}\ y_\theta$$

$$p_\theta = \pm\ r\ \sin\theta\ \sqrt{2\mu kT}\ y_\phi \ . \tag{2-30}$$

To randomly select the BC radial length, the Boltzmann weight of V(r) given in Eq. (2-23) is employed in a numerical partial sum technique that is equivalent to Eq. (2-1) (47). The Boltzmann weight for the variable r is

$$w(r)dr = e^{-V(r)/kT}\ r^2 dr \ . \tag{2-31}$$

Substituting w(r)dr into Eq. (2-1) the formal definition of $\xi(r)$ is

$$\xi(r) = \int_0^{r} r'^2 dr' \, e^{-V(r')/kT} \Big/ \int_0^{\infty} r^2 dr \, e^{-V(r)/kT} . \qquad (2\text{-}32)$$

The important contributions for the integrand of the denominator integral occur near $r = r_o$. One may replace the infinite upper limit with a finite upper limit r'' and obtain an approximation for the denominator integral. This approximation should be reasonable as long as the interval $[0, r'']$ contains the r values where the integrand makes its largest contribution to the integral. To implement the selection of r in this manner, one first evaluates the sequence of partial sums $\{S_k\}$ with

$$S_k = \sum_{i=1}^{k} r_i^2 \, e^{-V(r_i)/kT} , \qquad (2\text{-}33)$$

where $(k = 1, 2, 3, \ldots, n)$, $n = r''/\Delta r + 1$, where Δr is the interval spacing. The partial sum sequence $\{S_1, S_2, \ldots, S_n\}$ is then normalized with respect to S_n

$$W_k = S_k/S_n . \qquad (2\text{-}34)$$

To numerically solve the initial r, one employs the sequence $\{W_k\}$ and tests by incrementing over k for randomly chosen $\xi(r)$ the condition

$$\xi(r) - W_k \leq 0 . \qquad (2\text{-}35)$$

The first k value for which condition (2-35) holds, one chooses $r = r_k$.

To complete the specification of the relative cartesian coordinates and mementa of BC, one randomly chooses the orientation angles θ and ϕ according to Eq. (2-15). So the initial cartesian coordinates for BC are

$$\begin{aligned} Q_1 &= r \sin\theta \cos\phi \\ Q_2 &= r \sin\theta \sin\phi \\ Q_3 &= r \cos\theta \ . \end{aligned} \tag{2-36}$$

Letting $y = \pm y$ in Eq. (2-28) and substituting the randomly chosen p_r, p_θ, p_ϕ into the spherical polar expressions for the relative cartesian momenta of BC one has

$$\begin{aligned} P_1 &= \sin\theta \cos\phi \sqrt{2\mu kT}\, y_r + \cos\theta \cos\phi \sqrt{2\mu kT}\, y_\theta - \sin\phi \sqrt{2\mu kT}\, y_\phi \\ P_2 &= \sin\theta \sin\phi \sqrt{2\mu kT}\, y_r + \cos\theta \sin\phi \sqrt{2\mu kT}\, y_\theta + \cos\phi \sqrt{2\mu kT}\, y_\phi \\ P_3 &= \cos\theta \sqrt{2\mu kT}\, y_r - \sin\theta \sqrt{2\mu kT}\, y_\theta \ . \end{aligned} \tag{2-37}$$

The only remaining difference between method I and method II in specifying the initial conditions for an A, BC collision is the selection of the initial relative velocity. In method I, cross sections are computed at fixed relative velocities in the interval $[V_o, V_r']$ so that Eq. (2-21) may be evaluated by a given quadrature formula. However in method II V_r is randomly selected and Eq. (2-21) is evaluated by Monte Carlo techniques. The Boltzmann weight factor associated with V_r is (46)

$$w(V_r)dV_r = e^{-\mu_{A,BC} V_r^2/2kT} V_r^3 \, dV_r \ . \tag{2-38}$$

Substituting the appropriate limits into Eq. (2-1) $\xi(V_r)$ becomes

$$\xi(V_r) = \int_{V_o}^{V_r} e^{-\mu_{A,BC} V_r'^2/2kT} V_r'^3 \, dV_r' \Big/ \int_{V_o}^{\infty} e^{-\mu_{A,BC} V_r^2/2kT} V_r^3 \, dV_r \, . \tag{2-39}$$

After the integrals have been evaluated, V_r is the solution of the expression

$$(1 - \xi(V_r))(V_o^2 + \frac{2kT}{\mu_{A,BC}}) e^{-\mu_{A,BC} V_o^2/2kT} - (V_r^2 + \frac{2kT}{\mu_{A,BC}}) e^{-\mu_{A,BC} V_r^2/2kT} = 0 \, . \tag{2-40}$$

Once V_r has been specified, the A relative to BC center of mass coordinates and momenta are selected according to Eq. (2-16), which completes the specification of initial conditions in the method II formulation.

After numerical integration of a set of N trajectories containing a subset of N_r reactive trajectories, the rate coefficient is given by (46)

$$K(T) = \sqrt{\frac{2}{\pi}} (\mu_{A,BC}/kT)^{3/2} (kT/\mu_{A,BC}) (V_o^2 + 2kT/\mu_{A,BC}) \chi \, e^{-\mu_{A,BC} V_o^2/2kT} 2\pi b_M^2 (1/N) \sum_{i=1}^{N_r} \xi(b_i) \tag{2-41}$$

with statistical error determined by Eq. (2-20).

Formulation of the Variational Rate Coefficient

The variational rate coefficient for an (A, BC) exchange process

at thermal equilibrium has been expressed by Keck (22) as the equilibrium flux across S,

$$K'(\beta) = -\frac{1}{Q(\beta)} \int_{\substack{S \\ \vec{v}.\hat{n} > 0}} e^{-\beta H} \vec{v}.\hat{n}_s \, d\sigma, \qquad (2\text{-}42)$$

where $d\sigma$ is the differential surface element obtained by fixing the value of one of the generalized coordinates of the relative A-B-C phase space. S is the trial surface separating the reactant phase space from the product phase space with the position of S being described by a fixed value of the coordinate q_1. $\vec{v}$ is the generalized velocity of a phase point crossing the surface S; $\hat{n}_s$ is the vector normal to the surface S; $\vec{v}.\hat{n}_s$ is therefore the component of $\vec{v}$ normal to S, and the integration limit $\vec{v}.\hat{n}_s > 0$ only counts that portion of the flux crossing S in the direction of the product phase space. $Q(\beta)$ is the classical partition function per unit volume for reactants given by

$$Q(\beta) = \frac{1}{\gamma} \int_{\omega} e^{-\beta H_o} \prod_{i=1}^{6} dp_i dq_i \qquad (2\text{-}43)$$

where γ is the normalization volume in configuration space, and ω is the volume of the reactant phase space. The classical Hamiltonian initially expressed in spherical polar coordinates shown in Figure 1 is

$$H = \frac{1}{2\mu}(p_r^2 + p_\theta^2/r^2 + p_\phi^2/r^2\sin^2\theta) + \frac{1}{2\mu_{A,BC}}(P_R^2 + P_\Theta^2/R^2 + P_\Phi^2/R^2\sin^2\Theta) + v(r, \theta, \phi, R, \Theta, \Phi)$$

$$= T + v(r, \theta, \phi, R, \Theta, \Phi) \, , \qquad (2\text{-}44)$$

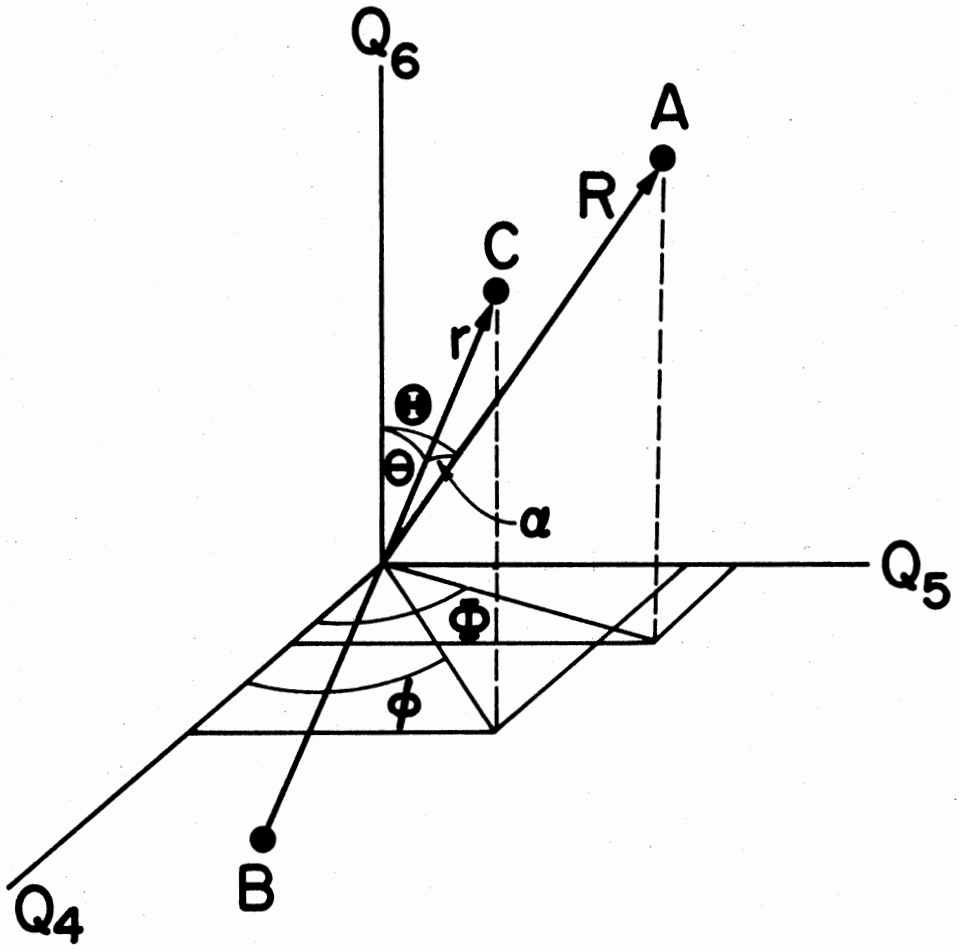

Figure 1. Spherical Polar Coordinate System to Initially Formulate the Variational Rate Coefficient

where $\nu(r, \theta, \phi, R, \Theta, \Phi)$ is the three body A-B-C potential. As the radial vector $\vec{R}$ gets large $\nu(r, \theta, \phi, R, \Theta, \Phi)$ goes to V(r) and Eq. (2-44) reduces to

$$H_o = T + V(r), \qquad (2\text{-}45),$$

where V(r) is taken to be the Morse potential given by Eq. (2-23).

In order to obtain the parameterization of S, a linear transformation is made from $(r, \theta, \phi, R, \Theta, \Phi)$ space to $(W, V, \theta, \phi, \Theta, \Phi)$ space. The transformation is

$$\begin{aligned} W &= AR - Br \\ V &= R + r \end{aligned} \qquad (2\text{-}46)$$

with no changes in the other coordinates. To express the Hamiltonian in terms of the new momenta, one requires the Lagrangian in spherical polar coordinates. The expression is

$$L = \frac{\mu}{2}(\dot{r}^2 + r^2\,\dot{\theta}^2 + \dot{\phi}^2\, r^2 \sin^2\theta) + \frac{\mu_{A,BC}}{2}(\dot{R}^2 + R^2\,\dot{\Theta}^2 +$$

$$\dot{\Phi}^2\, R^2 \sin^2\Theta) - \nu(r, \theta, \phi, R, \Theta, \Phi)\ . \qquad (2\text{-}47)$$

Taking the time derivatives of Eq. (2-46) and inverting to obtain the old velocities in terms of the new, one obtains

$$\begin{aligned} \dot{r} &= (A\dot{V} - \dot{W})/(A + B) \\ \dot{R} &= (B\dot{V} + \dot{W})/(A + B). \end{aligned} \qquad (2\text{-}48)$$

Substituting $\dot{r}$ and $\dot{R}$ into Eq. (2-47) one obtains the new Lagrangian as,

$$L = \frac{\mu}{2}\left(\left((A\dot{V} - \dot{W})/(A + B)\right)^2 + \left((AV - W)/(A + B)\right)^2 \dot{\theta}^2\right.$$

$$\left. + \left((AV - W)/(A + B)\right)^2 \dot{\phi}^2 \sin^2\theta\right) +$$

$$\frac{\mu_{A,BC}}{2}\left(\left((B\dot{V} + \dot{W})/(A + B)\right)^2 + \left((BV + W)/(A + B)\right)^2 \dot{\Theta}^2\right.$$

$$\left. +\left((BV + W)/(A + B)\right)^2 \dot{\Phi}^2 \sin^2\Theta\right) -$$

$$\nu(r(W,V),\ \theta,\ \phi,\ R(W,V),\ \Theta,\ \Phi)\ . \qquad (2\text{-}49)$$

The new momenta are obtained from (61)

$$p_i = \partial L(\dot{q}_i,\ q_i)/\partial\dot{q}_i\ . \qquad (2\text{-}50)$$

Applying Eq. (2-50) to Eq. (2-49) one obtains $P_w(\dot{V},\ \dot{W})$ and $P_v(\dot{V},\ \dot{W})$. Substitution of Eq. (2-48) and noting $\dot{r} = p_r/\mu$ and $\dot{R} = P_R/\mu_{A,BC}$ yields

$$\begin{aligned} P_w &= (-p_r + P_R)/(A + B) \\ P_v &= (Ap_r + BP_R)/(A + B). \end{aligned} \qquad (2\text{-}51)$$

Inversion of Eqs. (2-51) gives

$$\begin{aligned} p_r &= P_v - BP_w \\ P_R &= P_v + AP_w \end{aligned} \qquad (2\text{-}52)$$

Substitution of Eq. (2-52) into the Hamiltonian Eq. (2-44) yields the Hamiltonian in the new coordinate system.

$$H = \left(\frac{1}{2\mu} + \frac{1}{2\mu_{A,BC}}\right)P_v^2 + \left(\frac{A}{\mu_{A,BC}} - \frac{B}{\mu}\right)P_v P_w + \left(\frac{B^2}{2\mu} + \frac{A^2}{2\mu_{A,BC}}\right)P_w^2$$

$$+ \frac{1}{2\mu}\left(p_\theta^2/((AV - W)/(A + B))^2 + p_\phi^2/((AV - W)/(A + B))^2\sin^2\theta\right)$$

$$+ \frac{1}{2\mu_{A,BC}}\left(P_\Theta^2/((BV + W)/(A + B))^2 + P_\Phi^2/((BV + W)/(A + B))^2\sin^2\Theta\right)$$

$$+ \nu(r(W, V), \theta, \phi, R(W, V), \Theta, \Phi). \qquad (2\text{-}53)$$

In order to integrate Eq. (2-42), one requires $\vec{v}.\hat{n}_s = v_{n_s}$ expressed in terms of the new coordinates and momenta. The dividing surface S is defined to be:

$$S \equiv W - C = AR - Br - C = 0 . \qquad (2\text{-}54)$$

Thus, one has two variational parameters with which vary the location of S since

$$R - (B/A)r - C/A = 0. \qquad (2\text{-}55)$$

The unit vector normal to S is given by

$$\hat{n}_s = (\vec{\nabla S}/|\vec{\nabla S}|)_{S=0}. \qquad (2\text{-}56)$$

The dot product $\vec{v}.\hat{n}_s$ may be written

$$\vec{v}.\hat{n}_s = \frac{\vec{v}.\vec{\nabla S}}{|\vec{\nabla S}|} = [dS/dt]/|\vec{\nabla S}|. \qquad (2\text{-}57).$$

However, S has no explicit time dependence, so the total time variation of S is given by the Poisson bracket of S with H (61). That is,

$$dS/dt = [S, H] \ . \tag{2-58}$$

Combining Eqs. (2-57) and (2-58) one has

$$v_{n_s} = [S, H] \ / |\vec{\nabla S}| \ . \tag{2-59}$$

Expansion of the Poisson bracket leads to

$$[S, H] = (\frac{B^2}{\mu} + \frac{A^2}{\mu_{A,BC}})P_w + (\frac{A}{\mu_{A,BC}} - \frac{B}{\mu})P_v \ . \tag{2-60}$$

Obtaining $|\vec{\nabla S}|$ in the (W, V, θ, ϕ, Θ, Φ) coordinate system is somewhat involved and its derivation is given in Appendix A. If $\vec{\nabla S}$ is expressed in relative cartesian coordinates of the relative A-B-C configuration space, one obtains

$$\vec{\nabla S} = \hat{Q}_1(\partial S/\partial Q_1) + \hat{Q}_2(\partial S/\partial Q_2) + \hat{Q}_3(\partial S/\partial Q_3) + \hat{Q}_4(\partial S/\partial Q_4) +$$

$$\hat{Q}_5(\partial S/\partial Q_5) + \hat{Q}_6(\partial S/\partial Q_6), \tag{2-61}$$

where the $\hat{Q}_i$ are orthonormal vectors in the direction of the Q_i axes. Taking the magnitude of Eq. (2-61) provides

$$|\vec{\nabla S}| = \sqrt{A^2 + B^2}, \tag{2-62}$$

and substitution of Eqs. (2-60) and (2-62) into Eq. (2-59) the velocity component normal to S of a particle crossing S is,

$$v_{n_s} = ((\frac{B^2}{\mu} + \frac{A^2}{\mu_{A,BC}})P_w + (\frac{A}{\mu_{A,BC}} - \frac{B}{\mu})P_v)/\sqrt{A^2 + B^2} \ . \tag{2-63}$$

To obtain the upper limit of integration for $v.n_s > 0$ in Eq. (2-42) for the (W, V, θ, ϕ, Θ, Φ) coordinate system, the requirement $v_{n_s} < 0$ must be satisfied. This leads to the condition,

$$P_w < -\left(\frac{A}{\mu_{A,BC}} - \frac{B}{\mu}\right)P_v \Big/ \left(\frac{B^2}{\mu} + \frac{A^2}{\mu_{A,BC}}\right) . \qquad (2\text{-}64).$$

In order to evaluate the configuration integrals in Eq. (2-42), one must integrate over all (r, R) space accessible to the system on the surface S given by Eq. (2-54). Substituting W = C into r(W, V) and R(W, V) yields the expressions,

$$\begin{aligned} r(C, V) &= (AV - C)/(A + B) \\ R(C, V) &= (BV + C)/(A + B) . \end{aligned} \qquad (2\text{-}65)$$

To find the lower limit of the V integral for $C > 0$, set r(C, V) in Eq. (2-65) equal to zero and solve for V. For $C < 0$, treat R(C, V) in the same manner. This yields the following equation for V′, the lower integration limit of V,

$$V' = \begin{cases} C/A, & C > 0 \\ 0, & C = 0 \\ -C/B, & C < 0 . \end{cases} \qquad (2\text{-}66)$$

Since the Jacobian determinant of the transformation to (W, V, θ, ϕ, Θ, Φ, P_w, P_v, P_θ, p_ϕ, P_Θ, P_Φ) phase space, factors into the product of the Jacobian for the configuration space and that of the momentum space one has,

$$d\sigma = \sqrt{\det \underset{\sim}{a_Q}(C)}\ \sqrt{\det \underset{\sim}{g_P}(C)}\ dV\, d\theta\, d\phi\, d\Theta\, d\Phi\, dP_w\, dP_v\, dp_\theta\, dp_\phi\, dP_\Theta\, dP_\Phi, \qquad (2\text{-}67)$$

where det $\underset{\sim}{a}_Q(C)$ is the determinant of the metric tensor for the five-dimensional hypersurface of the configuration space described by W = C. This may be obtained by taking the g_{11} cofactor of Eq. (A-8) of Appendix A and evaluating it at W = C. One evaluates det $\underset{\sim}{g}_P(C)$ by taking the determinant of $\underset{\sim}{g}_P(C)$ of Eq. (A-14) of Appendix A. Substituting the results of these operations into Eq. (2-67) yields the differential element of surface for the eleven-dimensional surface in phase space defined by W = C. The result is,

$$d\sigma = \sqrt{A^2 + B^2}\, dV\, d\theta\, d\phi\, d\Theta\, d\Phi\, dP_w\, dP_v\, dp_\theta\, dp_\phi\, dP_\Theta\, dP_\Phi \,. \qquad (2\text{-}68)$$

Substitution of Eqs. (2-53), (2-63), (2-64), (2-68), and the appropriate V′ from Eq. (2-66) into Eq. (2-42) yields the variational rate coefficient

$$K'(A, B, C, \beta) = -\frac{1}{Q(\beta)} \int_{V=V'}^{\infty} dV \int_0^{\pi} d\theta \int_0^{2\pi} d\phi \int_0^{2\pi} d\Phi \int_0^{\pi} d\Theta$$

$$\chi\, e^{-\beta v(r(C,V),\, \theta,\, \phi,\, R(C,V),\, \Theta,\, \Phi)} \int_{-\infty}^{\infty} dp_\theta\, e^{-\beta p_\theta^2 / 2\mu \left(\frac{AV-C}{A+B}\right)^2}$$

$$\chi \int_{-\infty}^{\infty} dp_\phi\, e^{-\beta p_\phi^2 / 2\mu \left(\frac{AV-C}{A+B}\right)^2 \sin^2\theta} \int_{-\infty}^{\infty} dP_\Theta\, e^{-\beta P_\Theta^2 / 2\mu_{A,BC} \left(\frac{BV+C}{A+B}\right)^2}$$

$$\chi \int_{-\infty}^{\infty} dP_\Phi\, e^{-\beta P_\Phi^2 / 2\mu_{A,BC} \left(\frac{BV+C}{A+B}\right)^2 \sin^2\Theta} \int_{-\infty}^{\infty} dP_v\, e^{-\beta \left(\frac{1}{2\mu_{A,BC}} + \frac{1}{2\mu}\right) P_v^2}$$

$$\chi \int_{-\infty}^{P_w < -\left(\frac{A}{\mu_{A,BC}} - \frac{B}{\mu}\right)P_v / \left(\frac{B^2}{\mu} + \frac{A^2}{\mu_{A,BC}}\right)} dP_w \left(\left(\frac{B^2}{\mu} + \frac{A^2}{\mu_{A,BC}}\right)P_w + \left(\frac{A}{\mu_{A,BC}} - \frac{B}{\mu}\right)P_v\right)$$

$$\chi\ e^{-\beta\left(\left(\frac{B^2}{2\mu} + \frac{A^2}{2\mu_{A,BC}}\right)P_w^2 + \left(\frac{A}{\mu_{A,BC}} - \frac{B}{\mu}\right)P_w P_v\right)} \quad . \tag{2-69}$$

The partition function for reactants Eq. (2-43) written in spherical polar coordinates gives the following phase space integral,

$$Q(\beta) = \frac{1}{\gamma}\int_0^\infty dr\ e^{-\beta V(r)} \int_0^{R'} dR \int_0^\pi d\theta \int_0^{2\pi} d\phi \int_0^\pi d\Theta \int_0^{2\pi} d\Phi$$

$$\chi \int_{-\infty}^{\infty} dp_\theta\ e^{-\beta p_\theta^2/2\mu r^2} \int_{-\infty}^{\infty} dp_\phi\ e^{-\beta p_\phi^2/2\mu r^2 \sin^2\theta} \int_{-\infty}^{\infty} dp_r\ e^{-\beta p_r^2/2\mu}$$

$$\chi \int_{-\infty}^{\infty} dP_\Theta\ e^{-\beta P_\Theta^2/2\mu_{A,BC}R^2} \int_{-\infty}^{\infty} dP_\Phi\ e^{-\beta P_\Phi^2/2\mu_{A,BC}R^2 \sin^2\Theta}$$

$$\chi \int_{-\infty}^{\infty} dP_R\ e^{-\beta P_R^2/2\mu_{A,BC}} \quad , \tag{2-70}$$

where $\gamma = 4\pi R'^3/3$. After evaluation of the phase space integrals in Eqs. (2-67) and (2-68) and substitution of the resulting expression for $Q(\beta)$ into $K'(A, B, C, \beta)$, one obtains

$$K'(A, B, C, kT) = \frac{1}{(A+B)} \sqrt{2\pi kT \left(\frac{B^2}{\mu} + \frac{A^2}{\mu_{A,BC}}\right)} \frac{I_1(A, B, C, kT)}{I_2(kT)} \tag{2-71}$$

where,

$$I_2(kT) = \int_0^\infty r^2 dr\ e^{-V(r)/kT} \tag{2-72}$$

$$I_1(A, B, V', kT) = \int_0^{\pi} \sin\theta d\theta \int_{V=V'}^{\infty} dV \left(\frac{BV+C}{A+B}\right)^2 \left(\frac{AV-C}{A+B}\right)^2$$

$$\chi\, e^{-\nu(r(C,V),\, R(C,V),\, \cos\theta)/kT} \qquad (2\text{-}73)$$

and θ is the A, BC center of mass, C angle. That is, in order to evaluate the configuration integrals in Eq. (2-67) that specify the arbitrary collision plane, one orients the vector $\vec{R}$ along the Q_6 axis, then $\alpha = \theta$ and the integrations over the orientation angles are carried out for fixed θ and V.

Questions have been raised about the convergence of Eqs. (2-72) and (2-73) (22) (47) (64). The argument being, that the potential becomes constant at large particle separations and the integrals are divergent. The current remedy is to replace the infinite upper limits of Eqs. (2-72) and (2-73) with finite upper limits V_{m1} and r_{m2} values of $V > V_{m1}$ and $r > r_{m2}$ might be considered a region of inaccessible phase space for the process under consideration. The new upper bounds define $I_2(r_{m_2}, kT)$ and $I_1(A, B, V', V_{m1}, kT)$ as the following:

$$I_2(r_{m2}, kT) = \int_0^{r_{m2}} r^2 dr\, e^{-V(r)/kT}$$

$$I_1(A, B, V', V_{m1}, kT) = \int_0^{\pi} \sin\theta d\theta \int_{V=V'}^{V_{m1}} dV \left(\frac{BV+C}{A+B}\right)^2$$

$$\chi \left(\frac{AV-C}{A+B}\right)^2 e^{-\nu(r(C,V),\, R(C,V),\, \cos\theta)/kT} . \qquad (2\text{-}74)$$

Examination of Eq. (2-69) reveals that it is a variational rate coefficient depending on two variational parameters. Taking the particular set B = 0, A = 1, and C = R_t in Eq. (2-54), one finds an interesting special case of Eq. (2-71). The surface S is now defines as,

$$S = R - R_t = 0 \tag{2-75}$$

Denoting I_1 of Eq. (2-74) as I_1' and making the change of variable r = V - C yields,

$$I_1'(r_{m1}, kT) = R_t^2 \int_0^{\pi} \sin\theta d\theta \int_0^{r_{m1}} r^2 dr\, e^{-\nu(r, R_t, \cos\theta)/kT}$$

$$= R_t^2 I_1(r_{m1}, kT) . \tag{2-76}$$

Substitution of Eq. (2-76) into Eq. (2-71) gives the following expression:

$$K'(kT) = \sqrt{2\pi kT/\mu_{A,BC}}\; R_t^2 I_1(r_{m1}, kT)/I_2(r_{m2}, kT). \tag{2-77}$$

This is the result previously derived by Anderson (42) with finite upper limits for the integrals I_1 and I_2.

Selection of Initial Conditions for the Combined Phase Space/Trajectory Procedure

The derivation of the variational rate coefficient is based on the first of the two CPST assumptions: The thermal rate coefficient K(T) evaluated from Eq. (1-1) is independent of the location of S. In order to select initial phase points on S for the CPST trajectories,

assumption 2 is invoked. That is, the initial phase point describing the remaining eleven classical degrees of freedom of S may be selected from an equilibrium thermal Boltzmann distribution for each degree of freedom.

The classical degrees of freedom θ and V have as their Boltzmann weight factor the integrand of Eq. (2-74). That is,

$$f(\theta_j, V_i)\,\Delta\theta_j\,\Delta V_i = \sin\theta_j \left(\frac{BV_i + C}{A+B}\right)^2 \left(\frac{AV_i - C}{A+B}\right)^2 \chi\, e^{-\nu(r(C,V_i),\, R(C,V_i),\, \cos\theta_j)/kT}\,\Delta\theta_j\,\Delta V_i \qquad (2\text{-}78)$$

where θ_j and V_i are the increment sizes along the θ and V axes, respectively. Notice that Eq. (2-78) implies $f(\theta, V)$ is constant over the (θ, V) region θ in the interval $[\theta_j, \theta_j + \Delta\theta_j]$ and V in the interval $[V_i, V_i + \Delta V_i]$. To implement the random sampling of the initial (θ_j, V_i) over the integration limits of Eq. (2-74), one requires the θ and V increment sizes be constant. The partial sums of Eq. (2-78) (47) may be used for the Boltzmann weight of θ values in the integral $[0, \theta_t]$ and V in the interval $[V', V_k]$. That is,

$$S_{tk} = \sum_{j=1}^{t} \sum_{i=1}^{k} f(\theta_j, V_i)\ . \qquad (2\text{-}79)$$

The partial sums S_{tk} are evaluated for every grid point, (θ_j, V_i), contained in the area bounded by θ_j in the interval $[0, \pi]$ and V_i in the interval $[V', V_{ml}]$. Denoting $\theta_m = \pi$ and $V_n = V_{ml}$ one forms the

sequence of partial sums,

$$\{S_{11}, S_{12}, \ldots, S_{tk}, \ldots, S_{nm}\}. \tag{2-80}$$

Normalizing this partial sum sequence with respect to S_{nm}, a normalized sequence of partial sums may be obtained,

$$\{W_{11}, W_{12}, \ldots, W_{tk}, \ldots, W_{nm}\}, \tag{2-81}$$

where

$$W_{tk} = S_{tk}/S_{nm}. \tag{2-82}$$

Random selection of the initial (θ_r, V_k) for a CPST trajectory proceeds by choosing a random number, $\xi(\theta, V)$, and searching the $\{W_{ij}\}$ sequence until the condition

$$\xi(\theta, V) - W_{tk} \leq 0 \tag{2-83}$$

is satisfied. Then, one may obtain the spherical polar variables $r(C, V_k)$ and $R(C, V_k)$ from Eq. (2-65).

To specify the initial momenta on S, one requires the indefinite integrals of Eq. (2-69). After integration over the P_w integral, the remaining integrals are all gaussians described by Eqs. (2-24) through (2-28). Replacing y with z as the solution to Eq. (2-27), absorbing the randomly chosen positive or negative sign into z, and substituting the appropriate σ's into Eq. (2-28), the initial P_v, p_θ, p_ϕ, P_Θ, P_Φ momenta for a given CPST trajectory on S are given by,

$$P_v = \frac{1}{(A+B)} \sqrt{2kT\ (\mu_{A,BC}\ B^2 + \mu A^2)}\ \ z_v$$

$$P_\Phi = z_\Phi\ R(C,V_k)\ \sin\Theta\ \sqrt{2\mu_{A,BC}kT}$$

$$P_\Theta = z_\Theta\ R(C,V_k)\ \sqrt{2\mu_{A,BC}kT}$$

$$P_\phi = z_\phi\ r(C,V_k)\ \sqrt{2\mu kT}$$

$$P_\theta = z_\theta\ r(C,V_k)\ \sqrt{2\mu kT}\ . \qquad (2\text{-}84)$$

If one defines

$$f(P_w) = \left(\frac{B^2}{2\mu} + \frac{A^2}{2\mu_{A,BC}}\right) P_w^{\,2} + \left(\frac{A}{\mu_{A,BC}} - \frac{B}{\mu}\right) P_w P_v\ , \qquad (2\text{-}85)$$

and $I_{P_w}(P_v)$ as the definite integral of P_w over the limits given by Eq. (2-69),

$$I_{P_w}(P_v) = -\frac{1}{\beta}\, e^{\frac{\beta(A/\mu_{A,BC} - B/\mu)^2}{2(B^2/\mu + A^2/\mu_{A,BC})} P_v^{\,2}}\ , \qquad (2\text{-}86)$$

then replacing the lower limit of $-\infty$ of the P_w integral by P_w, the Monte Carlo random number for the random selection of P_w may be written as,

$$\xi(P_w) = \frac{1}{\beta I_{P_w}(P_w)}\ e^{-\beta f(P_w)} + 1\ . \qquad (2\text{-}87)$$

Substituting the quantities defined by Eqs. (2-85) and (2-86) and solving Eq. (2-87) for P_w, one obtains,

$$P_w = \frac{1}{\left(\frac{B^2}{\mu} + \frac{A^2}{\mu_{A,BC}}\right)} \left(- \left(\frac{A}{\mu_{A,BC}} - \frac{B}{\mu}\right) P_v - \sqrt{-2kT\left(\frac{B^2}{\mu} + \frac{A^2}{\mu_{A,BC}}\right) \ln(1-\xi(P_w))} \right)$$

The orientation angles, ϕ, Θ, Φ, for the arbitrary collision plane are the only variables that have not been specified. Setting $\phi=\theta=\Phi=0$ and obtaining the radial momenta p_r and P_R from Eq. (2-52), one may write the initial phase space point on S as cartesian coordinates and momenta expressed in terms of spherical polar coordinates and momenta. The result is,

$$Q_1 = r(C, V_k) \sin\theta_t$$

$$Q_2 = 0$$

$$Q_3 = r(C, V_k) \cos\theta_t$$

$$Q_4 = 0$$

$$Q_5 = 0$$

$$Q_6 = R(C, V_k)$$

$$P_1 = \sin\theta_t \, p_r + \cos\theta_t \sqrt{2\mu kT} \, z_\theta$$

$$P_2 = \sqrt{2\mu kT} \, z_\phi$$

$$P_3 = \cos\theta_t \, p_r + \sin\theta_t \sqrt{2\mu kT} \, z_\theta$$

$$P_4 = \sqrt{2\mu_{A,BC} kT} \, z_\Theta$$

$$P_5 = \sqrt{2\mu_{A,BC} kT} \, z_\Phi$$

$$P_6 = P_R \, . \qquad (2\text{-}89)$$

Once the initial phase point on S has been determined by Eqs. (2-89) this provides the initial conditions for a CPST trajectory. Hamilton's equations are then numerically integrated (60) toward the product region of phase space, or one follows the time evolution of the trajectory in the relative A-B-C phase space until one of the following conditions is satisfied,

$$S = W - C > 0 \quad , \tag{2-90}$$

or

$$\rho_i^2 - R_o^2 > 0 \quad , \tag{2-91}$$

where ρ_i is the distance from the geometric center of molecule i to the separated atom.

If the condition of Eq. (2-90) is satisfied, the trajectory has recrossed S and started toward the reactant phase space. This is considered a nonreactive or unsuccessful trajectory. Any trajectory satisfying this criterion is terminated. If a trajectory starting from S going toward the product region of phase space does not satisfy Eq. (2-90), but does satisfy Eq. (2-91), then it is a possible candidate for a successful trajectory. To determine if a trajectory is successful after it reaches the product region of phase space, the trajectory is back integrated from the initial phase point on S. If it terminates in either of the product regions of phase space by satisfying Eq. (2-91), the trajectory is unsuccessful. If the trajectory terminates in the reactant region of phase space, it is a successful or reactive trajectory.

Considering the results of the previous section, a variational rate coefficient has been derived that depends on the variational parameters A, B, and C which describe the location of S in the configuration space of the (A, BC) system. One may vary S with respect to these parameters and determine a minimum variational rate coefficient by evaluation of $K'(A, B, C, kT)$ of Eq. (2-71) for each (A, B, C) triple. Once this minimum has been determined, one may evaluate the CPST rate coefficient by running trajectories with initial conditions chosen from the minimum corssing surface S_0. The CPST rate coefficient Eq. (1-1) becomes,

$$K(A, B, C, kT) = \xi(A, B, C, T)\, K'(A, B, C, kT), \tag{2-92}$$

where

$$\xi(A, B, C, T) = N_r(A, B, C, T)/N(A, B, C, T), \tag{2-93}$$

and N_r denotes the number of reactive trajectories computed from a set of N trajectories.

The statistical error associated with Eq. (2-92) is given by (47),

$$\sigma^2 = (N-N_r)/NN_r. \tag{2-94}$$

Once the A, B, C, triple describing S_0 has been found for a given temperature, these parameters are used to compute variational rate coefficients over a large temperature range.

Integration of the Equations of Motion

Once the initial conditions for a trajectory have been specified

by Eqs (2-11), (2-12), and (2-16) of method I, Eqs. (2-36), (2-37) and (2-16) for method II, or Eqs. (2-89) for a CPST trajectory, one has chosen a point on a trajectory in the phase space of the system. Following the time evolution of a trajectory through the phase space of the system is equivalent to knowing all values of the Q_i and P_i for the trajectory at each instant of time during the collision event. To obtain the P_j and Q_j, one must numerically solve Hamilton's equations for a conservative system. The equations are:

$$\dot{Q}_j = \partial H(Q_i, P_i)/\partial P_j$$
$$\dot{P}_j = -\partial H(Q_i, P_i)/\partial Q_j = -\partial v(Q_i)/\partial Q_j \qquad (2\text{-}95)$$

where both i and j assume values from 1 to 6. The procedure involves solving twelve simultaneous differential equations of the form $\dot{P}_j(Q_i)$ and $\dot{Q}_j(P_i)$. The expressions for the $\dot{P}_j$ and $\dot{Q}_j$ have been derived by Karplus, Porter and Sharma (58).

To implement the solution of this system of differential equations, a fourth order Runge-Kutta method with minimum error bounds is employed (60). Specifying one of the dependent variables as y at time t and y_o as its value at the previous time step t-h with h being the integration step size, the pertinent iterative equations are:

$$y = y_o + 0.17476028\ k_1 - 0.55148066\ k_2 + 1.20553560\ k_3 + 0.17718478\ k_4 \ . \qquad (2\text{-}96)$$

If the expression for y' is $y' = f(t, y)$, the expressions for the k_i are:

$$k_1 = h\, f(t_o, y_o)$$

$$k_2 = h\, f(t_o + 0.4h,\ y_o + 0.4\, k_1)$$

$$k_3 = h\, f(t_o + 0.45573725h,\ y_o + 0.29697761\, k_1 + 0.15875964\, k_2)$$

$$k_4 = h\, f(t_o + h,\ y_o + 0.21810040\, k_1 - 3.05096516\, k_2 + 3.83286476\, k_3). \quad (2\text{-}97)$$

The integration step size is determined by integrating a random sampling of ten classical trajectories for each temperature from initial conditions chosen in the reactant valley to final conditions and then back-integrating to the reactant state. The criterion a step size was required to satisfy in order to be acceptable is that it reproduce the initial conditions with less than ten percent relative error of the most inaccurate coordinate or momenta. The step sizes determined in this manner from the classical trajectory procedure are assumed valid for the CPST trajectories.

Determination of the Final State

The final state of a classical trajectory is determined by testing Eq. (2-91) at each time step during the numerical integration of a trajectory, a condition which is valid for both CTA and CPST trajectories. Once Eq. (2-91) is satisfied, one has the possibilities of three different final systems: A + BC, AB + C, and AC + B. These are the only considerations necessary, since, for the collision energies sampled processes that lead to products other than those mentioned are negligible. The cartesian coordinates necessary for the end test for product AB + C are:

$$x_2 = \frac{2m_B+m_C}{2(m_B+m_C)} Q_1 - Q_4/2$$

$$y_2 = \frac{2m_B+m_C}{2(m_B+m_C)} Q_2 - Q_5/2$$

$$z_2 = \frac{2m_B+m_C}{2(m_B+m_C)} Q_3 - Q_6/2 \ . \qquad (2\text{-}98)$$

The description of the final state of the system may be specified in terms of final relative velocity, orbital and molecular angular momenta, and internal energy of the product diatomic molecule expressed in terms of the final coordinates and momenta (58). Denoting the final state with primes, the scattering angle in the center of mass coordinate system is (46),

$$\Theta_c = \arccos\left(\frac{Vx' \, Vx + Vy' \, Vy + Vz' \, Vz}{V_R' \, V_R}\right), \qquad (2\text{-}99)$$

where, V_R' and V_R are the magnitudes of the final and initial relative velocity vectors, respectively, and the V_i are the cartesian components of the relative velocity, Eq. (2-99) must be used to compute the scattering angles for CPST trajectories, since the orientation of the initial relative velocity vector is random. However, in CTA trajectories, the initial relative velocity vector is oriented in the direction of the positive Q_6-axis and Eq. (2-99) reduces to,

$$\Theta_c = \arccos(V_z'/V_R'). \qquad (2\text{-}100)$$

If one wishes to separate the internal energy of the product diatomic molecule into rotational and vibrational components, this may

be partially accomplished by the Morse oscillator approximation. Denoting r_1 and r_2 as the inner and outer turning points for the product diatomic molecule one has for the classical vibrational action (59):

$$n = \frac{2}{h} \int_{r_1}^{r_2} p_r \, dr \, . \tag{2-101}$$

This integration may be accomplished by continuing the trajectory after the final state has been reached and searching for the inner turning point. That is, $p_r = 0$. The final relative coordinates are arbitrarily oriented in their coordinate system and one narrows the search for $p_r = 0$ by searching for the smallest r value found after continuation of the trajectory. The $\vec{r}$ and $\vec{p}$ vectors are then simultaneously oriented in a new coordinate system with the z-axis oriented along $\vec{r}$. If the new coordinate system is designated by primes, then $p_z' = p_r$. One may accomplish this orientation with the aid of the rotation matrices (46) (52). The newly oriented coordinates and momenta are:

$$\vec{r}' = \underset{\sim}{R}_y(\theta) \, \underset{\sim}{R}_z(\phi) \, \vec{r}$$

$$\vec{p}' = \underset{\sim}{R}_y(\theta) \, \underset{\sim}{R}_z(\phi) \, \vec{p} \, , \tag{2-102}$$

where

$$\phi = \arctan(y/x)$$

$$\theta = \arccos(z/r). \tag{2-103}$$

The procedure mentioned above must be repeated for each time step after the end of a trajectory storing the values of $p_z' = p_r$ at each time step until the outer turning point, r_2, is reached. This gives one a numerical compilation of $p_r(r)$ for r in the interval $[r_1, r_2]$ with

varying increment sizes along r. It would be difficult at best to attempt an accurate numerical integration of $p_r(r)$ over the limits r_1 ro r_2. However, $p_r(r)$ may be numerically interpolated at desired r values with the aid of the one dimensional cubic spline procedure (65). The two and three dimensional counterparts of the cubic spline procedure have proven more than adequate in several cases for numerical interpolation of potential energy surfaces (66). After one has numerically interpolated $p_r(r)$ at the necessary r values, Eq. (2-101) may be numerically integrated by one of the Newton Cotes quadrature formulas (67). After the vibrational action has been obtained, the vibrational energy in the Morse oscillator approximation is (46);

$$E_n = n\hbar\omega_o - (n\hbar\omega_o)^2/4D_1. \qquad (2\text{-}104)$$

The approximation for the rotational energy is the difference of internal and vibrational energy,

$$E_r = E_{vr} - E_n . \qquad (2\text{-}105)$$

Initial states in the CTA procedure for thermal processes are chosen from a Boltzmann distribution in the reactant valley with only final states of products being examined. The CPST procedure requires sampling of states on S from a Boltzmann distributions. Unless one examines both reactant and product state distributions, there is no knowledge about the original reactant distribution. At least if one compiles reactant distributions for reactive trajectories in both CPST and CTA procedures, it may be possible to determine if the reactive trajectories originate from equivalent distributions in the reactant valley.

Statistical Averaging for the CTA and CPST Procedures

To compile frequency distributions for a given dynamical variable p, whether it be the initial or final state, the usual method (46) is to divide the range of the dynamical variable into constant increment sizes and to sum the weights of each trajectory that produces the dynamical variables p in the range of p to p + Δp for the process being studied. That is, if p is in the interval, $[p_o, p_1]$, one defines the increment size as,

$$\Delta_p = (p_1-p_o)/n \ , \tag{2-106}$$

where n is the number of intervals contained in the range of p. For example, if one is studying reactive processes, one finds the integer k or increment label from,

$$k = (p-p_o)/\Delta_p \ . \tag{2-107}$$

After a set of N trajectories have been computed containing a subset of N_r reactive trajectories, the normalized frequency of occurrence of the dynamical variable p in the increment k is,

$$f(p_k) = \sum_{m=1}^{N_r} w_m(k) / \sum_{i=1}^{N_r} w_i, \tag{2-108}$$

where w_i is the weight attributed to trajectory i, and $w_m(k)$ is the weight associated with the trajectories m that produce the dynamical

variable p in the increment $[p_o+(k-1)\Delta_p, p_o+k\Delta_p]$. If one is computing classical trajectories and selecting the impact parameter with Eq. (2-17), each trajectory is weighted by the impact parameter weighting. That is, $w_i = \xi(b_i)$. If one is computing CPST trajectories, each trajectory has weight $w_i = 1$.

One example of this, is the computation of the normalized differential cross section with Θ_c in the interval $[0, \pi]$. The expression is,

$$\frac{d\sigma((\Theta_c)k)}{d\Omega_k} = \sum_{m=1}^{N_r} \frac{w_m(k)}{\sin(\Theta_c)_k} \Big/ \sum_{i=1}^{N_r} w_i, \qquad (2\text{-}109)$$

where the w_i take on the weights mentioned previously for either the CTA or CPST procedures.

CHAPTER III

RESULTS AND DISCUSSION

CTA Rate Coefficient - Method I

The CTA rate coefficient has been computed at 900 K by computation of reaction cross sections at six relative velocities with initial conditions chosen by the procedures described under method I. The maximum impact parameter was chosen to be 2.50 au for V_r = 2.0 vu. Since the number of reactions decrease at lower relative velocities, the impact parameter was reduced for the lower relative velocities in order to avoid the large standard error given by Eq. (2-20). All trajectories were computed with an integration step size of 0.02 tu. Computer codes were checked by computation of standard quasiclassical trajectories at 900 K. The result of 7563 trajectories produced K(900) = $7.9346 \times 10^{11} \pm 0.8823 \times 10^{11}$ cm^3/mole-sec. This result is in statistical accord with the previous SQCT result of K(900) = 7.3760×10^{11} cm^3/mole-sec. The reaction cross sections computed by Eq. (2-19) are given in Table I.

To evaluate the rate coefficient from Eq. (2-21), one requires reaction cross sections at relative velocities for which the integrand must be evaluated in the numerical integration procedure. The numerical values of the reaction cross sections along with the upper and lower bounds were obtained graphically as shown in Figure 2. Extrapolation

to zero cross section was employed to estimate the reaction threshold.

TABLE I

REACTION CROSS SECTION AS A FUNCTION OF RELATIVE VELOCITY

V_r vu	N[a]	b_{max} au[b]	$S(V_r)$ au^2
1.050	600	1.25	0.0481 ± 0.0184
1.088	600	1.25	0.1369 ± 0.0355
1.200	382	1.60	0.5265 ± 0.1006
1.400	400	1.80	1.7009 ± 0.2024
1.600	400	2.00	2.9220 ± 0.2601
2.000	400	2.50	4.8896 ± 0.3961

[a]N total number of trajectories computed at each relative velocity

[b]Molecular units are described in Appendix B

A nine-point Newton Cotes quadrature (67) was employed for the numerical integration of Eq. (2-21). Upper and lower bounds of $S(V_r)$ were obtained by graphical techniques with each value of $S(V_r)$ being weighted by the relative velocity weighting to form the integrand of Eq. (2-21). The results of these computations with their threshold velocities V_o are given in Table II.

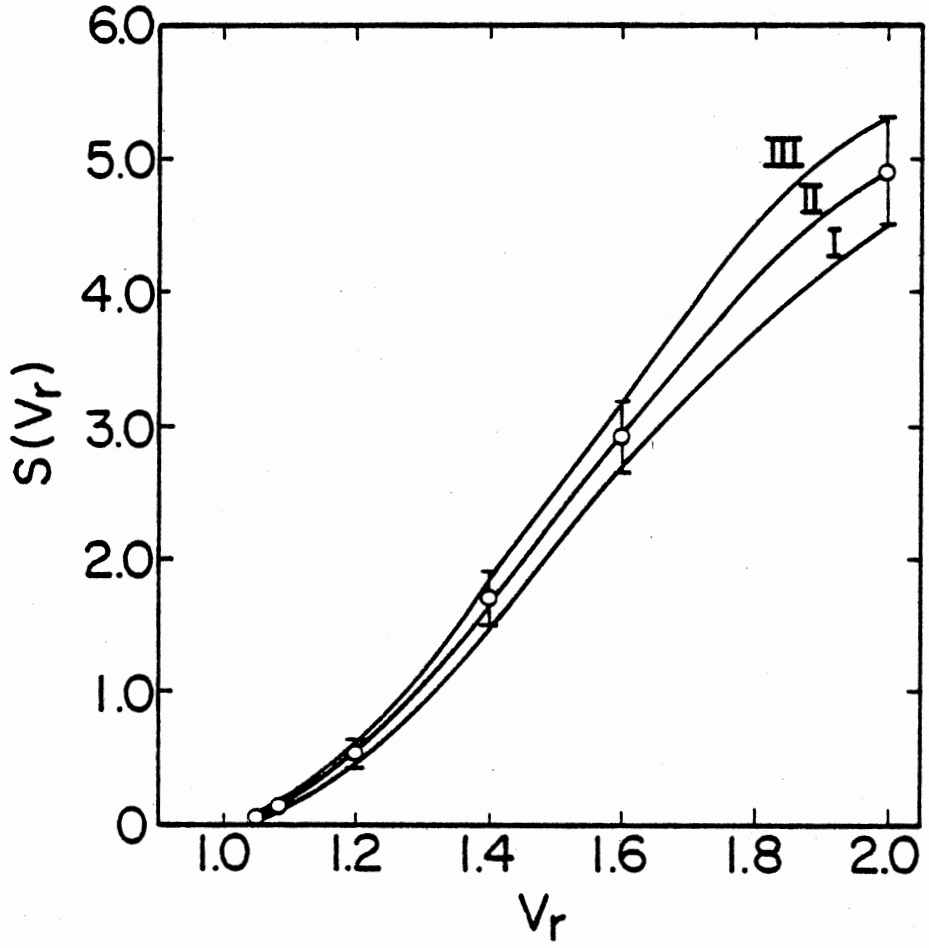

Figure 2. Plot of Reaction Cross Section vs. Relative Velocity, $S(V_r)$ and V_r Have Units of au^2 and Velocity Units, Respectively

TABLE II

RATE COEFFICIENT COMPUTED AT 900 K FROM METHOD I

Reference to Fig. 2	V_o vu	K(900) $\frac{cm^3}{mole\text{-}sec}$ [d]
I[a]	1.014	1.7760×10^{11}
II[b]	1.026	2.1202×10^{11}
III[c]	1.032	2.5374×10^{11}

Est. rel. error = 17.7%

[a] Lower bound

[b] From numerically computed cross sections

[c] Upper bound

[d] Eq. (2-21) $C = 1.65652 \times 10^{13}$

The primary purpose of evaluating this rate coefficient is to compare the rate coefficients obtained when the initial conditions for BC are chosen by methods I or II. However, it is worthwhile to compare this classical rate coefficient with that obtained in the previous SQCT study (58). The Porter-Korplus result is $K(900) = 7.3760 \times 10^{11}$ cm^3/mole-sec, roughly a three to four-fold factor larger than the method I CT rate coefficient. The SQCT cross sections are computed for v = 0 and J = 0, 1, ..., 5. Examination of the Boltzmann weight factor shows $S(V_r, J, v)$ for J = 1, 2, 3 to give the most important contributions to the sum over rotational states given in Eq. (41) of Ref. (58) for the evaluation of the rate coefficient. These reaction cross section

curves all exhibit threshold velocities below the threshold velocity for the classical barrier $V_o' \sim 1.09$ vu. Some are as low as 0.9 vu. Porter and coworkers point out that rotational energy probably does not enhance reaction for three dimensional trajectories. In fact, its major contribution is probably to provide a disorienting effect for the most favorable transition-state configuration, the collinear complex. Thus, the decrease of threshold below the classical value is due to the contribution of zero-point energy.

The CT rotationally vibrationally averaged cross section computed by method I does exhibit a threshold velocity below the V_o' value. If one applies arguments about rotational energy given above to the present case it appears that classical vibrational energy does lower the reaction threshold about 0.05 vu below the classical V_o' value. However, it does not seem to be nearly as significant as the zero point energy present in every trajectory sampled in the SQCT study.

CTA Rate Coefficients - Method II

The CTA rate coefficients for the $H + H_2$ thermal exchange reaction have been computed for temperatures of 300, 500, 900, and 1100 K with initial conditions selected by the procedures described by method II. Integration step sizes at the different temperatures have been determined by the criterion mentioned on p 45. Reaction thresholds were determined by computing nonstatistical trajectories with small impact parameters, $b_{max} = 0.25$ au, and relative velocities near the classical

threshold $V_o \sim 1.09$ vu. Initially 200 trajectory batches were computed to determine nonzero cross sections above threshold, then additional trajectories were computed to reduce statistical error. Results of the procedure described above at 300 K are given in Table III, with cross sections obtained from Eq. (2-19) and standard error given by Eq. (2-20). The trajectory computed cross sections with their upper and lower error bounds are shown in Figure 3.

TABLE III

REACTION CROSS SECTION NEAR THRESHOLD AT 300 K

V_r vu	N	$S(V_r) \times 10^3$ au^2 [a]
1.10	603	4.847 ± 1.494
1.15	600	11.598 ± 2.112
1.20	400	26.006 ± 3.773

[a] $b_{max} = 0.25$ au

Extrapolation to zero cross section yields a reaction threshold $V_o \sim 1.04$ vu to be used as the lower bound of Eq. (2-40) to select the initial relative velocity for a classical trajectory.

The maximum impact parameter was determined by computing the reaction probability $P_r(V_r, b)$ from Eq. (2-18) with $V_r = 1.20$ vu and

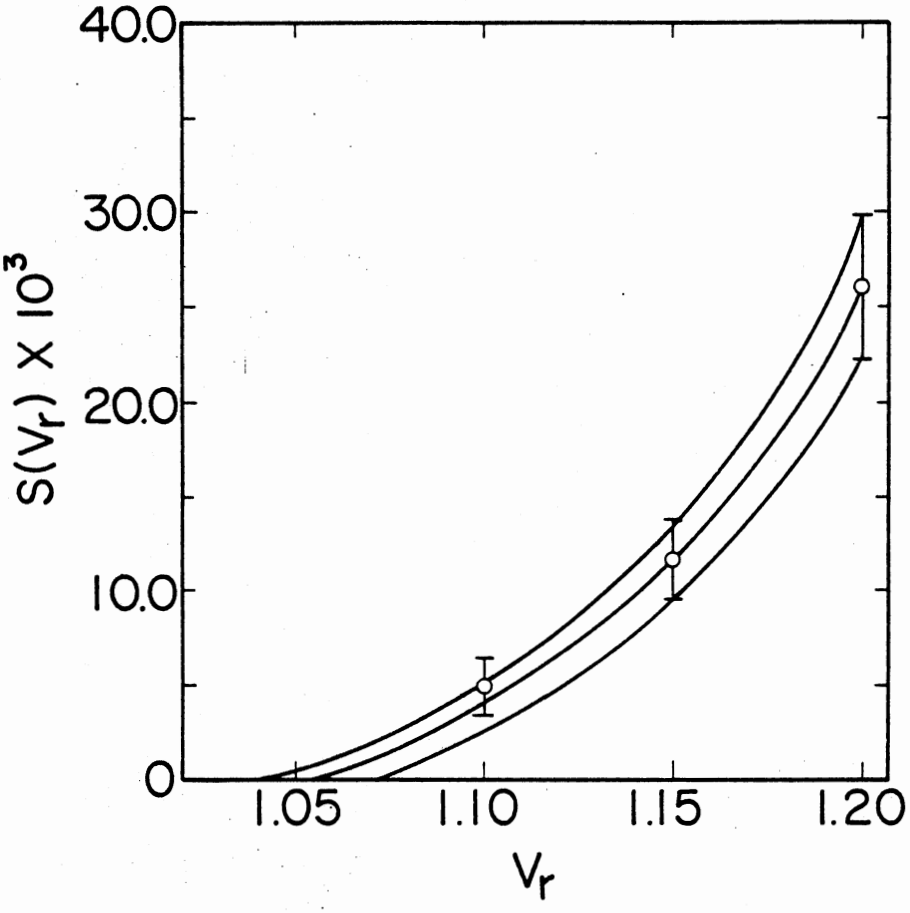

Figure 3. Reaction Cross Section Near Threshold at 300 K from Method II, $S(V_r)$ has Units of au^2, V_r is in Velocity Units

N = 200 at each value of b. When b was sufficiently large so that $P_r \rightarrow 0$ for the 200 trajectories sampled, b_{max} was set equal to that value of b. The b_{max} value so determined was used to select the initial impact parameter for a classical trajectory from Eq. (2-17).

The procedures discussed above were repeated for each temperature with the exception, that the threshold velocity at 900 K was the one determined from the method I procedure. The results are summarized in Table IV.

TABLE IV

INTEGRATION STEP SIZE AND PARAMETERS DETERMINED BY NONSTATISTICAL TRAJECTORIES

T K	Δt^a tu	V_o vu	b_{max} au
300	0.04	1.040	1.20
500	0.04	1.006	1.50
900	0.02	1.014	2.00
1100	0.02	0.870	2.10

[a]Integration step size

Classical trajectories were computed at the four temperatures given in Table IV with initial conditions chosen by the procedures

described in method II. The results of these computations along with the previous SQCT rate coefficients are given in Table V.

TABLE V

CT AND SQCT COMPUTED RATE COEFFICIENTS FOR THE $H + H_2$ THERMAL EXCHANGE REACTION

T K	N[a]	$K_{CT}(T)$ $\frac{cm^3}{mole\text{-}sec}$ [b]	$K_{SQCT}(T)$ $\frac{cm^3}{mole\text{-}sec}$ [c]
300	16328	$(1.6140 \pm 0.1564) \times 10^{6}$	2.0080×10^{8}
500	10314	$(1.4869 \pm 0.1414) \times 10^{9}$	2.3200×10^{10}
900	4836	$(1.8462 \pm 0.1477) \times 10^{11}$	7.3760×10^{11}
1100	3664	$(7.3613 \pm 0.7958) \times 10^{11}$	-------

[a] Number of trajectories computed for CT rate coefficient

[b] CT rate coefficient

[c] SQCT rate coefficient (Reference 58)

Comparison of the 900 K CT rate coefficient of Table V determined by method II and the upper and lower bounds for the method I CT rate coefficient given in Table II show the two results are in statistical agreement.

The rate coefficients of the SQCT study have been fitted to an Arrhenius expression (58), which resulted in a computed activation energy E_A = 7.435 kcal/mole. A similar treatment of the CT rate

coefficients listed in Table V yields E_A = 10.593 kcal/mole. It is possible from these results to make a qualitative statement about the contribution of zero-point energy to the reaction. However, it must be remembered the classical trajectories do exhibit classical vibrational energy. The zero-point vibrational energy of the H_2 molecule is $E_o \sim 6.386$ kcal/mole. The difference of the CT and SQCT activation energies mentioned above is 3.158 kcal/mole, from this, one may say a fraction of 0.495 or about half the zero-point energy aids the quasi-classical trajectories in crossing the barrier. A more precise determination of the effective zero-point energy involved in reaction could be obtained if one were to compute rate coefficients from trajectories having no vibrational energy. These computations have been done at temperatures of 300, 500, 700, and 900 K. The resulting activation energy is 11.652 kcal/mole, which suggests that 4.2 kcal/mole of the zero-point energy is effective in promoting reaction. This result is in reasonable accord with that obtained in the SQCT study, where collinear trajectories were computed both with and without zero-point energy. The resulting difference in the relative translational energy necessary to transverse the barrier was determined to be 4.1 kcal/mole. This agreement must be regarded with some caution since it involves a comparison between a three dimensional and a collinear study. If such comparison of activation energies is a valid method to estimate the contribution of vibrational energy to reaction, one may compare the activation energies from rate coefficients obtained by trajectories without vibrational energy and the CT rate coefficients to estimate the classical

vibrational energy contribution to reaction. The result is 1.059 kcal/mole of classical vibrational energy contributes to reaction.

Investigation of the Variational Rate Coefficient

The final form of the variational rate coefficient given by Eq. (2-71) intuitively suggests that one could study the variation of $K'(A, B, C, T)$ with respect to the variational parameters A, B, and C, possibly finding local minima, that must be upper bounds to the classical rate coefficient (22).

To assess the reliability of the computed variational rate coefficients one must determine the accuracy of the numerically computed values of the integrals, $I_2(r_{m2}, kT)$ and $I_1(A, B, V', V_{m1}, kT)$ given by Eqs. (2-74). Some of the tests that have been performed to evaluate the accuracy of the integrals are comparison of simple definite integrals computed both analytically and numerically, evaluation of I_1 by two different numerical integration procedures for the (H, H_2) system, evaluation of I_1, I_2 and $K'(T)$ for the (H, I_2) system and comparing with previous results (47), evaluation of I_1 for the reactant asymptotic limit, and comparison of I_1 and the normalization factor S_{nm} defined in Eqs. (2-79) and (2-80).

The simple definite integrals used to test the numerical integration procedures are:

$$\int_0^1 dx\, x^2 = 1/3 \qquad (3\text{-}1a)$$

$$\int_0^1 dy \int_0^1 dx\, x^2 y^2 = 1/9 \qquad (3\text{-}1b)$$

The result of a Simpson's rule integration of Eq. (3-1a) with seven integrand evaluations produces a value of 0.333333. With seven points to evaluate the inner integral and seven for the outer integral of Eq. (3-1b), a result of 0.11111 was obtained.

The results of numerical integration by both Simpson's rule and a five-point Newton Cotes procedure for I_1 given in Eq. (2-74) evaluated at 900 K are shown in Table VI. The results in Table VI show that as the values of N_v and N_θ are increased, the computed values of I_1 show an oscillatory convergence. Comparison of the results for Simpon's rule $I_S(N_v, N_\theta)$ and the Newton Cotes procedure $I_{NC}(N_v, N_\theta)$ shows that $I_S(49, 15)$ and $I_{NC}(49,17)$ are converging to the same value. The values of I_1 for $I_S(143, 91)$ and $I_{NC}(161, 93)$ are practically identical. In addition, if one rejects $I_{NC}(29,17)$ and $I_{NC}(33, 17)$, the computed relative standard deviations are less than 1.8%. Computing the relative deviations from the mean for $I_{NC}(29, 17)$ and $I_{NC}(33, 17)$, one finds both are greater than 10 s.

If one sets A = 1.0, B = 0.0, and C = R_t, I_1 assumes the form of Eq. (2-76) with the variational rate coefficient given by Eq. (2-77). The integrals I_1, I_2 and the variational rate coefficient have been computed for the (H, I_2) system and the results compared with the previous CPST study (47) at 600 K. The results are given in Table VII with the results of the previous CPST study taken as the correct values. Table VII shows the results of this work are good in accord with those of the previous CPST study with the relative error of each computed quantity being on the order of a fraction of a percent.

TABLE VI

NUMERICAL INTEGRATION OF I_1 AT 900 K
FOR THE (H, H_2) SYSTEM[a]

Integration Procedure	N_v[b]	N_θ[c]	I_1 au^5
Simpson's Rule	31	15	0.9966116×10^{-2}
	49	15	0.1002501×10^{-1}
	143	91	0.9854186×10^{-2}
Newton Cotes	29	17	0.1216127×10^{-1}
	33	17	0.8222695×10^{-2}
	49	17	0.1027321×10^{-1}
	161	93	0.9854142×10^{-2}
Rel. std. dev.[d] = 1.7%			

[a] A = 1.0, B = 1.5, C = 0.0

[b] Number of integrand evaluations along V

[c] Number of integrand evaluations along θ

[d] Based on rejection of $I_{NC}(29, 17)$ and $I_{NC}(33, 17)$

TABLE VII

COMPARISON OF PRESENT WORK WITH A = 1.0, B = 0.0, AND C = R_t WITH PREVIOUS WORK ON THE (H, I_2) SYSTEM

Quantity	Numerical Procedure	Numerical[a,b] Result	Numerical[c] Result
$I_2(600)$ au^3	Simpson's Rule	8.58407	---------
	Newton Cotes	8.58372	8.56446
$I_1(600)$ au^5 [d]	Simpson's Rule	34.8725	---------
	Rhomberg Method	34.7172	---------
	Newton Cotes	34.7771	34.6140
$K'(600)$ $\frac{cm^3}{mole\text{-}sec}$		2.518×10^{15}	2.514×10^{15} [e]
	$e_1 = 0.22\%$[f]	$e_2 = 0.47\%$	$e_3 = 0.16\%$

[a] Reference 47

[b] I_1 and I_2 of Ref. 47 multiplied by $e^{-D_1/kT}$ to adjust energy zero to that of this work. D_1 is the Morse well depth for I-I

[c] This work

[d] I_1 Eq. (2-74)

[e] $K'(600)$ Eq. (2-71)

[f] Rel. error, e_1, e_2, e_3 of I_2, I_1, and $K'(T)$ respectively work of Ref. 47 taken as the correct results

If one evaluates the variational rate coefficient for the case of A = 1.0, B = 0.0, and C = R_t for very large R_t, I_1 from Eq. (2-77) goes into the form,

$$I_1 = 2\ I_2 \ . \tag{3-2}$$

The integration has been done for the (H, I_2) system at 600 K the result is,

$$I_1 = 2.00034\ I_2 \ , \tag{3-3}$$

with R_t = 16.0 au.

The definition of the Reimann sum (68) of f defined and continuous over a rectangle R described by $a \leq x \leq b$ and $c \leq y \leq d$ is,

$$S(N,\ f,\ \{p_{ij}\}) = \sum_{i=0}^{n-1} \sum_{j=0}^{m-1} f(p_{ij})\ \Delta x_i\ \Delta y_j \ , \tag{3-4}$$

where p_{ij} is the point (x_i, y_j), $\Delta x_i\ \Delta y_j$ is the area of the subrectangle R_{ij} containing p_{ij} and N is the grid partitioning R. As the grid N is made finer, the diagonal length d(N) of the largest of the R_{ij} decreases, and as $d(N) \to 0$ the value of the Reimann sum approaches the value of the integral of f over the rectangle R. The Reimann sum may serve as a method to approximate double integrals. If Δx_i and Δy_j are constant, that is they have the same value for every i and j Eq. (3-4) becomes,

$$S(N,\ f,\ \{p_{ij}\}) = \Delta x\ \Delta y \sum_{i=0}^{n-1} \sum_{j=0}^{m-1} f(x_i,\ y_j), \tag{3-5}$$

that is the area element $A(R_{ij}) = \Delta x\ \Delta y$ may be factored outside the double sum. This double sum is of the same form as S_{nm} of Eq. (2-79). A value for S_{nm} has been computed for n = m = 250, A = 0.56, B = 0.95, and C = -0.25 at a temperature of 900 K for the (H, H_2) system the results are compared with I_1 evaluated by the five-point Newton Cotes procedure in Table VIII.

TABLE VIII

COMPARISON OF I_1 AND S_{nm}[a]

Quantity	Numerical Result
I_1[b]	8.892371×10^{-3}
S_{nm}[c]	15.35830
$\Delta\theta\ \Delta V$[d]	5.788712×10^{-4}
$\Delta\theta\ \Delta V\ S_{nm}$	8.890477×10^{-3}

[a] (H, H_2) system, T = 900 K, A = 0.56, B = 0.95, and C = -0.25

[b] Five-point Newton Cotes quadrature

[c] Eq. (2-79), n = m = 250

[d] $\Delta\theta$ and ΔV obtained from upper and lower limits on θ and V integrals divided by 249 the number of intervals, upper and lower limits on θ and V integrals are 0.0, 3.14159, 0.26316 and 11.68750 respectively

The search for local minima of $K'(A, B, C, T)$ was carried out by a numerical grid search, where values of $K'(A_i, B_j, C_k, T)$ were computed at each grid point (A_i, B_j, C_k). The boundaries of the A, B, C grid were defined as $0.2 \leq A \leq 1.1$, $0.2 \leq B \leq 1.1$ with C taking values of -0.30, -0.25, -0.20, 0.0, and 0.25. The mesh of the grid in the A-B plane for a fixed value of C is given by $A_{i+1} - A_i = 0.1$ and $B_{j+1} - B_j = 0.1$. Some numerically computed values of $K'(A,B,C,T)$ for the (H, H_2) system at 900 K are given in Table IX. Variational rate coefficients computed for these grid points are arranged from the maximum found for each value of C_k to the minimum with a few intermediate values. A numerical grid search of 500 computed values of $K'(A, B, C, T)$ reveals a minimum for (A, B, C) = (0.60, 1.00, -0.25). Taking a finer mesh of the grid about the region (A, B, C) = (0.60, 1.00, -0.25) produced the last value listed in Table IX, $K'(0.56, 0.95, -0.25, 900) = 2.3340 \times 10^{11}$ cm^3/mole-sec. Further refinement of the grid possibly would yield lower variational rate coefficients. However, the reduction in mesh size only produced a change in the third significant digit of the computed variational rate coefficient, and it is entirely possible that other values of C_k would yield lower variational rate coefficients. A more detailed search of this grid would soon become prohibitive for practical computer time requirements, and would, in essence, defeat the purpose of the entire procedure. In addition a comparison of $K'(0.56, 0.95, -0.25, 900)$ with the CT rate coefficient listed in Table V shows $K(900) = 1.8462 \times 10^{11}$ cm^3/mole-sec, which shows the variational rate coefficient is certainly an upper bound to

TABLE IX

COMPUTED VALUES OF K (A, B, C, T) FOR THE (H, H_2) SYSTEM AT 900 K

A	B	C	K′(A, B, C, T) $\frac{cm^3}{mole\text{-}sec}$ [a]
0.20	1.10	-0.30	6.2726×10^{15}
0.30	1.10	-0.30	8.3245×10^{14}
0.30	0.30	-0.30	3.5766×10^{14}
0.30	0.40	-0.30	2.5293×10^{13}
0.30	0.50	-0.30	1.0740×10^{12}
0.30	0.60	-0.30	2.3422×10^{11}
0.20	1.10	-0.25	7.0765×10^{15}
0.60	0.50	-0.25	2.9754×10^{14}
0.60	0.60	-0.25	1.4283×10^{14}
0.60	0.70	-0.25	1.7062×10^{13}
0.60	0.80	-0.25	2.1503×10^{12}
0.60	0.90	-0.25	4.4133×10^{11}
0.60	1.00	-0.25	2.3402×10^{11}
0.20	1.10	-0.20	7.7925×10^{15}
0.20	0.90	-0.20	3.1929×10^{15}
0.20	0.70	-0.20	5.5506×10^{14}
0.20	0.60	-0.20	8.9066×10^{13}
0.20	0.50	-0.20	3.6467×10^{12}
0.20	0.40	-0.20	2.3422×10^{11}
0.20	1.10	0.0	1.0779×10^{16}
0.70	0.60	0.0	2.3485×10^{14}

TABLE IX (Continued)

A	B	C	K′(A, B, C, T) $\frac{cm^3}{mole\text{-}sec}$ [a]
0.70	0.70	0.0	2.3656×10^{13}
0.70	0.80	0.0	2.5119×10^{12}
0.70	0.90	0.0	4.6623×10^{11}
0.70	1.00	0.0	2.3697×10^{11}
0.20	1.10	0.25	1.4838×10^{16}
0.80	0.60	0.25	3.5957×10^{14}
0.80	0.70	0.25	3.5206×10^{13}
0.80	0.80	0.25	3.0535×10^{12}
0.80	0.90	0.25	5.0144×10^{11}
0.80	1.00	0.25	2.4263×10^{11}
0.56	0.95	-0.25	2.3340×10^{11} [b]

[a] Eq. (2-71) with I_1 and I_2 from Eq. (2-74)

[b] Fine mesh grid search C = -0.25, $0.55 \leq A \leq 0.65$, $0.95 \leq B \leq 1.05$, mesh: $A_{i+1} - A_i = 0.01$, $B_{j+1} - B_j = 0.01$

K(900) as it should be according to Keck (22), but it is still within reasonable agreement with K(900). In fact, K´(0.56, 0.95, -0.25, 900) $\sim$ 1.26 K(900).

In order to qualitatively examine the variation of K´(A, B, C, T) with respect to the parameters A, B, and C one may inspect the projection of S onto the potential $\nu(r, R, \theta)$. This is equivalent to following the integration path I_1 of Eq. (2-74) assumes along the curve S = 0, for different choices of A, B, and C. To implement this procedure contour maps of $\nu(r, R, \theta)$ were plotted for fixed θ with S of the form,

$$r = \frac{A}{B} R - \frac{C}{B} . \qquad (3-6)$$

These coordinates are shown in Figure 4.

Projections of S onto the (r, R) plane for (A, B, C) = (0.56, 0.95, -0.25) are shown for $\theta = \pi/3, \pi/2, 3\pi/4$, and π in Figures 5-8. This (A, B, C) triple produced the smallest computed variational rate coefficient. In addition, projections of S onto these contour maps are shown for other choices of (A, B, C) in Figures 9-13.

Figures 5-8 correspond to the smallest computed value of the variational rate coefficient while Figures 9(b), 11(a) and 12(a) correspond to the smallest variational rate coefficients computed for C = -0.25, 0.0, and 0.25 respectively from the initial grid search. The integration path for I_1 described by S = 0 shown in the figures is cut off at $r = r_{m1} = 4.50$ au, which is adequate to include the important contributions of the integrand of I_1. Mathematically speaking, one wishes to minimize K´(A, B, C, T), which is strongly dependent on

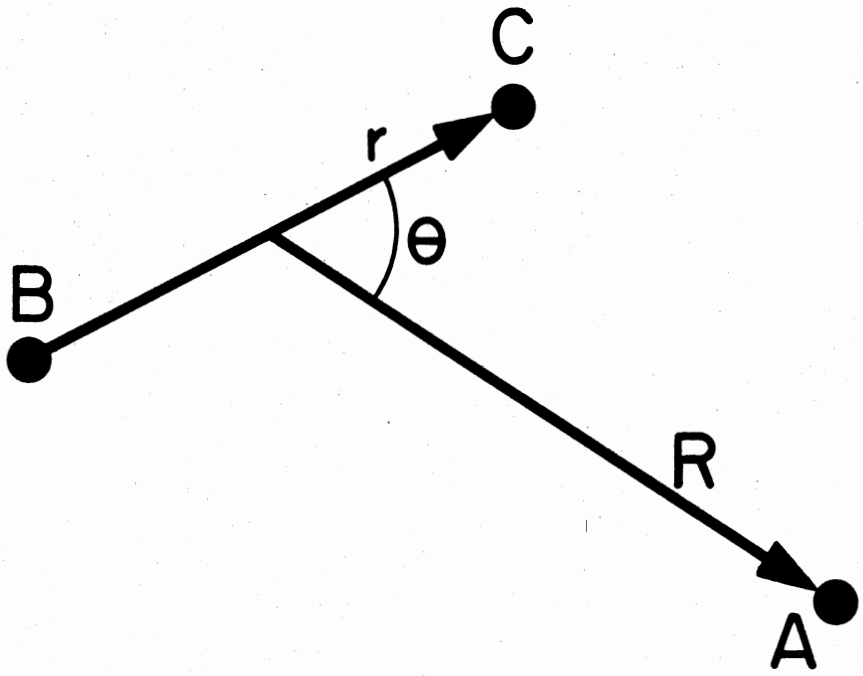

Figure 4. Coordinate System Employed to Plot Contours of $\nu(r,R,\theta)$ with the Projection of S onto the r-R plane, r is the Radial B-C Vector, R is the Radial Vector from the B-C Center of Mass to Atom A, and θ is the Angle Between r and R

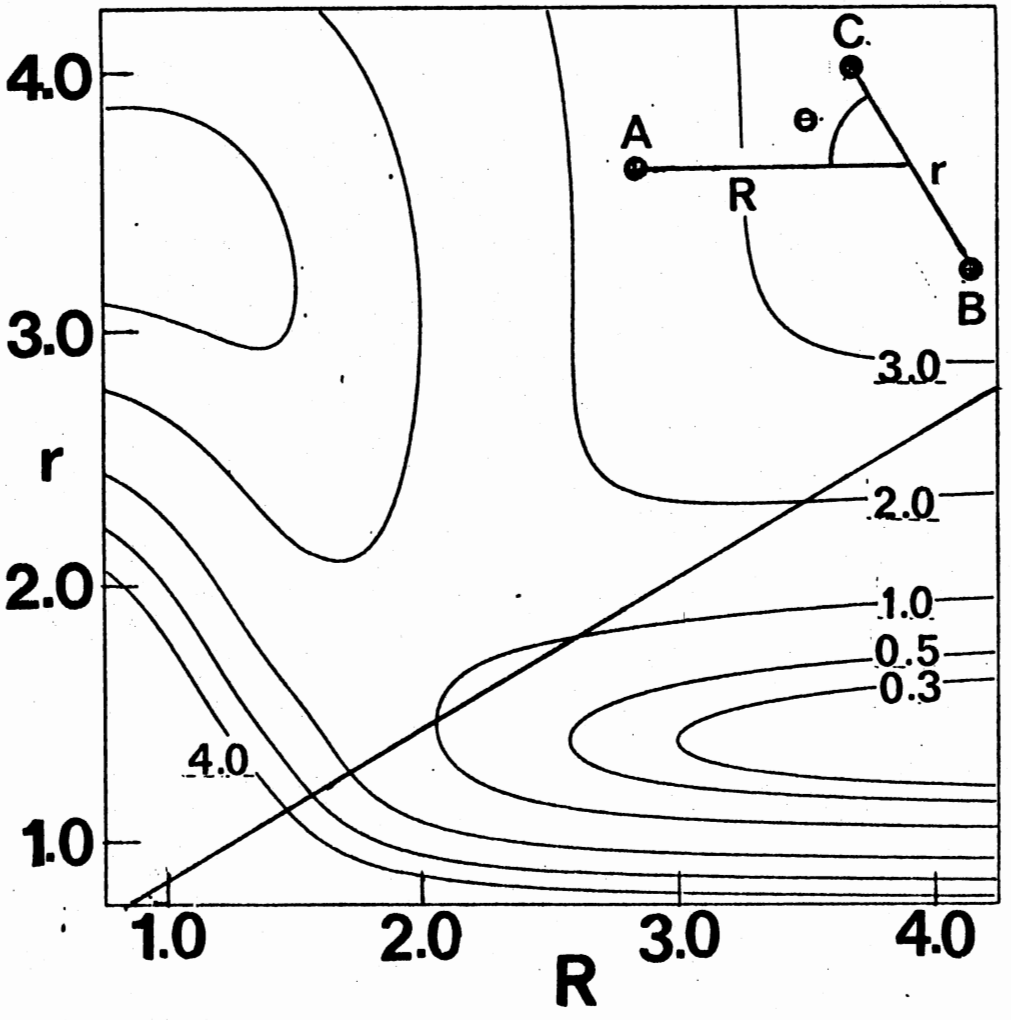

Figure 5. Projection of S onto the (r,R) Plane, A = 0.56, B = 0.95, C = -0.25, $\theta = \pi/3$, Potential Contours are in eV Referenced to H + H_2 at Infinite Separation as the Zero of Energy r and R in Atomic Units

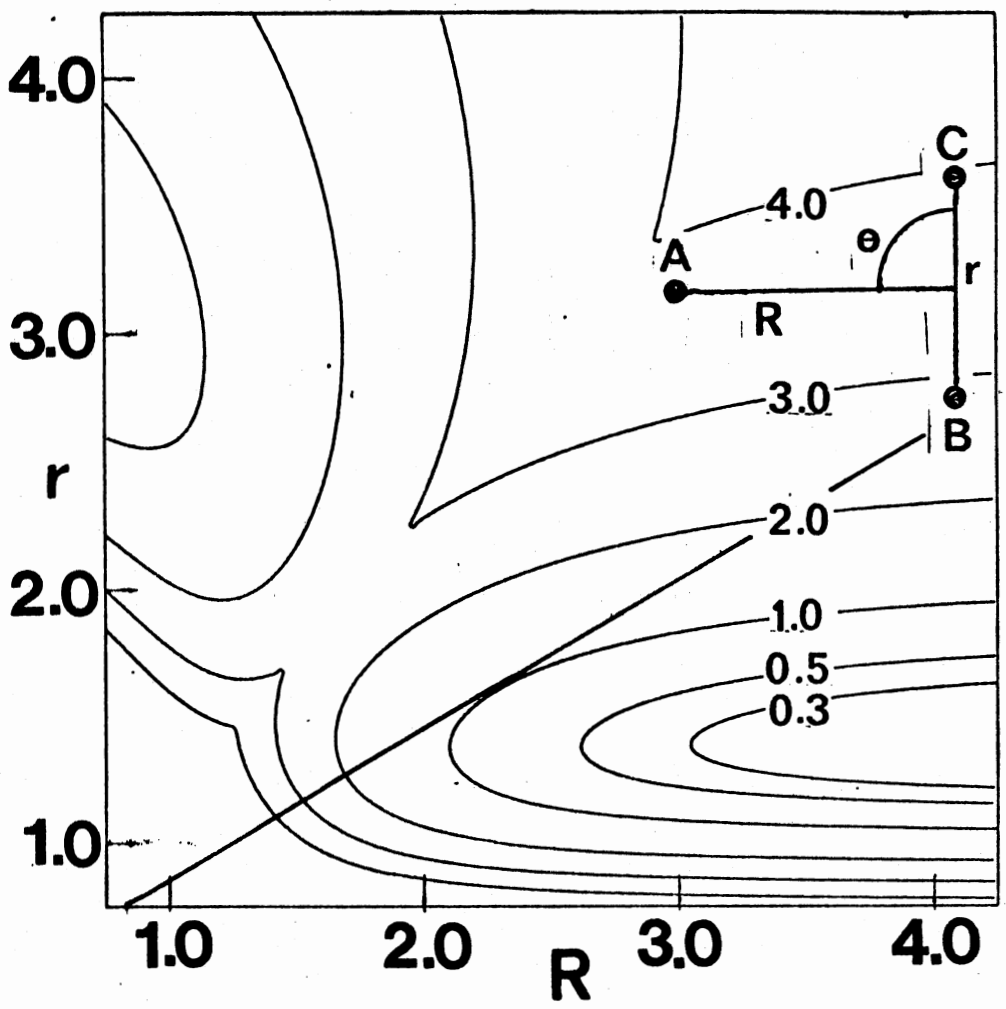

Figure 6. Projection of S onto the (r,R) Plane, A = 0.56, B = 0.95, C = -0.25, $\theta = \pi/2$, Potential Contours are in eV Referenced to H + H_2 at Infinite Separation as the Zero of Energy, r and R in Atomic Units

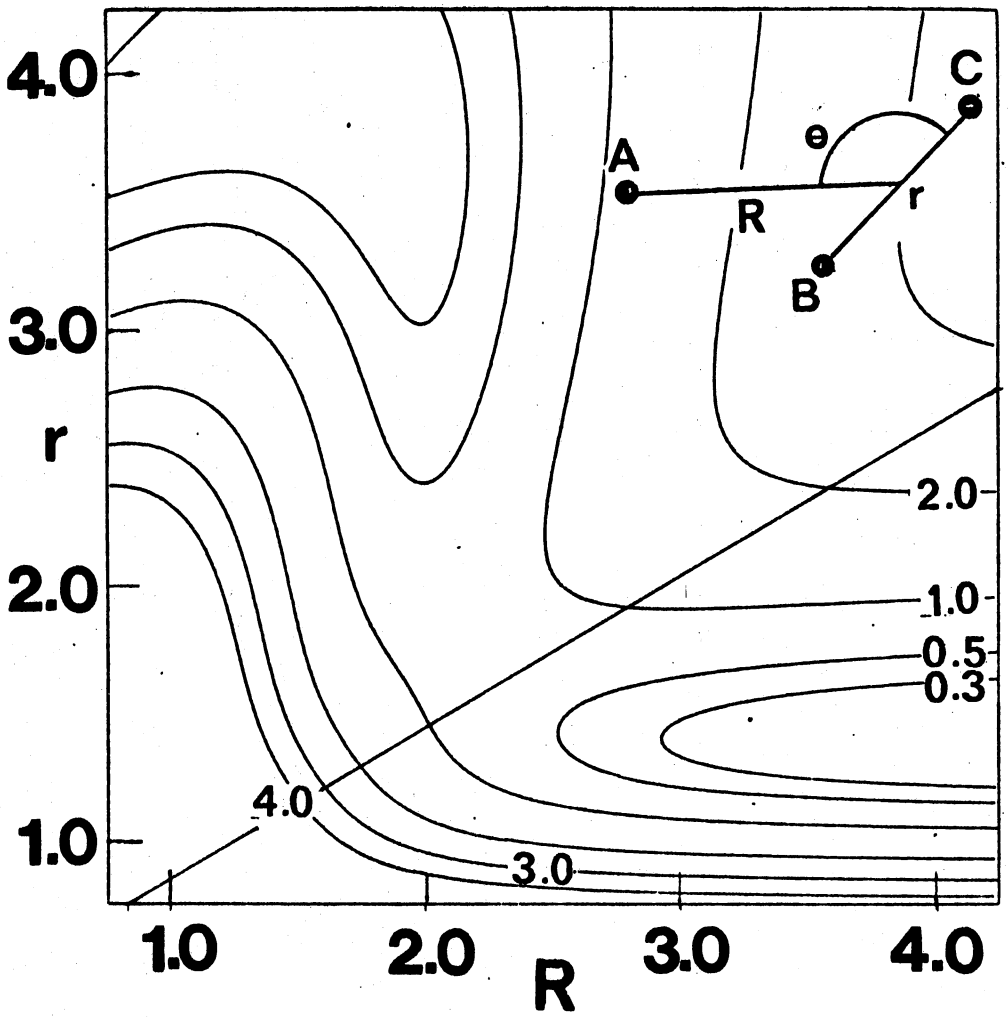

Figure 7. Projection of S onto the (r,R) Plane, A = 0.56, B = 0.95, C = -0.25, $\theta = 3\pi/4$, Potential Contours are in eV Referenced to H + H_2 at Infinite Separation as the Zero of Energy, r and R in Atomic Units

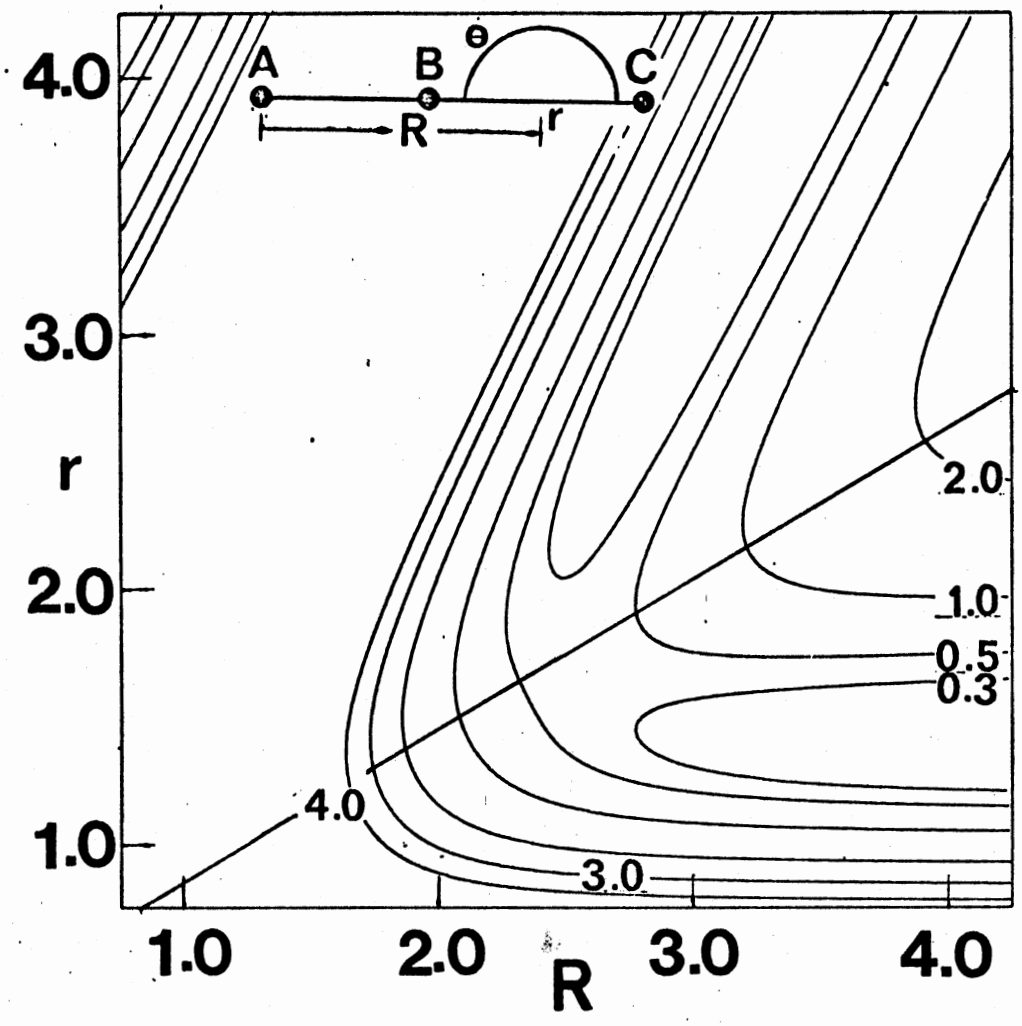

Figure 8. Projection of S onto the (r,R) Plane, A = 0.56, B = 0.95, C = -0.25, $\theta = \pi$, Potential Contours are in eV Referenced to H + H_2 at Infinite Separation as the Zero of Energy, r and R in Atomic Units

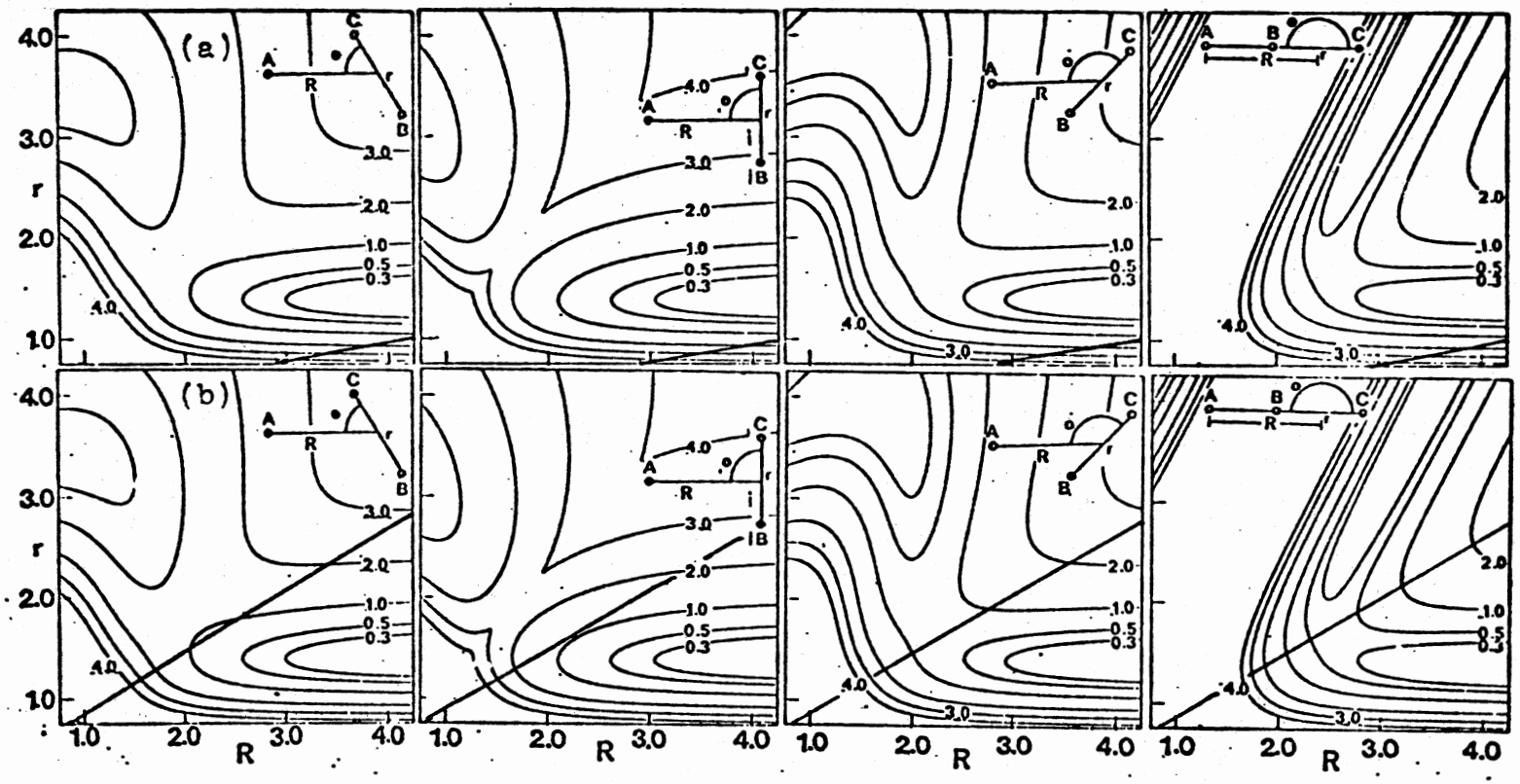

(a) A = 0.20, B = 1.10, C = -0.25
(b) A = 0.60, B = 1.00, C = -0.25

Figure 9. Projection of S onto the (r,R) Plane for the (H, H_2) System, Same as Figures 5, 6, 7, and 8, θ Follows Same Sequence from Left to Right as it Does in Figures 5-8

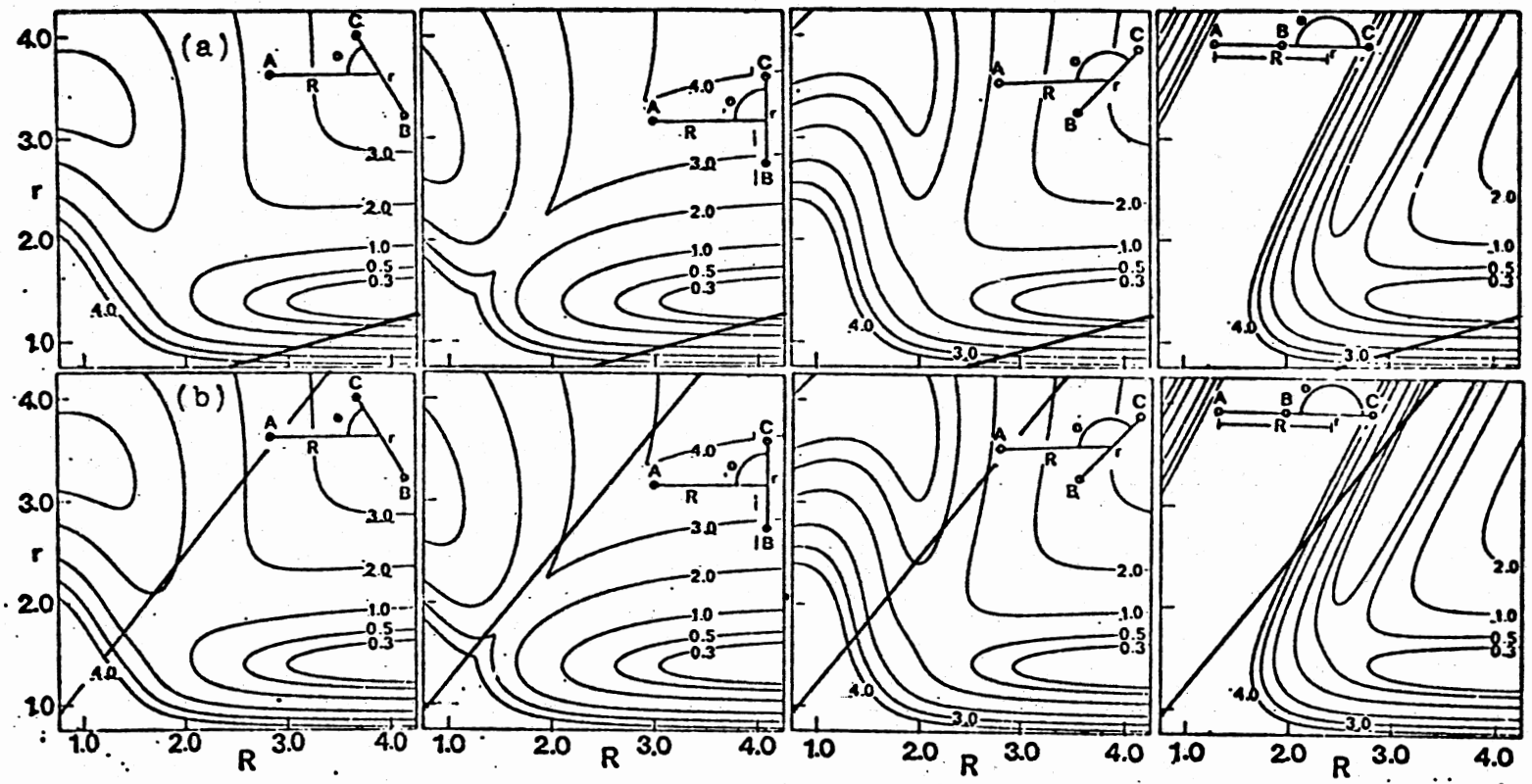

(a) A = 0.30, B = 1.00, C = 0.0, $K'(900) = 1.4025 \times 10^{15}$ cm^3/mole-sec.
(b) A = 1.00, B = 0.80, C = 0.0, $K'(900) = 3.9102 \times 10^{14}$ cm^3/mole-sec.

Figure 10. Projection of S onto the (r,R) Plane for the (H, H_2) System, Same as Figures 5, 6, 7, and 8, θ Follows Same Sequence from Left to Right as it Does in Figures 5-8

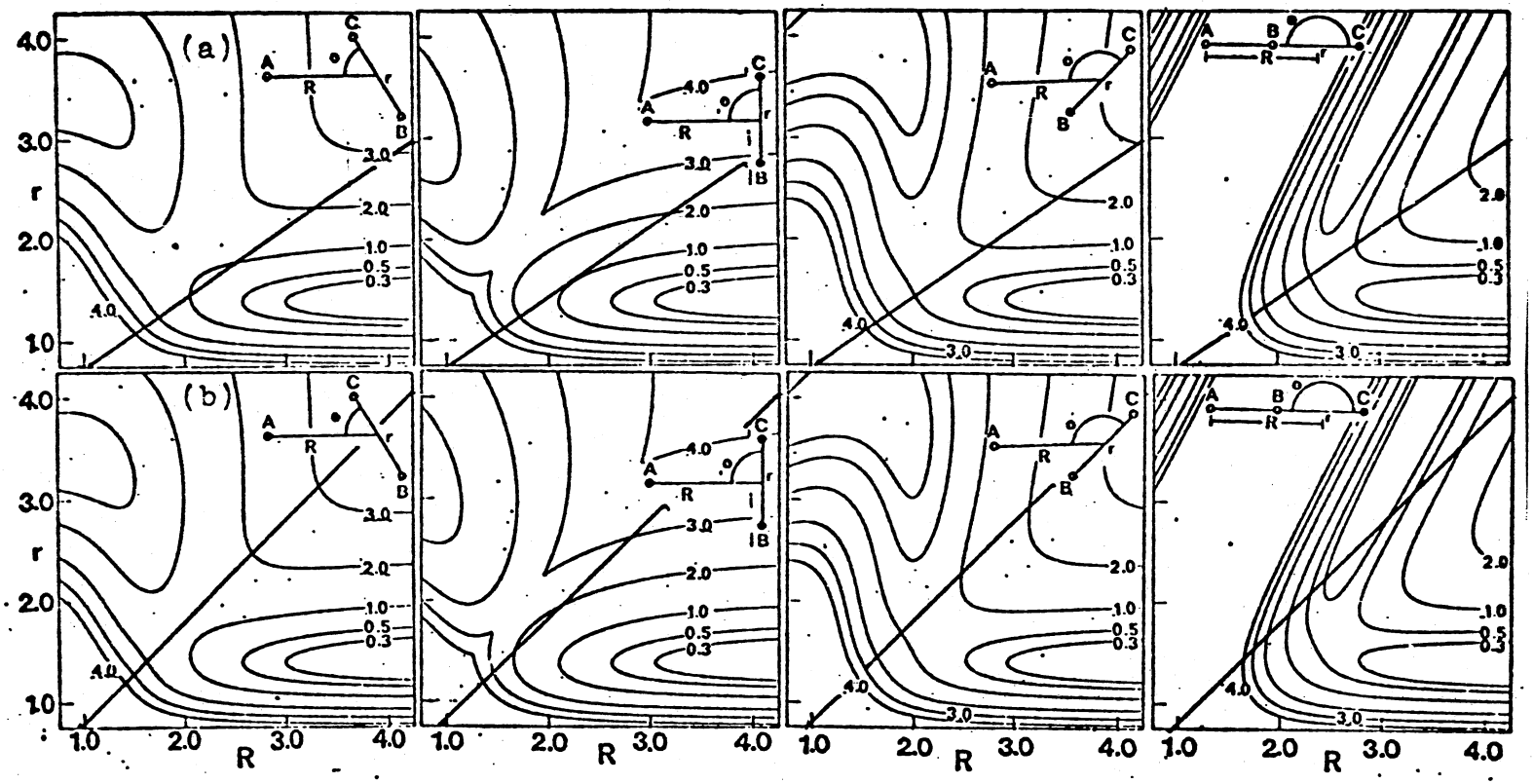

(a) A = 0.70, B = 1.00, C = 0.0
(b) A = 0.80, B = 0.70, C = 0.25

Figure 11. Projection of S onto the (r,R) Plane for the (H, H_2) System, Same as Figures 5-8, θ Follows Same Sequence from Left to Right as it Does in Figures 5-8

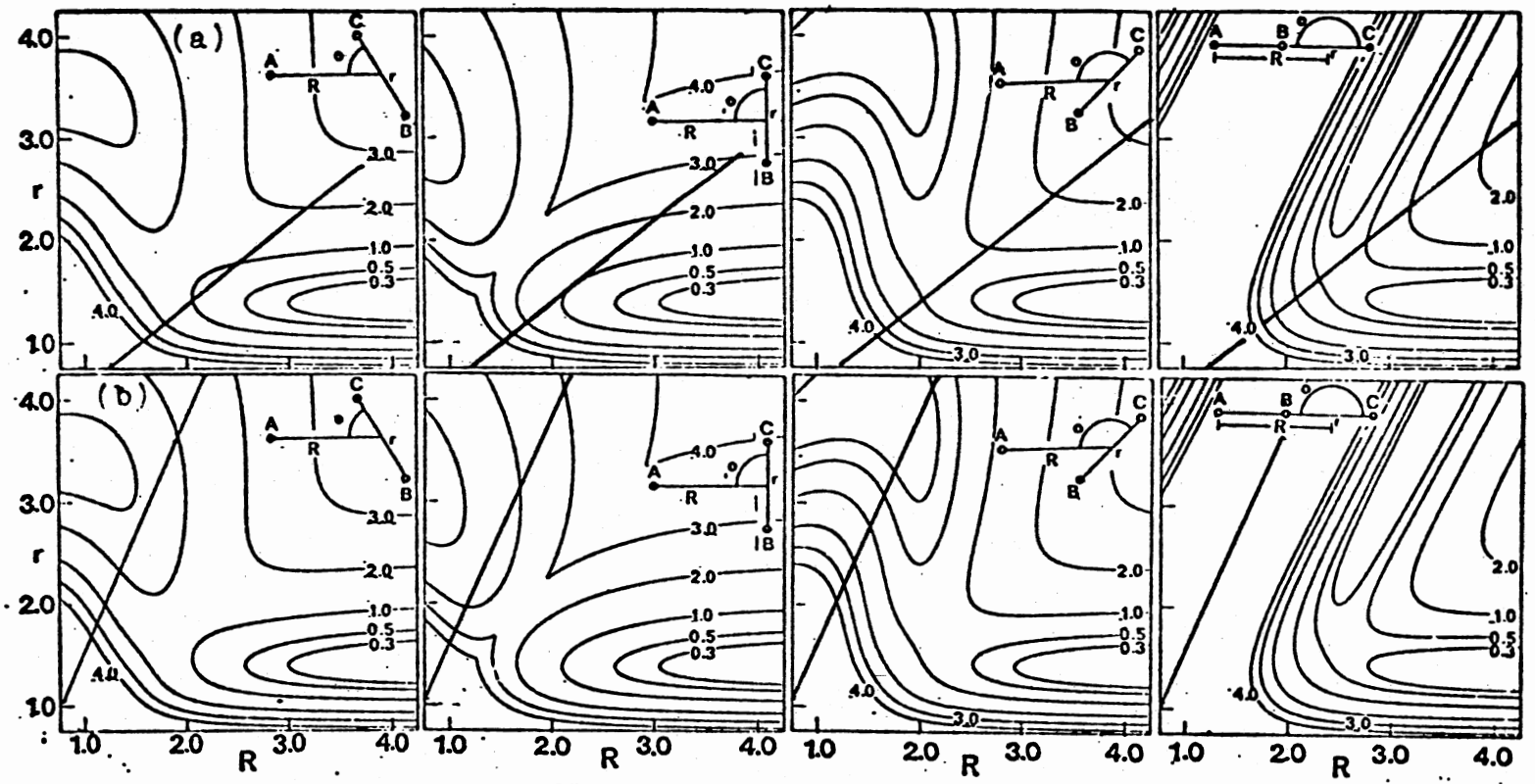

(a) A = 0.80, B = 1.00, C = 0.25
(b) A = 0.90, B = 0.40, C = 0.25, $K'(900) = 8.1804 \times 10^{13}$ cm^3/mole-sec.

Figure 12. Projection of S onto the (r,R) Plane for the (H, H_2) System, Same as Figures 5-8, θ Follows Same Sequence from Left to Right as it Does in Figures 5-8

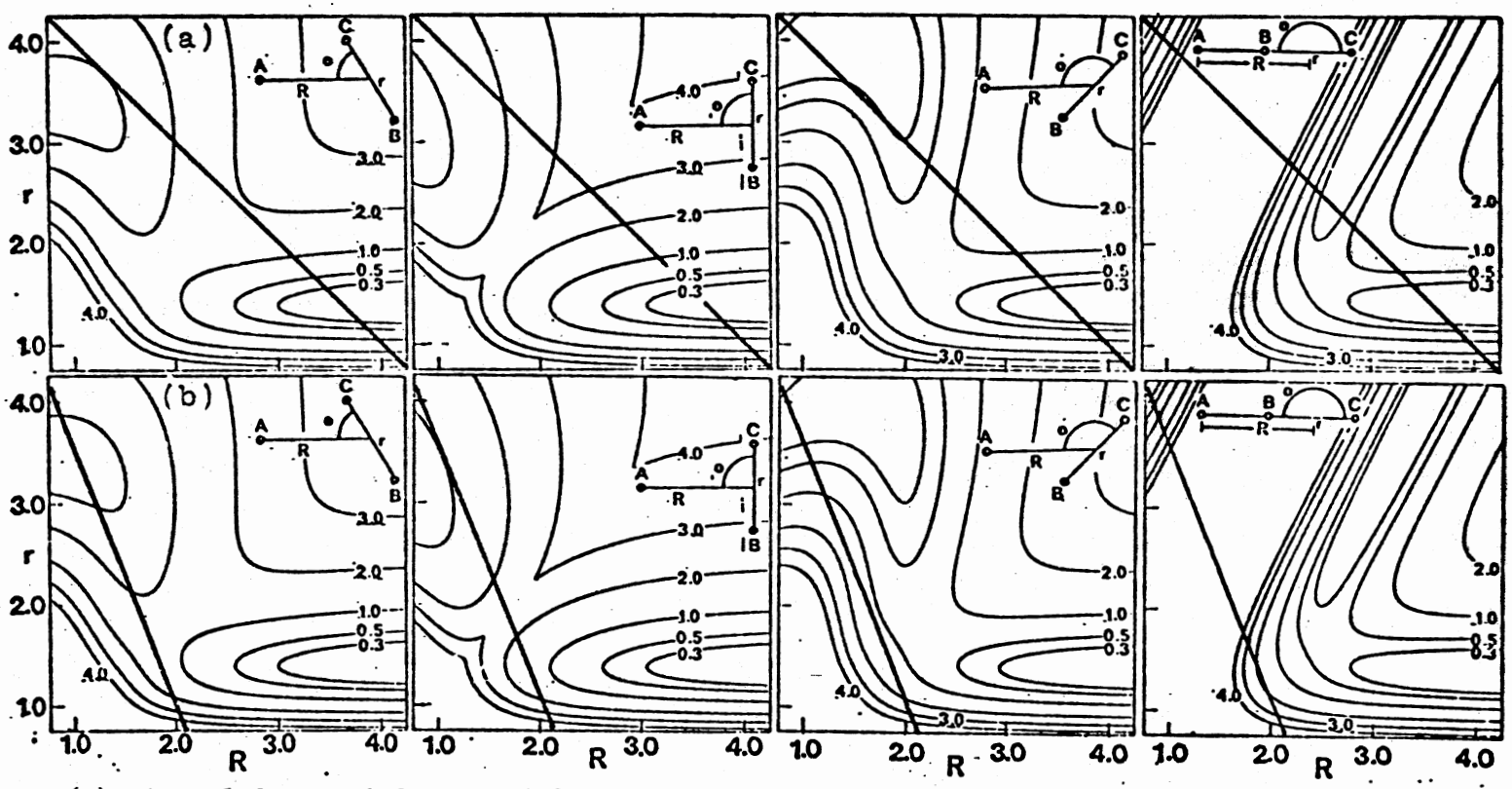

(a) A = -1.0, B = 1.0, C = -5.0
(b) A = -1.0, B = 0.4, C = -2.4

Figure 13. Projection of S onto the (r,R) Plane for the (H, H_2) System, Same as Figures 5-8, θ Follows Same Sequence from Left to Right as it Does in Figures 5-8

the value of I_1. The integrand of I_1 given in Eq. (2-74) is seen to depend strongly on the potential sampled by the integration path S = 0. An examination of the potential contours crossed by the projection of S onto the (r, R) plane in Figures 5-8, 9(b), 11(a), and 12(a) shows that S does cross high-energy regions of the potential-energy surfaces for different values of θ, particularly in the vicinity of the reaction path, where the important contributions to I_1 occur. Conversely, an inspection of Figures 9(a), 10(a), 11(b), and 12(b) shows S traversing regions of low energy, in particular Figure 9(a) shows S far out in the entrance valley, one of the lowest-energy regions of the potential surface.

A more pleasing interpretation of the variational rate coefficient may be obtained by discussing it in terms of "a flow of phase-space points across S", as described by Keck (22). According to this description, the variational rate coefficient becomes the flux of phase-space points across S. The parallelism between the flux analogy of the variational rate coefficient and collision theory is clear if one chooses S far out in the reactant valley. In such a case, the limiting form of the variational rate coefficient (flux across S) becomes the collision frequency. In order to investigate the flux for reactive processes, one must choose S so that it divides the phase space of the system into a reactant region and a product region. The flow of phase points traversing S from the reactant region to the product region of phase space will be an upper bound to the classical reaction rate coefficient if S is chosen properly. Proper choices of S have

been discussed by Keck (22) and Wigner (10). In essence, S must be chosen so that it has no wrinkles or holes. For instance, consider a trajectory that originates in the reactant region of phase space and terminates in the product region of phase space. If it traverses S in the vicinity of a wrinkle, the trajectory of the phase point could cross S more than once. This would correspond to counting the same trajectory more than once for its contribution to the flux. If it traverses S in a region of phase space where there is a hole, it might not cross S at all, and would make no contribution to the flux across S in the product direction. Choices of S that lead to multiple counting or complete neglect of a trajectory originating in the reactant phase space and terminating in the product region of phase space should be avoided. The motivating idea behind the variational study is to locate S in a region of phase space, where the density of reactive trajectories is largest. That is, S is located in a region of phase space where trajectories originating in the reactant phase space that are unable to reach the product phase space do not reach S. The flux also includes trajectories that reach S from the product region of phase space and are counted on the return trip to the product phase space. It is also possible a trajectory from either the product or reactant region of phase space may reach S recross it many times and go off in either direction. Each crossing of S toward the product region of phase space contributes to the flux.

The previous discussion indicates a proper choice of S for reactive processes is in a region of phase space that is inaccessible to

nonreactive trajectories. The (H, H_2) system has an energy barrier to reaction.

In order for a trajectory to be reactive, it must possess sufficient energy to traverse the barrier. Any trajectory not satisfying this requirement, whether approaching S from the product or reactant region of phase space, will turn back to its original region of phase space. It seems evident from the previous discussion that a good location for S is across the reaction path and as near the region of phase space that contains the top of the energy barrier as possible. It was considerations such as these that led to the concept of a "transition-state" at the top of the barrier.

Perhaps a qualitative illustration of the ideas discussed above may be obtained from the figures showing the projections of S onto the (r, R) plane. Figures 5-8, 9(a), 9(b), 10(a), 11(a), 11(b), and 12(a) show surfaces S that divide the system phase space into two different regions. However, the surfaces S shown in Figures 9(a) and 10(a) will be poor choices since trajectories crossing S in the forward direction still must traverse a 9 kcal/mole barrier to reach the product region of phase space. The majority of these trajectories return to the reactant region of phase space. Consequently, when S is located in this region of phase space, the density of phase points that possess the ability to cross S in the forward direction is very large. In fact, all reactive and nonreactive trajectories must cross this dividing surface. As a result, very large flux values are obtained for these particular choices of S. K´(0.30, 1.00, 0.0, 900) is given in Figure 10 and K´(0.20, 1.10, -0.25, 900) is given in Table IX. The choices of S shown in Figure 11(b) is beginning to resemble a

desirable choice of S, however, at the $\theta = \pi$ projection of the potential surface, one finds that trajectories originating from the product region of phase space that turn back recross S in the forward direction on the return trip. An examination of Table IX shows the flux computed for this particular S is easily two orders of magnitude larger than the lowest computed estimate of the reactive flux for C = 0.25. Examples of choices of S with holes that are only crossed once or not at all by phase-space points successfully completing the path from reactant to product phase space are shown in Figures 10(b) and 12(b). This is particularly noticeable for the surface on the $\theta = \pi$ map. Figure 10(b) shows S far out in the product region of phase space. Since, S is cut-off at r = 4.5 au, many reactive trajectories could reach the product region of phase space without ever crossing S. Figure 12(b) clearly shows a bad choice of S particularly for the $\theta = \pi$ map. S is situated on top of a ridge that is at least 180 eV above the zero of energy, this region of phase space is never sampled by any phase point at thermal energies. Any phase point that successfully travels the path from reactant to product regions of phase space near or on the $\theta = \pi$ projection of the potential-energy map will contribute nothing to the flux. One might call a dividing surface S of this type a "leaky surface". Figure 13 is another illustration of poor choices of S. For example, most reactive trajectories crossing the surface S shown in Figure 13(a) must cross S twice to reach the product region of phase space. This is an example of the "multiple crossings" of S mentioned earlier. Figure 13(b) is similar to 13(a) except that it is a "leaky surface". Any reactive trajectory that does reach S could cross S twice before it reaches the product region of phase

space. However, most reactive trajectories will never reach S at all, especially those that travel the minimum energy paths. The multiple crossing surfaces shown here result from a choice of $A < 0$, so for potential-energy surfaces resembling those of the (H, H_2) system choices of A or $B < 0$ should be avoided. In addition, Figures 5-8, 9(b), 11(a), and 12(a) all seem to represent good or "proper" choices of S in the sense that S crosses the reaction path near the high energy regions. These surfaces are in regions of phase space that are mostly inaccessible to nonreactive trajectories.

Examining the projections of S in Figures 5-8, one finds S does traverse high energy regions of the potential surface. However, it always seems to miss the regions of highest energy. A comparison of the variational rate coefficient $K'(0.56, 0.95, -0.25, 900)$ to $K(900)$ computed from CT trajectories of method II show the variational rate coefficient is about 20% larger. The problem seems to be that S does not depend on θ. It is easily seen by examining $\nu(r, R, \theta)$ for different values of θ, that the potential barrier in the reaction path shifts for different values of θ. The present formulation of the variational rate coefficient shows S has no way to compensate for this shifting of the barrier position, with respect to changing θ.

It would be very interesting to see if there was much improvement in the variational rate coefficient if θ was included in the description of S. There is definitely a connection between the degrees of freedom that are important in the description of the potential and the degrees of freedom that are important for the description of a proper choice of S. This appears encouraging enough to state a hypothesis that appears nearly axiomatic:

All degrees of freedom that are important in the description of the potential for a process under study by the variational procedure should be included in the description of S in order for the variational rate coefficient to converge to the true rate coefficient for the process.

The variational procedure has been applied to the (H, H_2) system. The parameters that yield the smallest value for the computed variational rate coefficient are (0.56, 0.95, -0.25). The dividing surface corresponding to this particular (A, B, C) triple was designated S_0. S_0 was then used to compute variational rate coefficients for the (H, H_2) thermal exchange reaction at several other temperatures. The results of these computations are given in Table X.

TABLE X

COMPUTED VARIATIONAL RATE COEFFICIENTS FOR THE (H, H_2) THERMAL EXCHANGE REACTION USING THE DIVIDING SURFACE S_0 [a]

T K	$K'(A, B, C, T)$ $\frac{cm^3}{mole\text{-}sec}$
300	1.8247×10^6
500	1.6804×10^9
700	3.7507×10^{10}
900	2.3340×10^{11}
1100	8.0052×10^{11}

[a] A = 0.56, B = 0.95, C = -0.25

A comparison of the variational rate coefficients with the CT rate coefficients given in Table V shows the variational rate coefficients are upper bounds to the CT rate coefficients computed at temperatures of 300, 500, and 900 K. However, at 1100 K the variational rate coefficient falls within the statistical error bounds of the CT rate coefficient.

The variational procedure has also been applied to the (H, I_2) system. The potential-energy surface employed was obtained from the asymptotic three-body limit of the (H_2, I_2) interaction potential (54). The initial grid search over the A-B plane was carried out in the same fashion as it was for the (H, H_2) system with values of C = -0.20, -0.10, 0.0, and 0.10 with r_{m1} = 7.50 au at a temperature of 600 K. Table XI lists the minimum variational rate coefficient obtained from the grid search for each value of C with the value obtained from the refined grid search as the last entry of Table XI.

TABLE XI

COMPUTED VALUES OF K′(A, B, C, T) FOR THE (H, I_2) SYSTEM AT 600 K

A	B	C	K′(A, B, C, T) $\frac{cm^3}{mole\text{-}sec}$
0.80	1.10	-0.20	2.2385×10^{15}
0.80	1.10	-0.10	2.2220×10^{15}
0.60	0.80	0.0	2.2205×10^{15}
0.60	0.80	0.10	2.2403×10^{15}
0.56	0.75	0.0	2.2170×10^{15} [a]

[a] Result of refined grid search

The (H, I_2) system has very little zero-point energy so the SQCT rate coefficient should be comparable to the CT rate coefficient. The SQCT rate coefficient computed in the previous CPST study is K(600) = 2.12 x 10^{14} cm^3/mole-sec, this corresponds to K'(0.56, 0.75, 0.0, 600) $\sim$ 10.5 K(600). The variational rate coefficient is roughly an order of magnitude greater than the SQCT result.

This result suggests S is located in a region of phase space that is accessible to nonreactive trajectories. The source of the problem may be found from an examination of the projection of S onto the (r, R) plane. These are shown in Figures 14-17.

One feature that is immediately apparent from the projections of S onto the (r, R) plane is that S traverses a region of attractive three-body interaction, a shallow well in the entrance valley. The greatest well depth δ occurs for the $\theta = \pi/2$ surface shown in Figure 15 with $\delta \sim$ -2.1 kcal/mole below the energy zero of separated reactants and reaches its highest value for $\theta = \pi$ with $\delta \sim$ -1.2 kcal/mole shown in Figure 17. In addition, there are small barriers in the entrance valley they are approximately 0.9, 0.7, 0.7 kcal/mole for $\theta = \pi/3$, $3\pi/4$, π respectively, and 16.6 kcal/mole for $\theta = \pi/2$.

It is apparent from Figures 14-17 that there will be virtually no contribution to the flux from phase-space points that originate in the product phase space, cross S, and return since the difference in elevation between stable products and reactants is 36.9 kcal/mole. The average translational energy at 600 K of phase-space points originating in the reactant region of phase space is more than adequate to traverse the barrier except for θ values near $\pi/2$. Although, it

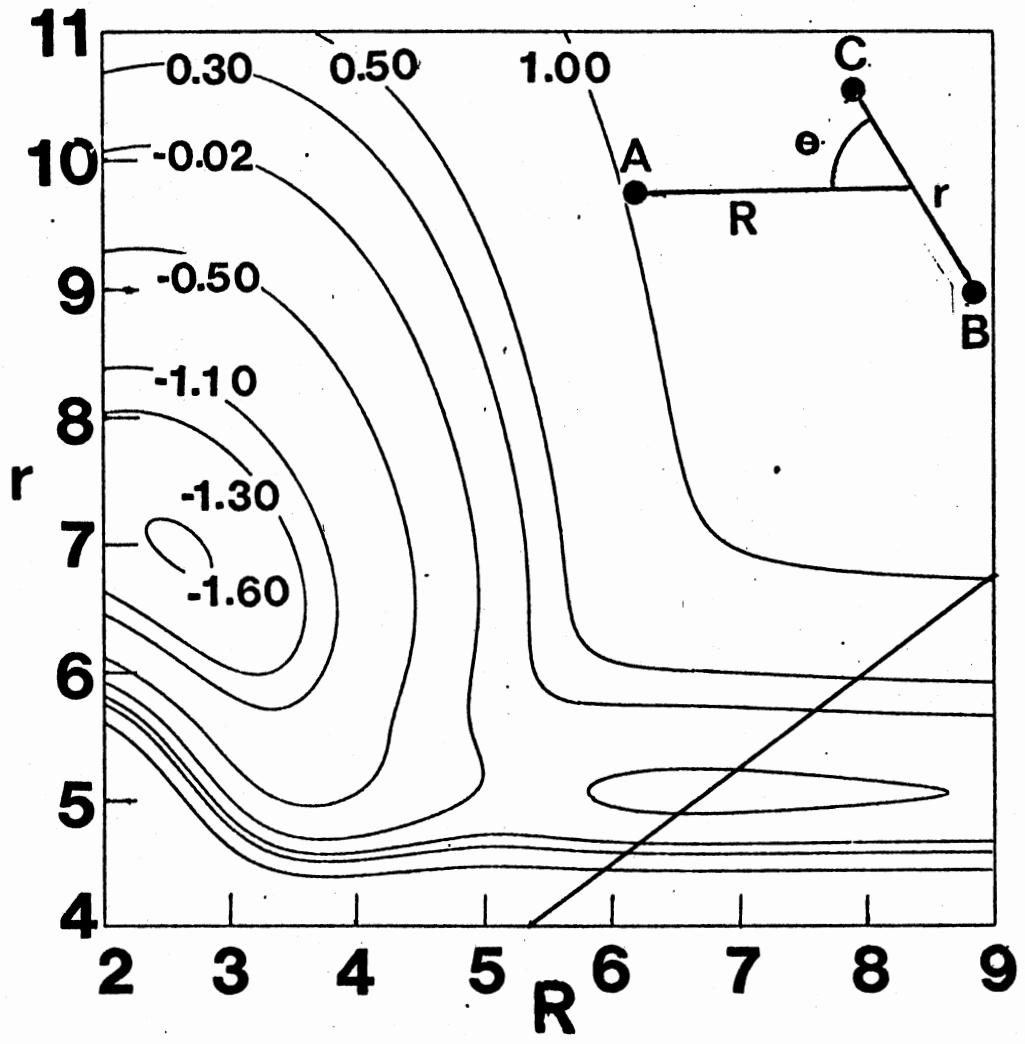

Figure 14. Projection of S onto the (r,R) Plane, A = 0.56, B = 0.75, C = 0.0, $\theta = \pi/3$, Potential Contours are in eV Referenced to H + I_2 at Infinite Separations as the Zero of Energy, r and R in Atomic Units

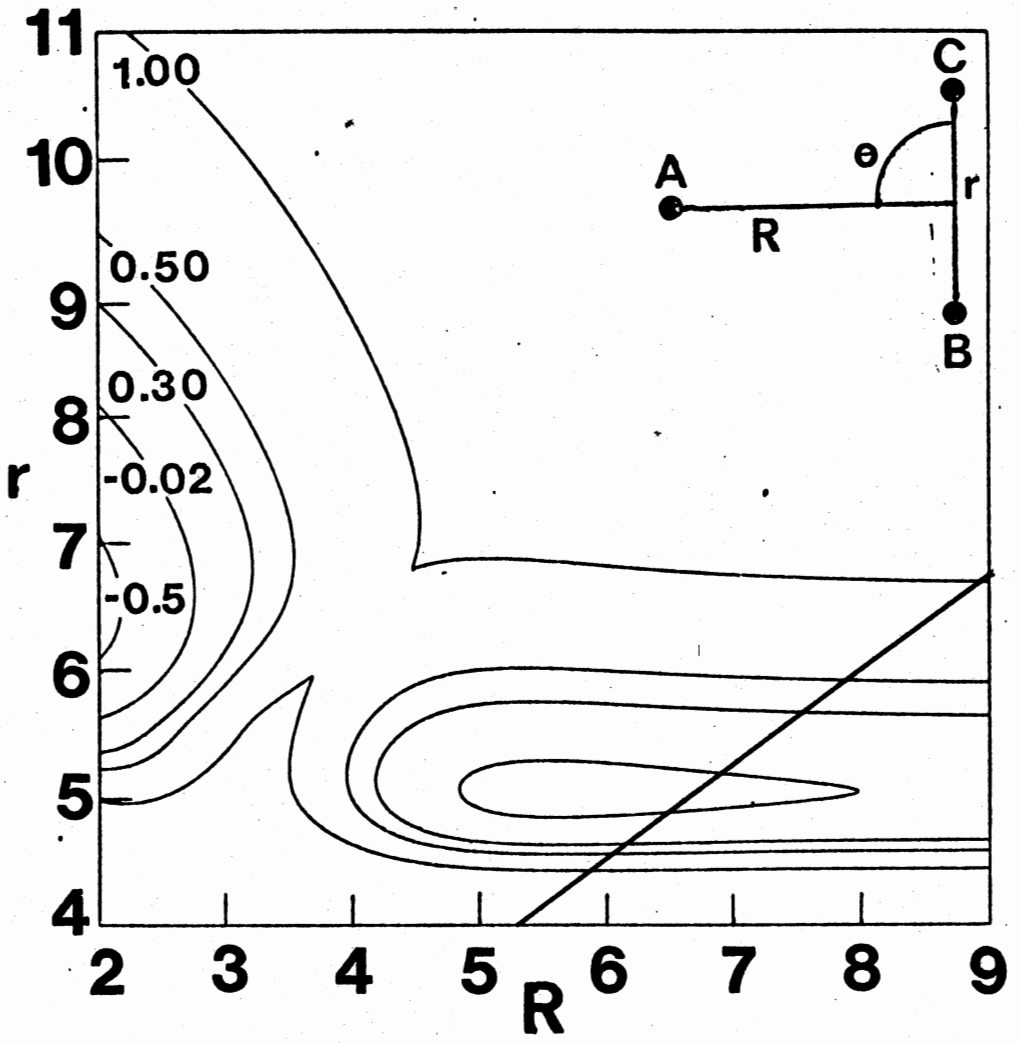

Figure 15. Projection of S onto the (r,R) Plane, A = 0.56, B = 0.75, C = 0.0, $\theta = \pi/2$, Potential Contours are in eV Referenced to H + I_2 at Infinite Separation as the Zero of Energy, r and R in Atomic Units

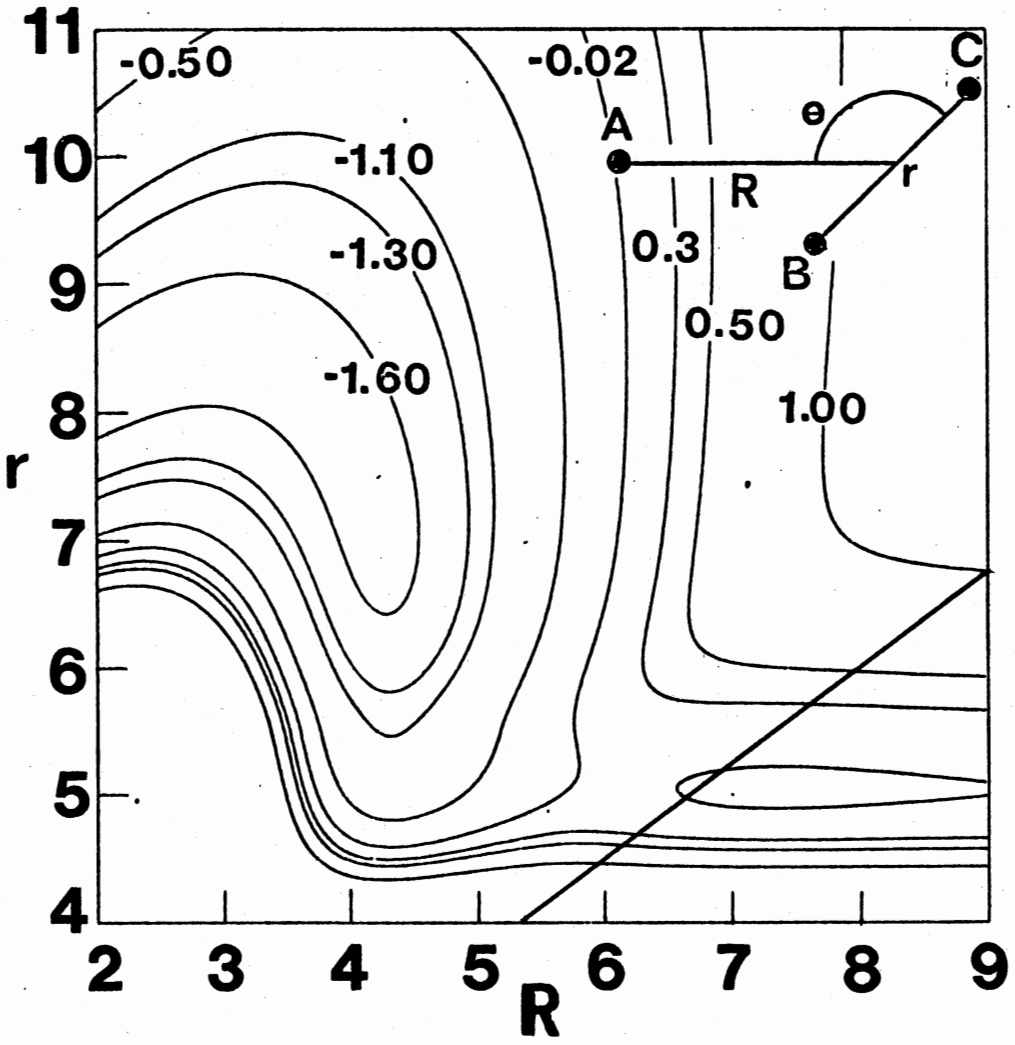

Figure 16. Projection of S onto the (r,R) Plane, A = 0.56, B = 0.75, C = 0.0, $\theta = 3\pi/4$, Potential Contours are in eV Referenced to H + I_2 at Infinite Separation as the Zero of Energy, r and R in Atomic Units

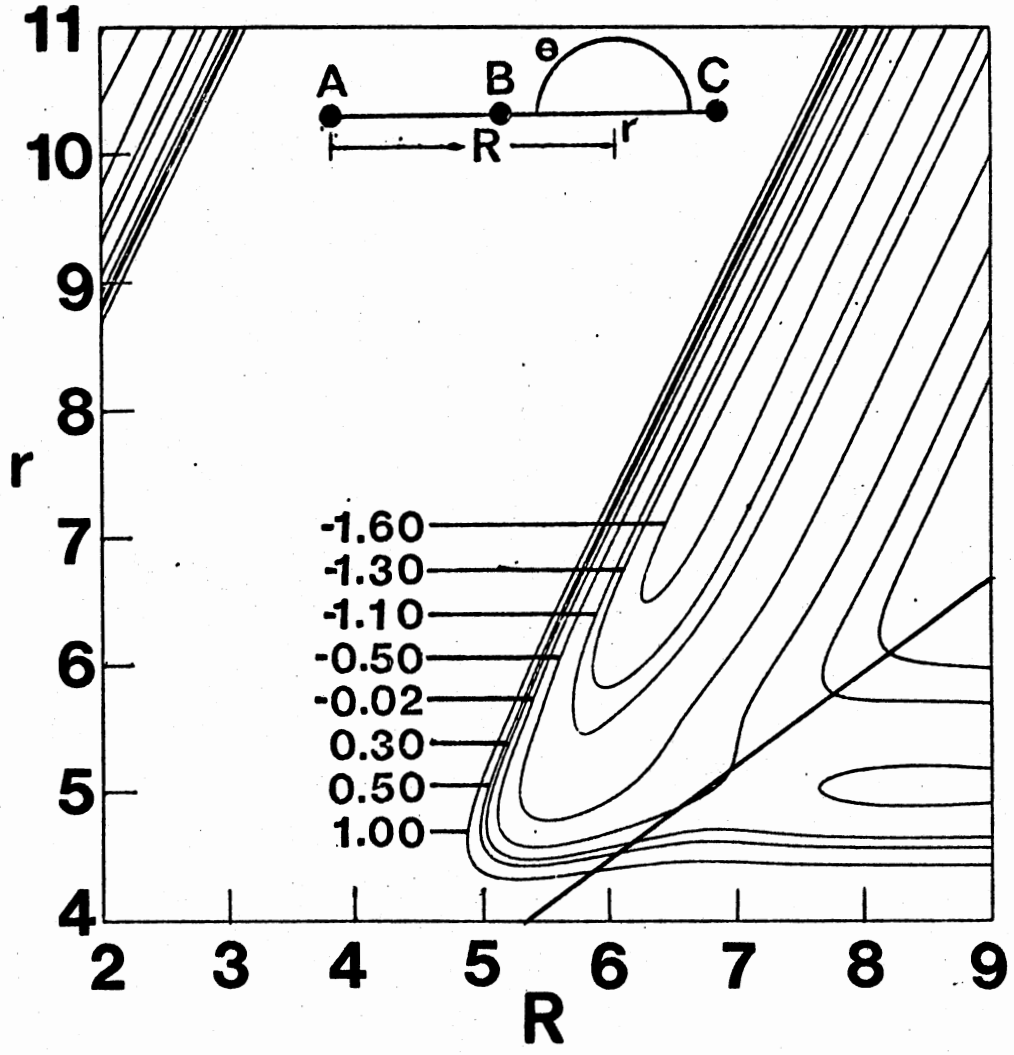

Figure 17. Projection of S onto the (r,R) Plane, A = 0.56, B = 0.75, C = 0.0, $\theta = \pi$, Potential Contours are in eV Referenced to H + I_2 at Infinite Separation as the Zero of Energy, r and R in Atomic Units

appears S must be located near the barrier for $3\pi/4<\theta<\pi$ and $0<\theta<\pi/4$ shown in Figures 16 and 17, for $\pi/4 < \theta < 3\pi/4$ S traverses the well in the entrance valley. Notice this includes the $\theta = \pi/2$ surface. Since the average relative translational energy is 1.77 kT $\sim$ 2.1 kcal/mole, virtually all phase-space points originating in the reactant zone with θ near $\pi/2$ in the vicinity of the barrier will return. An examination of the relative velocity distribution of the (H, I_2) system shown in Figure 8 of reference 47 shows the most probable relative translational energy is about 1.9 kcal/mole at 600 K. Considering barrier heights and relative translational energies alone, it appears that more than half of the phase points originating in the reactant phase space will react, this discussion does not include phase points traveling on potential-energy surfaces where θ is near $\pi/2$ in the vicinity of the barrier. However, all phase points originating in the reactant region of phase space will reach S. Indeed, one would expect the flux to significantly overestimate the true reaction rate coefficient. Although, this is the best result obtained for S described by the degrees of freedom r and R, it appears that S does include substantial regions of phase space that are accessible to nonreactive trajectories originating in the reactant region of phase space.

Once, S_0 was determined with (A, B, C) = (0.56, 0.75, 0.0) variational rate coefficients were evaluated for the (H, I_2) system over the temperature range 300-1100 K. The results are reported in Table XII. In addition, Table XII includes rate coefficients evaluated from Sullivan's (69) experimentally determined temperature fit of the rate coefficient for the (H, I_2) system. The rate coefficient is of

TABLE XII

COMPUTED VARIATIONAL RATE COEFFICIENTS
FOR THE REACTION $H + I_2 \rightarrow HI + I$
USING THE DIVIDING SURFACE
S_0 [a]

T K	K(T) $\frac{cm^3}{mole\text{-}sec}$ [b]	K′(A, B, C, T) $\frac{cm^3}{mole\text{-}sec}$
300	1.73×10^{14}	4.4290×10^{15}
500	2.24×10^{14}	2.4695×10^{15}
600	2.45×10^{14}	2.2167×10^{15}
700	2.65×10^{14}	2.0850×10^{15}
900	3.00×10^{14}	1.9791×10^{15}
1100	3.32×10^{14}	1.9647×10^{15}

[a] A = 0.56, B = 0.75, C = 0.0

[b] Reference 69

the form,

$$K(T) = AT^{\frac{1}{2}} e^{-E_A/kT} , \qquad (3\text{-}6)$$

with $A = 10^{13.0 \pm 0.2}$ and essentially no activation energy. The experimental uncertainty in the frequency factor gives upper and lower bounds of $6.3 \times 10^{12} < A < 1.6 \times 10^{13}$. At low temperatures the experimental rate coefficients show that phase points originating in the reactant zone have a small region of phase space available to follow to the product zone because the majority of these trajectories are of low energy and unable to traverse the small barrier. As the temperature is increased, the phase points begin to populate the regions of higher energy. Hence, more phase points are able to follow trajectories leading to the product phase space. Consequently, one observes an increase in the rate coefficient. However, the variational rate coefficients certainly do not behave in this manner. This flux is a measure of phase points reaching S from the reactant zone with S located in the region of phase space containing the well in the entrance valley.

The most striking feature of the temperature study of the variational rate coefficient is its decrease with respect to temperature. At low temperatures one may think of the phase space points clustered closely together in the region of phase space containing the well in the entrance valley with other phase space points more sparsely distributed in the complementary regions of phase space. That is, there is a high density of systems in this region of phase space. Since S does span this region of phase space, one would expect the flux across S in the product direction to be large. As the temperature is increased,

this low-energy region of phase space becomes less important and the phase-space points are redistributed more sparsely over a much larger region of available phase space. In essence, the phase-space points are spread out over the accessible regions. Now the region of phase space corresponding to the well is not as densely populated. Consequently, the flux across S in the direction of the product region of phase space decreases, and the variational rate coefficients decreases with temperature.

The comparison between Sullivan's experimental results on the (H, I_2) system and the variational rate coefficients is, at best, poor. An examination of the projection of S onto the (r, R) plane shows S does span the well in the entrance valley for certain values of θ. Furthermore, there is no way to avoid this with S being described by the two degrees of freedom, r and R. If one were to include the additional degree of freedom, θ, in the description of S, there might be a substantial improvement in the variational rate coefficients.

Such a study has been done for (H, I_2) system with S defined by,

$$S = AR - Br - D\theta - C = 0 \qquad (3\text{-}7).$$

The derivation of $K'(A, B, C, D, T)$ is given in Appendix C. The final result is:

$$K'(A, B, C, D, T) = \frac{\sqrt{2\pi kT}}{(A+B)} \quad \frac{I_1(A, B, C, D, kT)}{I_2(kT)}, \qquad (3\text{-}8)$$

where,

$$I_1(A, B, C, D, kT) = \int_0^{\pi} \sin\theta \, d\theta \int_{V'}^{V_{ml}} dV \, R^2(\theta,V,C) \, r(\theta,V,C) \, x$$

$$\sqrt{\frac{r^2(\theta,V,C)\, B^2}{\mu} + \frac{D^2}{\mu} + \frac{r^2(\theta,V,C)\, A^2}{\mu_{A,BC}}} \quad x$$

$$e^{-v(r(\theta,V,C),\, R(\theta,V,C),\, \cos\theta)/kT}, \qquad (3\text{-}9)$$

with I_2 given by Eq. (2-74). Notice V' and V_{ml}, both depend upon θ and if A and B are considered positive, V' depends upon the sign of C and D. Another point worth noting is if D = 0, $K'(A, B, C, D, T)$ reduces to $K'(A, B, C, T)$.

An examination of the potential-energy contours for the H + I_2 system suggests that one might expect a substantial improvement in the variational rate using equations (3-8) and (3-9). In Figures 14-17, it is seen the location of S is fixed whereas the potential is a function of θ. During the integration over θ, S traverses low-energy regions of the potential, in particular, the well in the entrance valley. Since the flux is large in such regions, the variational rate is much larger than the reaction rate. This difference will be magnified at lower temperatures.

One may utilize the previous discussion as additional information that may prove helpful in the grid search for local minima of $K'(A,B,C,D,T)$. The (A,B,C) set that yielded the smallest $K'(A,B,C,T)$

will be used as the initial guess for the minimization of K′(A,B,C,D,T) at a temperature of 300 K. Taking advantage of the symmetry of the potential about $\theta = \pi/2$, S is defined as,

$$S = \begin{cases} AR - Br - D\theta - C, & 0 \leq \theta \leq \pi/2 \\ AR - Br - D'\theta - C', & \pi/2 < \theta \leq \pi \end{cases} \quad D' = -D, \; C' = C - D\pi. \qquad (3\text{-}10)$$

An inspection of the contour maps of Figures 14-17 show that the high-energy regions of the potential in the reaction path moves toward smaller R values for $0 \leq \theta \leq \pi/2$. For $\pi/2 < \theta \leq \pi$ this region backtracks toward larger R values. If one rewrites S of Eq. (3-10) in the form,

$$r = \frac{A}{B} R - \frac{D}{B} \theta - \frac{C}{B} , \qquad (3\text{-}11)$$

it is seen that a choice of $D < 0$ for $0 \leq \theta \leq \pi/2$ will increase the r-intercept, which will result in moving S out of the small well in the entrance valley.

Using the initial guess to aid in the grid search, B is fixed at 0.75 while an (A, D) grid is searched for a local minima of K′(A, B, C, D, T) at different values of C. Results of such a grid search for the (H, I_2) system for different values of C are shown in Table XIII with the smallest K′(A, B, C, D, T) computed being the last entry. The projections of S onto the (r, R) plane are shown in Figure 18-21.

An examination of Table XII shows $K(300) = 1.73 \times 10^{14}$ cm^3/mole-sec evaluated from Sullivan's expression Eq. (3-6) for the (H, I_2) thermal exchange reaction. The results listed in Table XIII show that

TABLE XIII

RESULTS OF THE GRID SEARCH OF K′(A, B, C, D, T) FOR THE (H, I_2) SYSTEM AT 300 K [a]

A	C	D	K′(A, B, C, D, T) [b,c]
0.54	0.100	-0.92	5.4037×10^{14}
0.54	0.0	-0.80	1.3943×10^{15}
0.54	-0.100	-0.60	4.1346×10^{15}
0.54	0.100	-0.90	5.6366×10^{14}
0.52	0.200	-1.10	3.0456×10^{14}
0.52	0.175	-1.10	2.6397×10^{14}
0.52	0.125	-1.10	2.4442×10^{14}
0.52	0.150	-1.10	2.4280×10^{14}
0.51	0.150	-1.20	2.0643×10^{14} [d]

[a] B = 0.75

[b] units of K′ are cm^3/mole-sec

[c] K′(A, B, C, D, T) given by Eq. (3-8)

[d] Refined grid search

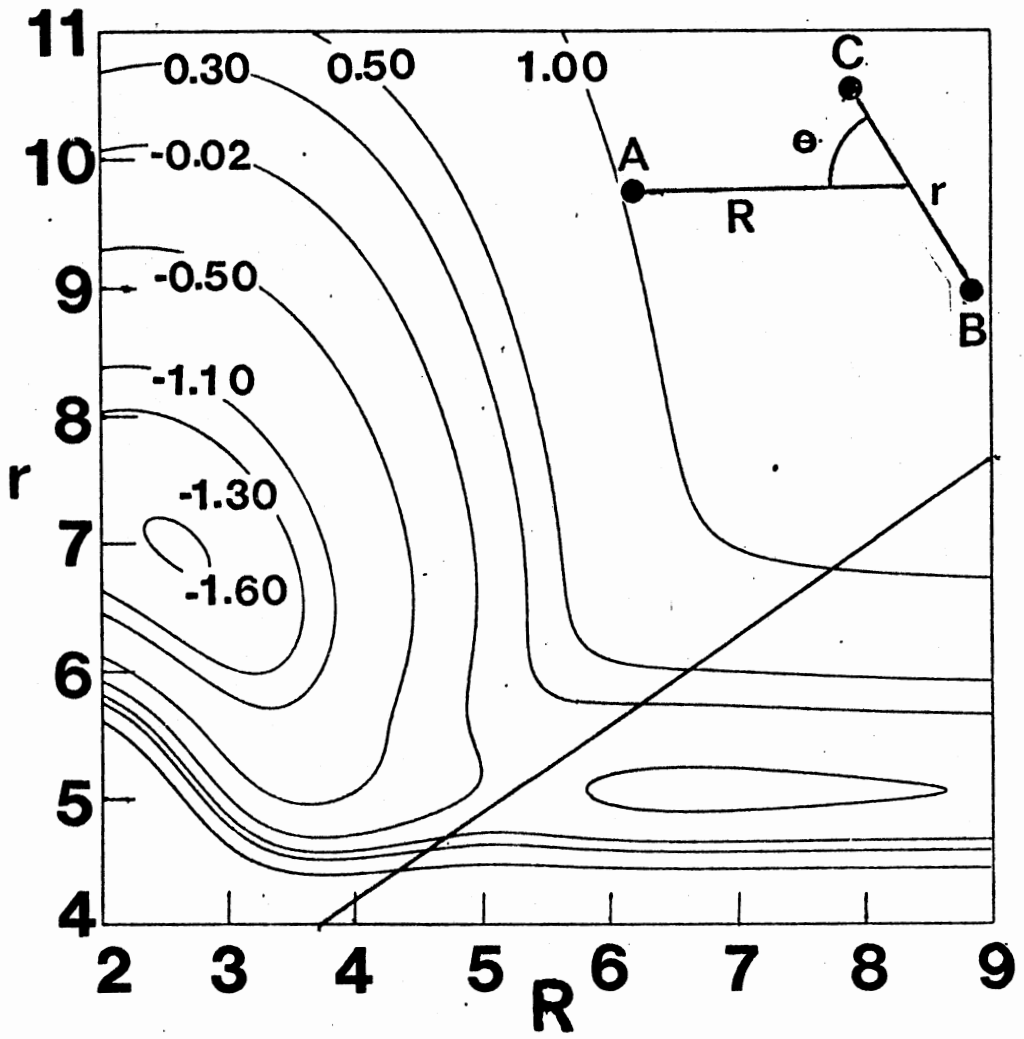

Figure 18. Projection of S onto the (r,R) Plane, A = 0.51, B = 0.75, C = 0.150, D = -1.20, $\theta = \pi/3$, Potential Contours are in eV Referenced to H - I_2 at Infinite Separation as the Zero of Energy, r and R in Atomic Units

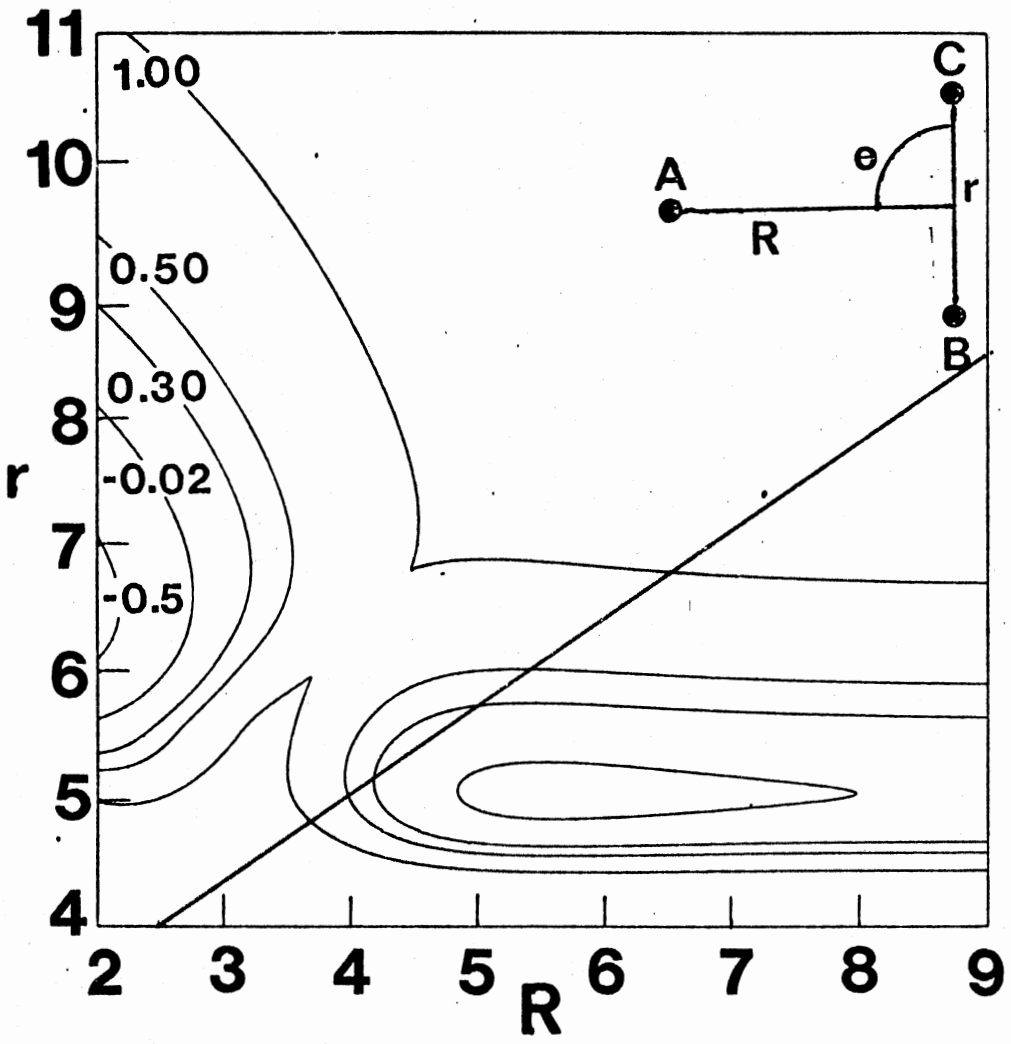

Figure 19. Projection of S onto the (r,R) Plane, A = 0.51, B = 0.75, C = 0.150, D = -1.20, $\theta = \pi/2$, Potential Contours are in eV Referenced to H - I_2 at Infinite Separation as the Zero of Energy, r and R in Atomic Units

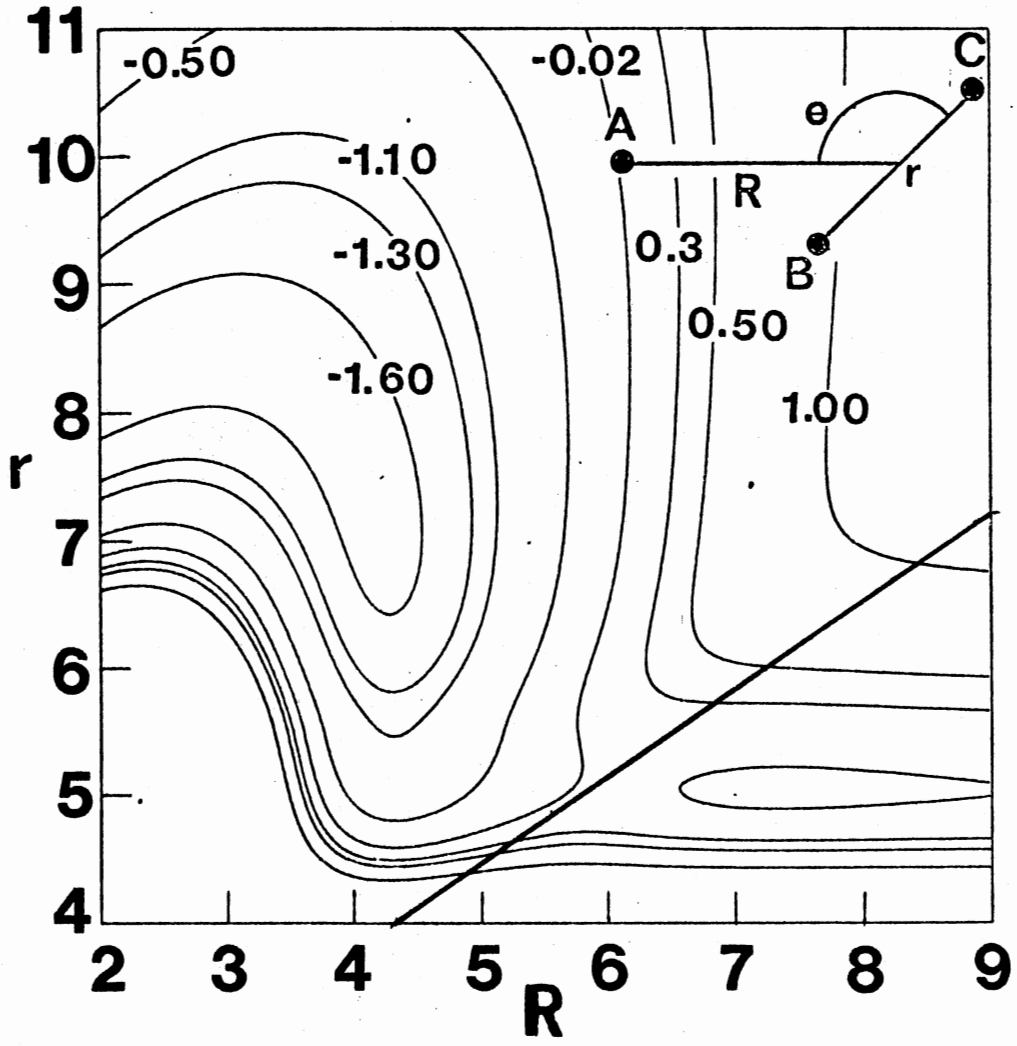

Figure 20. Projection of S onto the (r,R) Plane, A = 0.51, B = 0.75, C = 0.150, D = -1.20, $\theta = 3\pi/4$, Potential Contours are in eV Referenced to H - I_2 at Infinite Separation as the Zero of Energy, r and R in Atomic Units

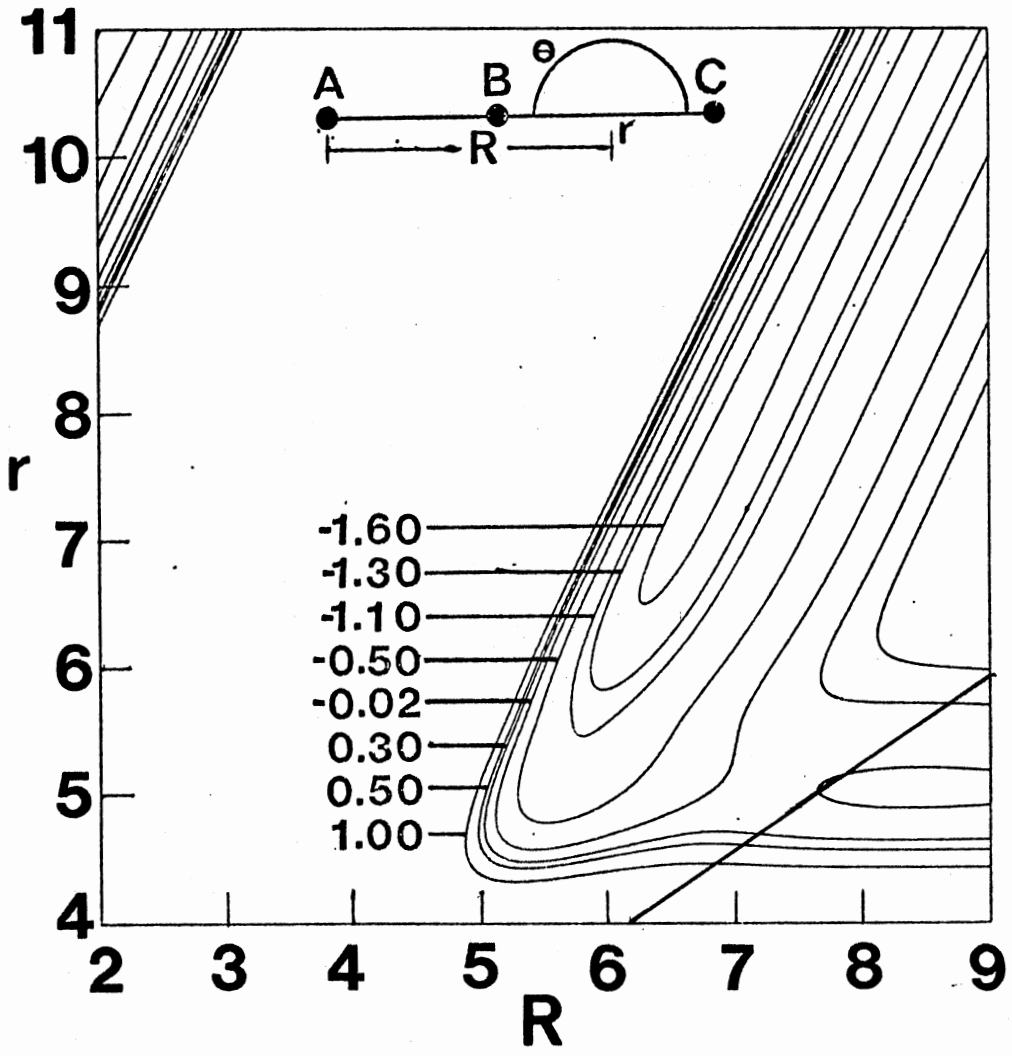

Figure 21. Projection of S onto the (r,R) Plane, A = 0.51, B = 0.75, C = 0.150, D = -1.20, $\theta = \pi$, Potential Contours are in eV Referenced to H - I_2 at Infinite Separation as the Zero of Energy, r and R in Atomic Units

K′(A, B, C, D, T) is nearing this value. Of the 285 K′(A, B, C, D, T) computed, K′(0.51, 0.75, 0.15, -1.20, 300)~1.2 K(300) was the smallest found. This result could be improved somewhat by searching a grid of finer mesh over C and D in this vicinity. If one considers the projections of S onto the (r, R) plane in Figures 18-21, it is seen from $\theta = \pi$ surface, Figure 21, that S does touch the -0.02 eV contour. Thus, it is not surprising that K′(300) is still about 19% too large. However, the essential question is: How good is the variational procedure in providing reliable classical rate coefficients? Clearly, the (H, H_2) and (H, I_2) systems give very good results. Furthermore, if one considers the different classes of potential these two systems represent, the two examples prove more enlightening than they first appear. The (H, H_2) system potential has a wide region of very high potential between the reactant and product regions with no potential minima. Consequently, it should not prove too difficult to locate a satisfactory S. As a matter of fact, K′(A, B, C, T) proved quite adequate. On the other hand the (H, I_2) system has a very narrow, modestly repulsive potential between the reactant and product regions and also has a well in the entrance valley. In order to obtain a satisfactory variational rate coefficient, S must pass between the regions of low potential always avoiding the potential well. Certainly K′(A, B, C, 600)~10.5 K(600) is inadequate, where K(600) is the SQCT result reported in a previous study (47), and K′(600) is from Table XII. However, if one employs K′(A, B, C, D, T) and takes advantage of the symmetry of the potential about $\theta = \pi/2$, a result K′(0.51, 0.75, 0.150, -1.20, 600)~

2.0 K(600) is obtained. Clearly, the variational procedure can provide reasonable approximations to classical rate coefficients provided the parameterization of S is sufficiently flexible.

Choosing the set (A, B, C, D) = (0.51, 0.75, 0.150, -1.20) as the set of parameters describing S_0, variational rate coefficients were computed over the temperature range 300-1100 K. The results are given in Table XIV. These results show reasonable agreement with Sullivan's experimental values at 300 K and increase to K (A,B,C,D,T)$\sim$ 2.33 K(T) at 1100 K. A refined grid search could improve the results. The result at 1100 K is larger than the upper bound, 5.3 x 10^{14} cm^3/mole-sec, from Sullivan's experimental uncertainty. In addition, it may not be valid to compare experimental results over the temperature range of 667-800 K to variational rate coefficients computed over the temperature range of 300-1100 K. Furthermore, the experimental study reports an activation energy E_A = 0, whereas the H-I_2 potential-energy surface has a barrier of 0.49 kcal/mole. Essentially, the potential surface employed in the variational study may not represent the true system potential accurately in all regions.

CPST Rate Coefficients

Once S_0 has been determined by the variational procedure, it is employed in a CPST computation of the rate coefficient. If the variational study has been reasonably successful, one would expect the CPST correction factor, ξ(A, B, C, T) defined by Eqs. (2-92) and (2-93), to approach unity. That is, if a set of N trajectories are sampled from S_0, the number of reactive trajectories N_r should approach N.

TABLE XIV

TEMPERATURE BEHAVIOR OF K′(A, B, C, D, T)[a]

T K	K′(A, B, C, D, T)[b]
300	2.0643×10^{14}
500	3.6385×10^{14}
600	4.3342×10^{14}
700	4.9854×10^{14}
900	6.1822×10^{14}
1100	7.7272×10^{14}

[a] A = 0.51, B = 0.75, C = 0.150, D = -1.20

[b] K′ in units of cm^3/mole-sec

S_0 for the (H, H_2) system is described by (A, B, C) = (0.56, 0.95, -0.25). CPST rate coefficients have been computed from initial conditions sampled from S_0 as described in Chapter II at temperatures of 300, 500, 700, 900, and 1100 K using 100 trajectories to compute the CPST rate coefficient at each temperature. The results of these computations along with the correction factor ξ(A, B, C, T) and standard error σ given by Eq. (2-94) are given in Table XV.

The upper and lower error bounds for the CPST and CT rate coefficients overlap indicating statistical agreement with the exception of

the 900 K rate coefficients. A possible source of the disagreement between the two rate coefficients could be an overestimate of the reaction threshold in the CT procedure. An examination of threshold velocities from Table IV does show a decrease in reaction threshold with temperature except at 900 K. Probably the cause of this descrepancy is the use of a larger b_{max} for the estimate of the 900 K threshold. Consequently, the smaller impact parameters are not as heavily sampled as those at other temperatures.

TABLE XV

RATE COEFFICIENTS COMPUTED BY THE CPST PROCEDURE FOR THE H + H_2 THERMAL EXCHANGE REACTION[a]

T K	ξ(A, B, C, T)	K(A, B, C, T) $\frac{cm^3}{mole=sec}$ [b]
300	0.89	$(1.6240 \pm 0.0571) \times 10^6$
500	0.98	$(1.6468 \pm 0.0235) \times 10^9$
700	0.94	$(3.5256 \pm 0.0891) \times 10^{10}$
900	0.94	$(2.1939 \pm 0.0554) \times 10^{11}$
1100	0.88	$(7.0446 \pm 0.2602) \times 10^{11}$

[a] 100 trajectories computed for each CPST rate coefficient

[b] Eq. (2-92)

It should be noted that the number of trajectories required to obtain the CT coefficients with statistical accuracy on the order of 10% is significantly larger than the 100 trajectories used to compute the CPST rate coefficients with statistical error bounds on the order of 2-4%. This increased efficiency of the CPST procedure is not always obtained, however. It is strongly dependent upon the particular system under investigation (47). For example, for the (H, I_2) system studied in the previous section with S described by the two degrees of freedom r and R, the best choice of (A,B,C) found was (0.56, 0.75, 0.0) which yields $K'(A,B,C,T) \sim 6.6\ K(T)$ at 900 K. One would expect optimization of the CPST procedure to be poor for this case. This has previously been found to be true for $S = R - C = 0$, where $C = R_t$ (47).

Temperature Study by the CTA, CPST and Variational Methods

The temperature behavior of the (H, H_2) system has been studied by the CT, variational, and CPST procedures. The computed rate coefficients as a function of temperature are given in Tables V, X, and XV, respectively. The temperature dependence of the rate coefficients was expressed in the Arrhenius form,

$$K(T) = A\, e^{-E_A/RT}, \qquad (3\text{-}12)$$

and the results of a linear least squares fit to ln K(T) vs. $10^3/T$ for the three methods are shown in Figures 22, 23, and 24. The

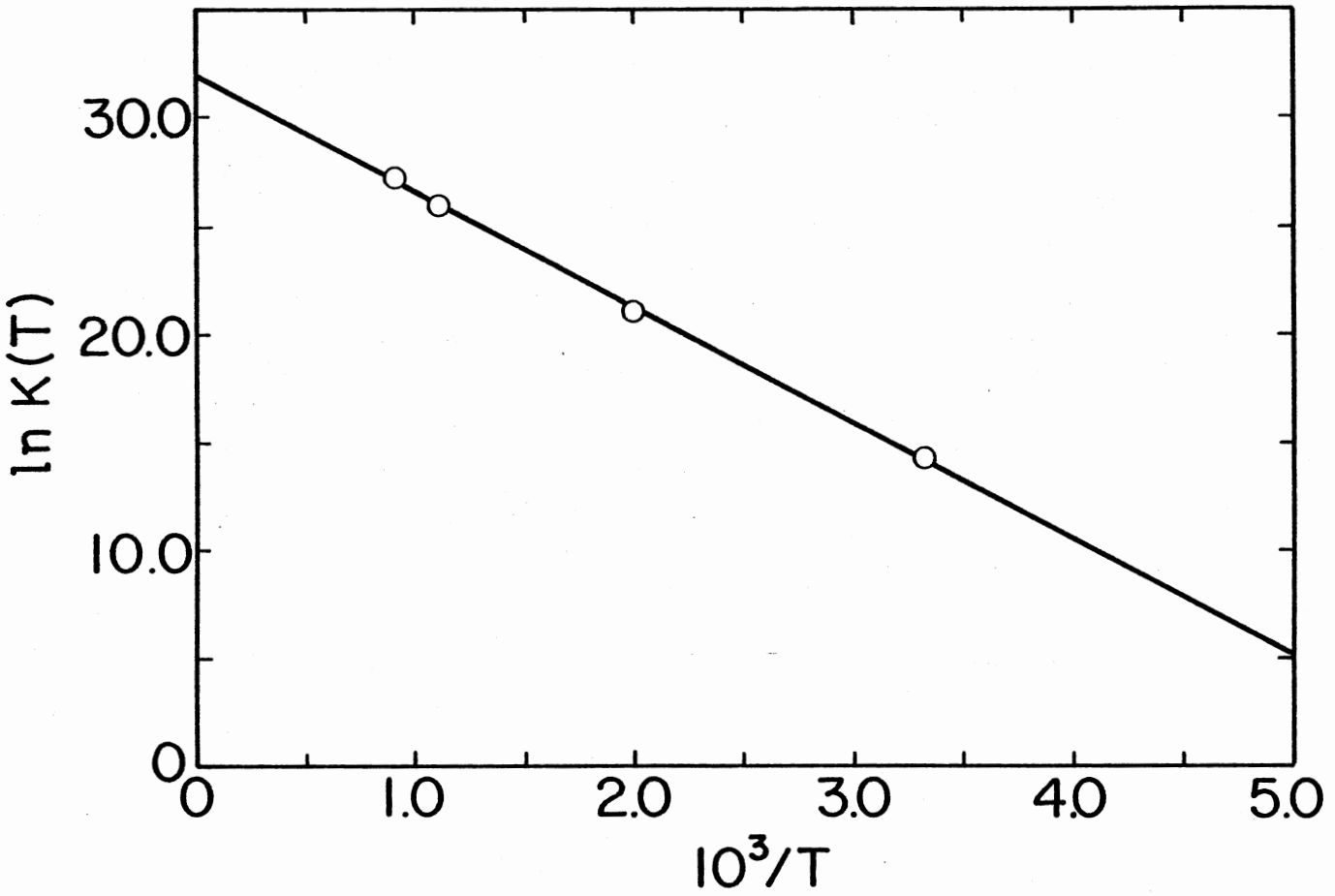

Figure 22. Arrhenius Fit to CT Rate Coefficients for the (H, H_2) System, K(T) is in Units of cm^3/mole-sec

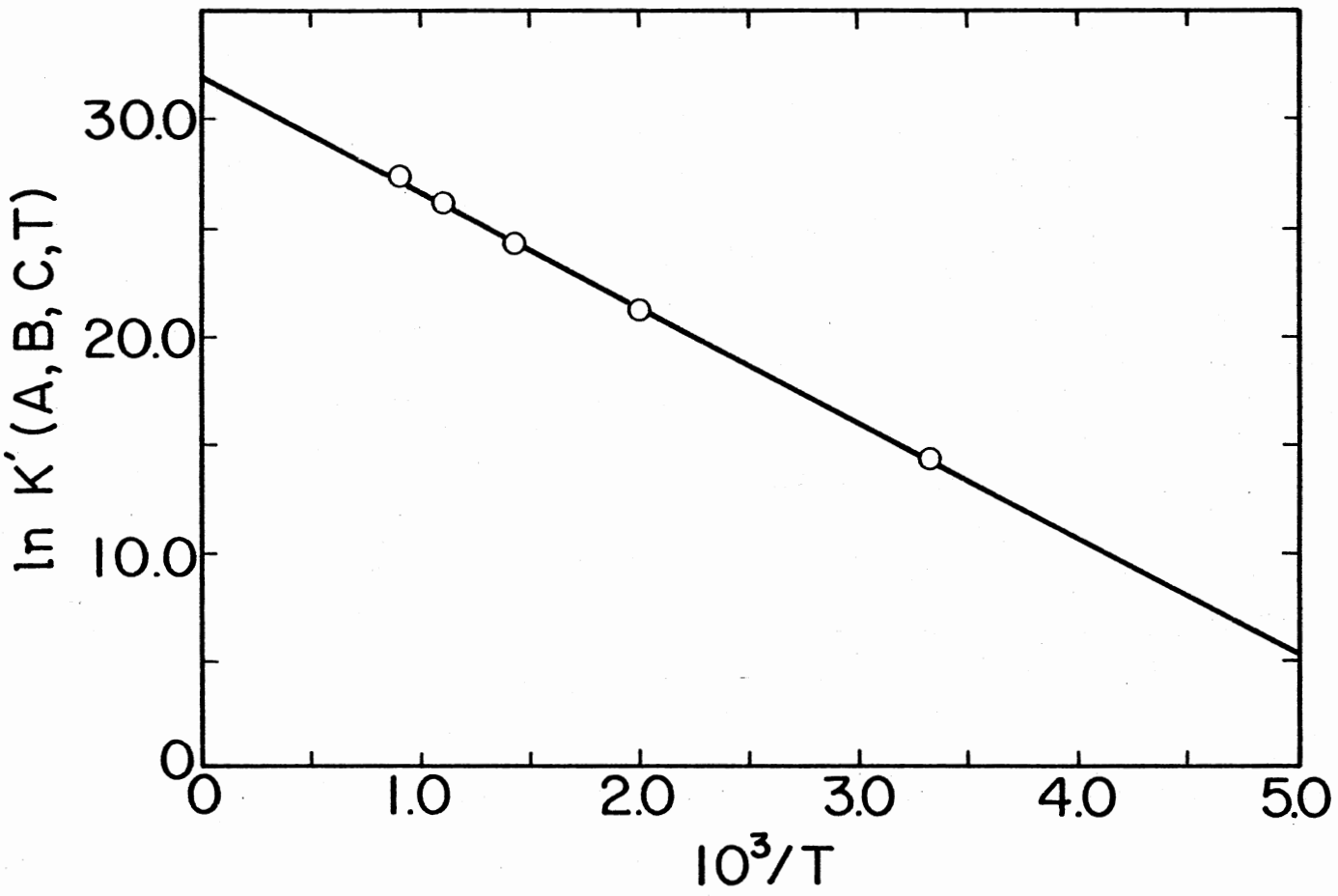

Figure 23. Arrhenius Fit to Variational Rate Coefficients for the (H, H_2) System, A = 0.56, B = 0.95, C = -0.25, Units of K'(T) are cm^3/mole-sec

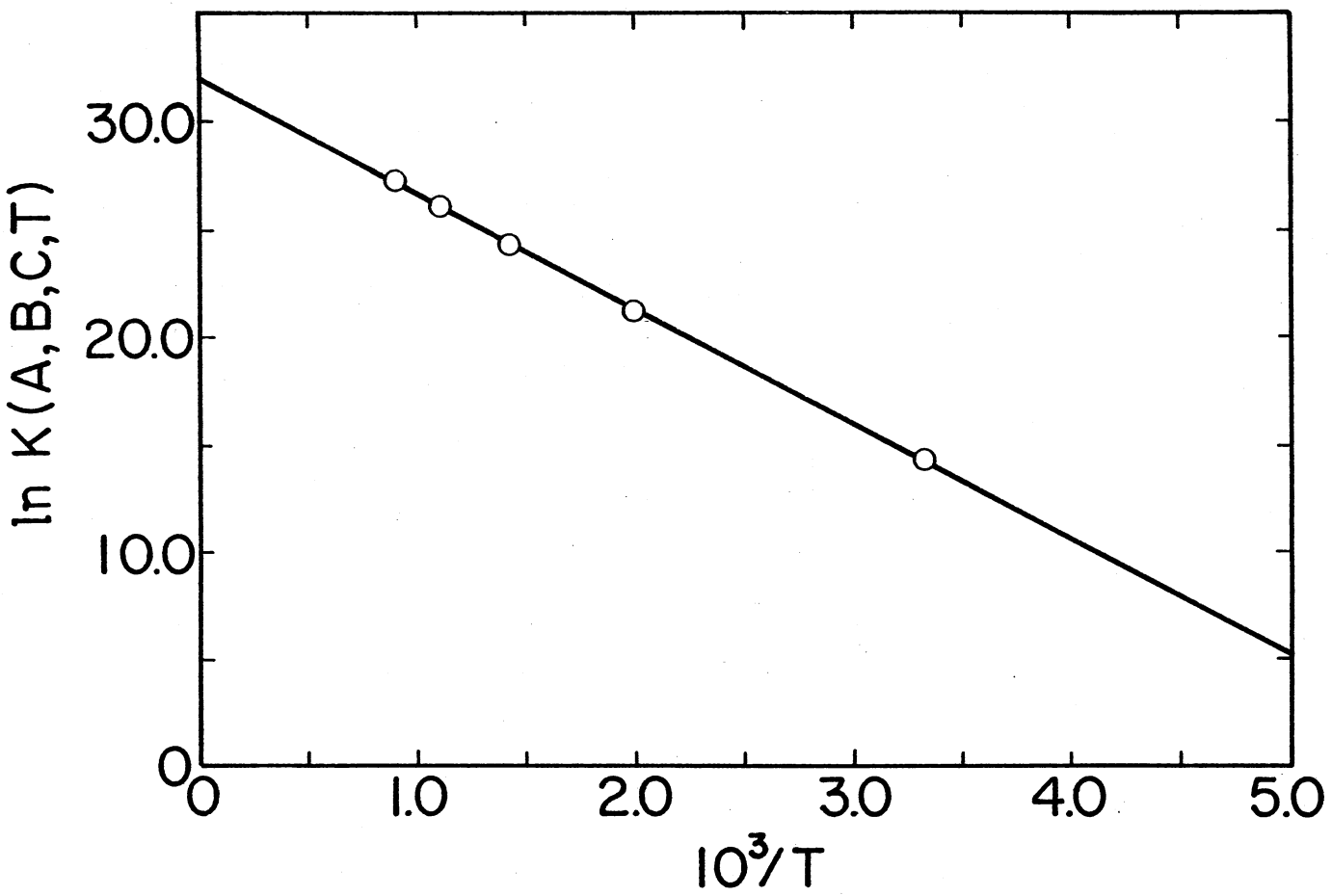

Figure 24. Arrhenius Fit to CPST Rate Coefficients for the (H, H_2) System, A = 0.56, B = 0.95, C = -0.25, Units of K(A,B,C,T) are cm^3/mole-sec

frequency factors and activation energies predicted by the three methods are given in Table XVI.

TABLE XVI

RESULTS OF THE ARRHENIUS TEMPERATURE FIT OF THE RATE COEFFICIENT FOR THE (H, H_2) THERMAL EXCHANGE REACTION INVESTIGATED BY THE CT, VARIATIONAL, AND CPST PROCEDURE

Procedure	ln A	E_A $\frac{kcal}{mole}$
CT	31.97 ± 0.16[a]	10.59 ± 0.15
Variational[b]	32.08 ± 0.12	10.59 ± 0.12
CPST[b]	32.02 ± 0.08	10.60 ± 0.08

[a]Probable error of slope and intercept of linear least squares line Reference 70

[b]A = 0.56, B = 0.95, C = -0.25

In this comparison of predicted temperature behavior of the rate coefficient, the CT results are considered to be the correct values. Essentially, one is comparing the results of two other procedures to the results from trajectory calculations with initial conditions sampled from a Boltzmann distribution in the reactant valley, which is correct for thermal processes.

An examination of Figures 22, 23, and 24 shows the Arrhenius description of the rate coefficient provides a good fit for all three methods. The Arrhenius fit to the CT rate coefficients shown in Figure 22 depicts a small deviation from Arrhenius behavior, there is a slight increase in slope at the low temperature end. This feature also appears in the Arrhenius fit to the Variational and CPST rate coefficient. It seems the temperature behavior predicted by the variational and CPST procedures does mimic the CT results with regard to the characteristics mentioned above. The CPST and variational frequency factors and activation energies shown in Table XVI indicate very good agreement with CT results with the uncertainty of each computed quantity being less than 2%.

Consider an isolated system composed of a mixture of A and BC particles at temperature T with A and BC capable of reaction. If one defines the activation energy of the system as the difference between the ensemble average of energy of A and BC particles that do react and the ensemble average energy of the system, we have

$$E_A = \langle E_R \rangle - \langle E \rangle , \qquad (3\text{-}13)$$

where $\langle E \rangle$ is the ensemble average of the system energy and $\langle E_R \rangle$ is the ensemble average energy of A and BC particles in the system that do react. This quantity may be computed by CT methods. An analogous variational definition could be the difference between the ensemble average energy of A and BC particles that reach S and the ensemble average of the system energy. Or,

$$(E_s)_A = \langle E_s \rangle - \langle E \rangle \quad , \tag{3-14}$$

where $\langle E_s \rangle$ is the ensemble average energy of A and BC particles that reach S and $(E_s)_A$ is the predicted activation energy from the variational procedure. Notice one might be able to computed $(E_s)_A$ from,

$$(E_s)_A = \frac{\int_{\substack{S=0 \\ \vec{v}.\hat{n}_s>0}} H\, e^{-\beta H}\, d\sigma}{\int_{\substack{S=0 \\ \vec{v}.\hat{n}_s>0}} e^{-\beta H}\, d\sigma} - \frac{\int_{\omega} H_o\, e^{-\beta H_o} \prod_{i=1}^{6} dp_i\, dq_i}{\int_{\omega} e^{-\beta H_o} \prod_{i=1}^{6} dp_i\, dq_i} \quad , \tag{3-15}$$

where the Hamiltonian has been described by Eqs. (2-44) and (2-45). It might prove worthwhile to attempt the evaluation of Eq. (3-15) notice $(E_s)_A$ does exhibit temperature dependence and unless actual computations are performed, it is difficult to say how strong this temperature dependence would be.

According to Keck (22), there exists a surface S^0 that is crossed once and only once by trajectories traveling from reactant to product phase space. If one considers the conditions required for a "proper" choice of S, that is S must completely separate reactant and product phase space and be as inaccesible to nonreactive trajectories as possible, it is clear that the variational procedure essentially tries to approximate S^0. This implies no nonreactive trajectories will reach S^0. It appears that a necessary criterion for a given trajectory to belong to the set of reactive trajectories is that the set of phase

space coordinates composing a trajectory contain a point on S^0 as a limit point (68).

Clearly a proper choice of S is in order, since, if S were chosen to lie far out into the reactant phase space $(E_s)_A \rightarrow 0$, and certainly E_A is a least upper bound for $(E_s)_A$. As S begins to resemble S^0 more closely, one expects $(E_s)_A$ to approach E_A from below, or

$$\lim_{S \rightarrow S^0} (E_s)_A = \text{lub } (E_s)_A = E_A. \qquad (3\text{-}16).$$

If one considers the activation energies of Table XVI, it is obvious that S must be approaching S^o for the (H, H_2) system. However, it is not S^o since, K´(A, B, C, T)>K(T) for every temperature. This is also evident from the CPST trajectories in which some phase-space points selected on S_0 do recross S_0 and return to the reactant phase space.

Temperature studies have also been performed with the variational procedure applied to the (H, I_2) system with S_0 described by (A,B,C) = (0.56, 0.75, 0.0). The variational rate coefficients given in Table XII were assumed to follow the temperature dependence of Eq. (2-6) as suggested by Sullivan (69) and a plot of ln $(K'(A,B,C,T)/\sqrt{T})$ vs. $10^3/T$ is shown in Figure 25. The resulting frequency factor and activation nergy are given in Table XVII along with Sullivan's results.

The activation energy obtained from the temperature study of K (A, B, C, T) does not suggest any agreement at all with Sullivan's experimental results, neither does it agree with what one expects from the potential-energy surface for the (H, I_2) system with a barrier of

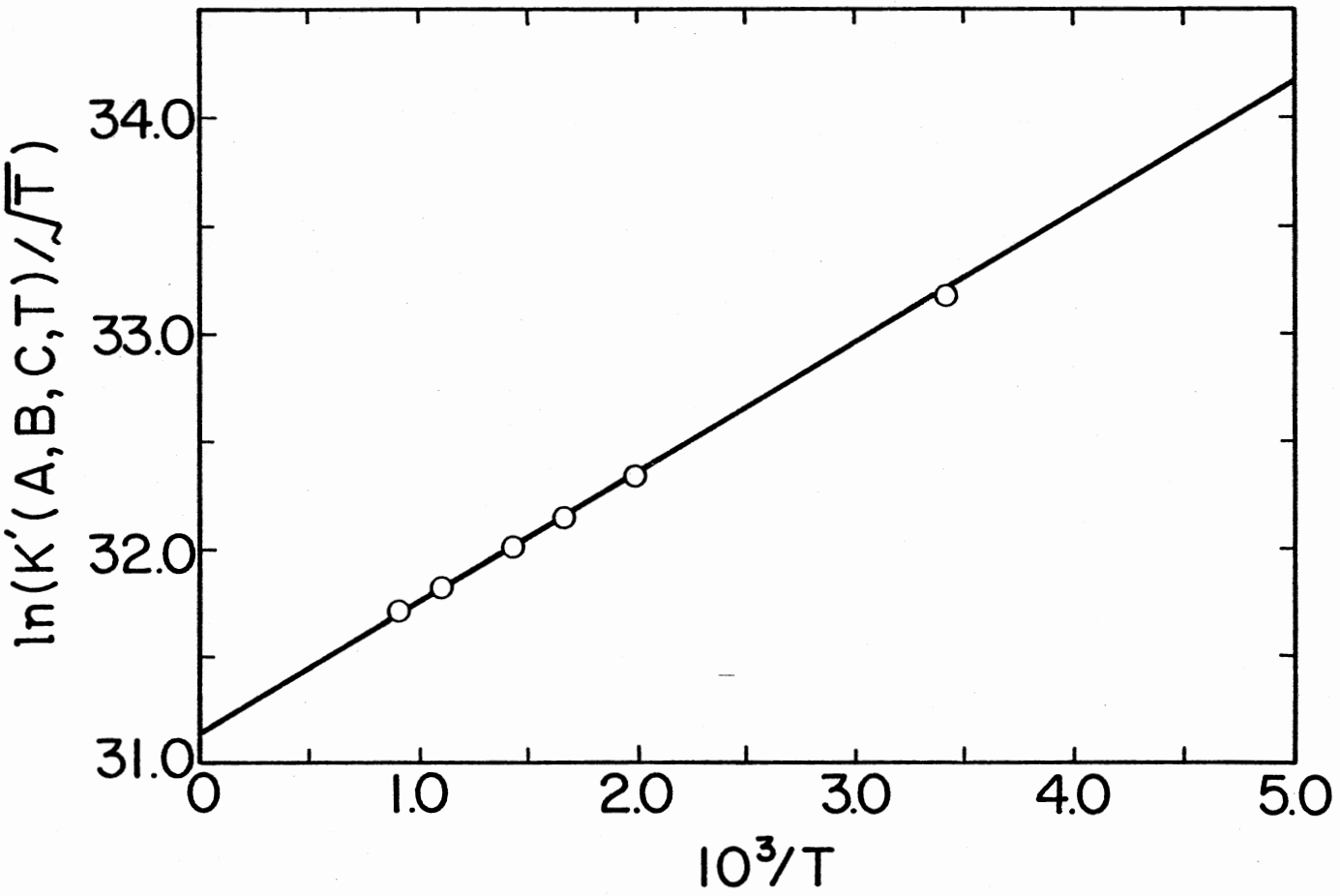

Figure 25. Ln $(K'(A,B,C,T)/\sqrt{T})$ vs. $10^3/T$ for the (H, I_2) System, Units of K´ are cm^3/mole-sec, A = 0.56, B = 0.75, C = 0.0

approximately 0.7 kcal/mole. However, if one considers the definition of $(E_s)_A$ given by Eq. (3-14) as the energy difference between the average energy of particles in the reactant phase space and those reaching S, it is not necessary that $(E_s)_A$ always be greater than zero. Certainly S_0 is not a good approximation to S^o. An inspection of Figures 14-18 shows S_0 traversing the well in the entrance valley which has a depth $-2.1 \leq \delta \leq -1.2$ kcal/mole for different values of θ.

TABLE XVII

RESULTS OF THE TEMPERATURE STUDY OF THE (H, I_2) THERMAL EXCHANGE REACTION BY THE VARIATIONAL PROCEDURE

Procedure	ln A	E_A $\frac{kcal}{mole}$
Variational		
K'(A, B, C, T)[a]	31.141 ± 0.012	-1.205 ± 0.012
K'(A, B, C, D, T)[b]	30.930 ± 0.008	0.495 ± 0.009
Experiment[c]	29.99 ± 0.46	0.0 ± 0.50

[a] $S = AR - Br - C = 0$, $A = 0.56$, $B = 0.75$, $C = 0.0$

[b] $S = AR - Br - D\theta - C = 0$, $A = 0.51$, $B = 0.75$, $C = 0.150$, $D = -1.20$

[c] Reference 69

It is perhaps useful to analyze the grid search algorithim to understand what led to this choice of S_0. The search was performed over a grid of (A, B) points for different choices of C at an arbitrary temperature. For this case, the search was conducted at 600 K. At this temperature $-1.76 \leq \delta/kT \leq -1.01$ or the integrand of I_1 may assume values as large as $e^{1.76} \sim 5.8$ as the integration over θ is performed. However, at 300 K $-3.52 \leq \delta/kT \leq -2.01$ the integrand of I_1 may assume values as large as $e^{3.52} \sim 33.8$ during the integration over θ. The effect of the small well is not as significant at the higher temperature. Consequently, one obtains variational rate coefficients that decrease with temperature. Thus, it appears that one should perform the grid search at low temperatures where the low-energy attributes of the potential will be maximized in the variational study.

The set (A, B, C, D) = (0.51, 0.75, 0.150, -1.20) yielded the smallest computed variational rate coefficient at 300 K with S_0 described by Eq. (3-10). Computed values of $K'(A, B, C, D, \bar{T})$ are given in Table XIV as a function of temperature for this particular S_0, and a plot of $\ln (K'(A,B,C,D,T)/\sqrt{T})$ vs. $10^3/T$ is given in Figure 26. The computed frequency factor and activation energy from the linear least squares fit are given in Table XVII.

The results of the temperature fit of $K'(A,B,C,D,T)$ show $E_A \sim 0.5$ kcal/mole, certainly not unreasonable for a potential-energy surface with a 0.49 kcal/mole barrier (47). It is difficult to compare the variational and experimental frequency factors considering the uncertainty of the experimental results. Essentially the variational frequency factor is 2.6 times larger than the experimental result.

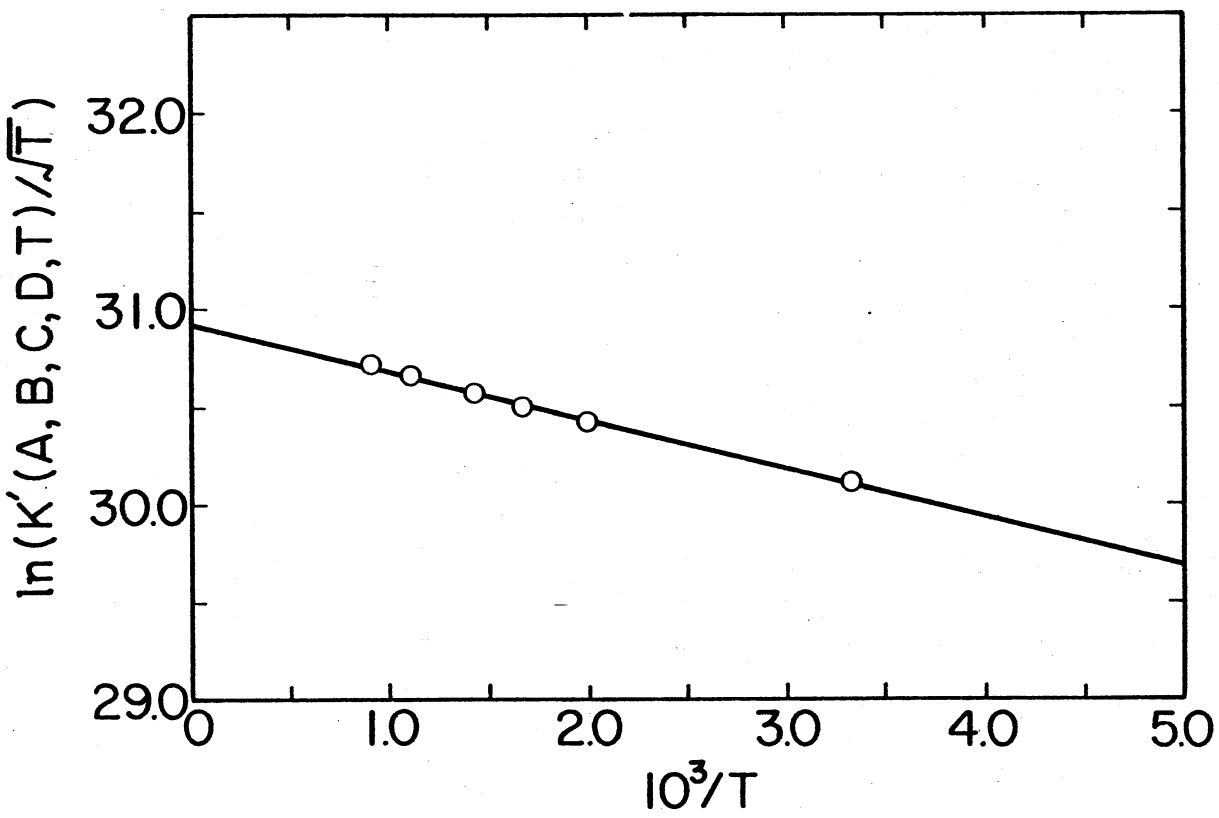

Figure 26. Ln(K´(A,B,C,D,T)/$\sqrt{T}$) vs. 10^3/T for the (H, I_2) System, A = 0.51, B = 0.75, C = 0.150, D = -1.20, K´ in Units of cm^3/mole-sec

However, the variational procedure does seem to provide reliable classical rate coefficients, activation energies, and possibly frequency factors requiring small amounts of computer time in comparison with Monte-Carlo classical trajectory procedures. For example, to compute K(900) to within 10% statistical uncertainty for the (H, H_2) system by CT procedures required 27 CPU hours on an IBM 370/158 computer, while the search for a local minima of K′(A,B,C,900) required 7.8 CPU hours. However, it must be remembered that the (H, H_2) system is one of the worst cases to examine by CT procedures. For other systems it may not be possible to find an adequate S or the resulting grid search may prove more cumbersome than the actual trajectory calculation. Of course, one obtains no information on collision details, reaction cross sections, differential cross sections, or product energy distributions that are readily available from Monte Carlo procedures.

A Comparison of Initial and Final State Properties Predicted by the CPST and CT Procedures

The CPST procedure has shown it can produce reliable classical rate coefficients within statistical agreement with CT results with just a few trajectories if an optimum S has been chosen. Another interesting test would be to examine the final state distributions of the dynamical variables predicted by the CPST procedure. Such a problem was seriously addressed in the study of the (H, I_2) system at 600 K. These authors found that it required 15,000 trajectories to obtain adequate statistical accuracy to determine very small

differences in differential cross sections predicted by the two procedures.

Since the (H, I_2) system is a highly reactive system, compared to the (H, H_2) system, this essentially eliminates any chance of making quantitative comparisons between the two procedures for the (H, H_2) system. The best one may hope for is qualitative comparisons and conclusions. A total of 4750 classical trajectories were examined for the final state distributions by the CT procedure which produced a weighted sum of reactive trajectories of 60.8, or essentially 1 out of 80 trajectories react. To study the final state distributions produced by the CPST procedure, 500 trajectories were sampled from S_0, of which 461 were reactive. Certainly one would expect much better statistical accuracy in the final state distributions of the CPST procedure, however, the question is how well do these results compare with the CT results.

The differential scattering cross sections predicted by the CT and CPST procedures are shown in Figure 27 (a) and (b), respectively. Qualitatively they are both similar, both predict backward scattering peaked at 175-180 degrees. This predicts a rebound type of mechanism, essentially, this agrees with the reaction cross section. An examination of Figure 2 shows reaction cross sections less than 5 au^2 according to Laidler (1), processes with reaction cross less than 10$(\text{Å})^2$ will undergo backward scattering. However, any fine details of the scattering cannot be obtained, one might examine Figure 27 (a) and conclude the CT results predict stronger backward scattering, but

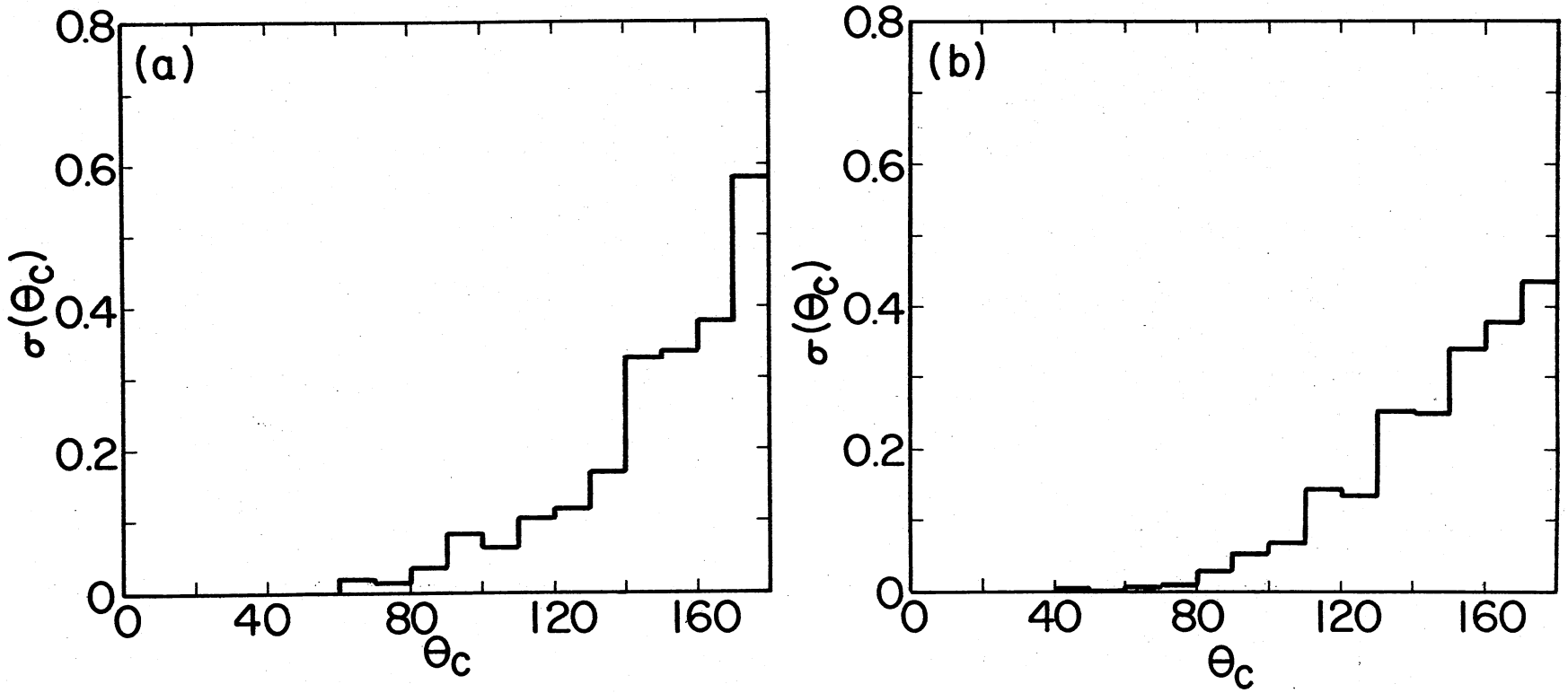

(a) Computed from the CT Procedure

(b) Computed from the CPST Procedure

Figure 27. Differential Scattering Cross Section as a Function of Center of Mass Scattering Angle for the (H, H_2) Thermal Exchange Reaction at 900 K

these results have large statistical uncertainty, hence such conclusions may not be reliable.

The final state rotational energy of a trajectory is obtained from Eqs. (2-101), (2-104), and (2-105) as the difference of internal and vibrational energy in the Morse oscillator approximation. The rotational energy distributions from the CT and CPST procedures are shown in Figure 28 (a) and (b), respectively. The CPST result shown in Figure 28 (b) appears to predict a higher occurence of low rotational energy products, but again large differences may be absorbed in the large statistical error. Essentially, this rules out quantitative assessment of the CT and CPST product rotational energy distributions. Again, there is qualitative resemblence of the distribution of product rotational energies predicted by the two procedures.

The distribution of product vibrational energy is shown in Figure 29 (a) and (b), for the CT and CPST procedures, respectively. Here again, one has qualitatively similar vibrational energy distribution predicted by the two procedures. However, on the low energy end 0-3 kcal/mole, there is a consistently higher occurrence of low product vibratonal energy predicted by the CT method, which might not be as easily dismissed as statistical uncertainty.

Further comparisons may yet be made, for instance, one is reasonably assured of a Boltzmann distribution of initial conditions in the reactant region of phase space. In fact, this is how the initial conditions are selected in the CT study of thermal processes. To determine if the Boltzmann weighting of states on S_0 was appropriate, one might back-integrate from initial conditions chosen on S_0 to the

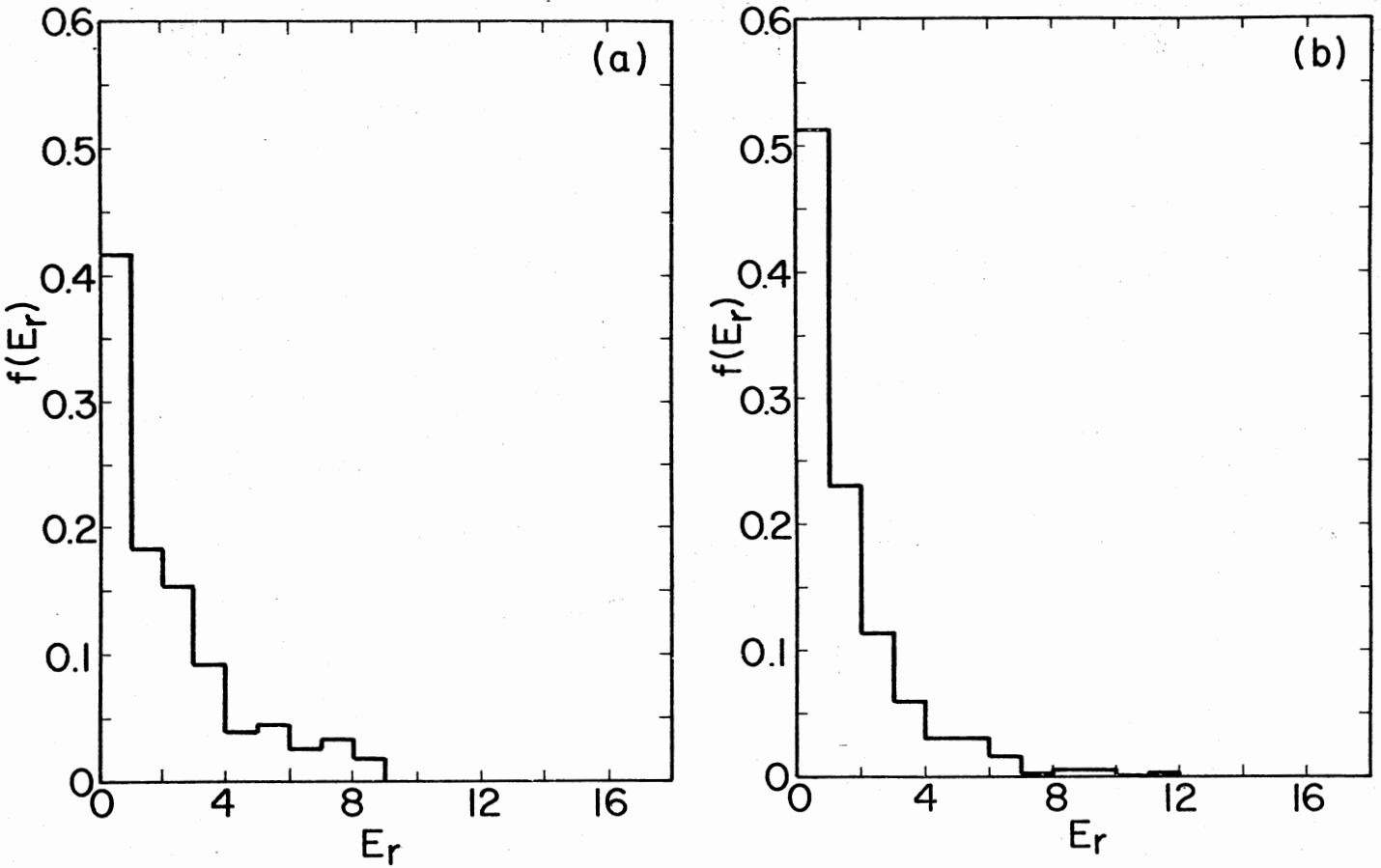

(a) Computed by the CT Procedure

(b) Computed by the CPST Procedure

Figure 28. Product Rotational Energy Distribution $f(E_r)$ for the (H, H_2) Thermal Exchange Reaction at 900 K, E_r in kcal/mole

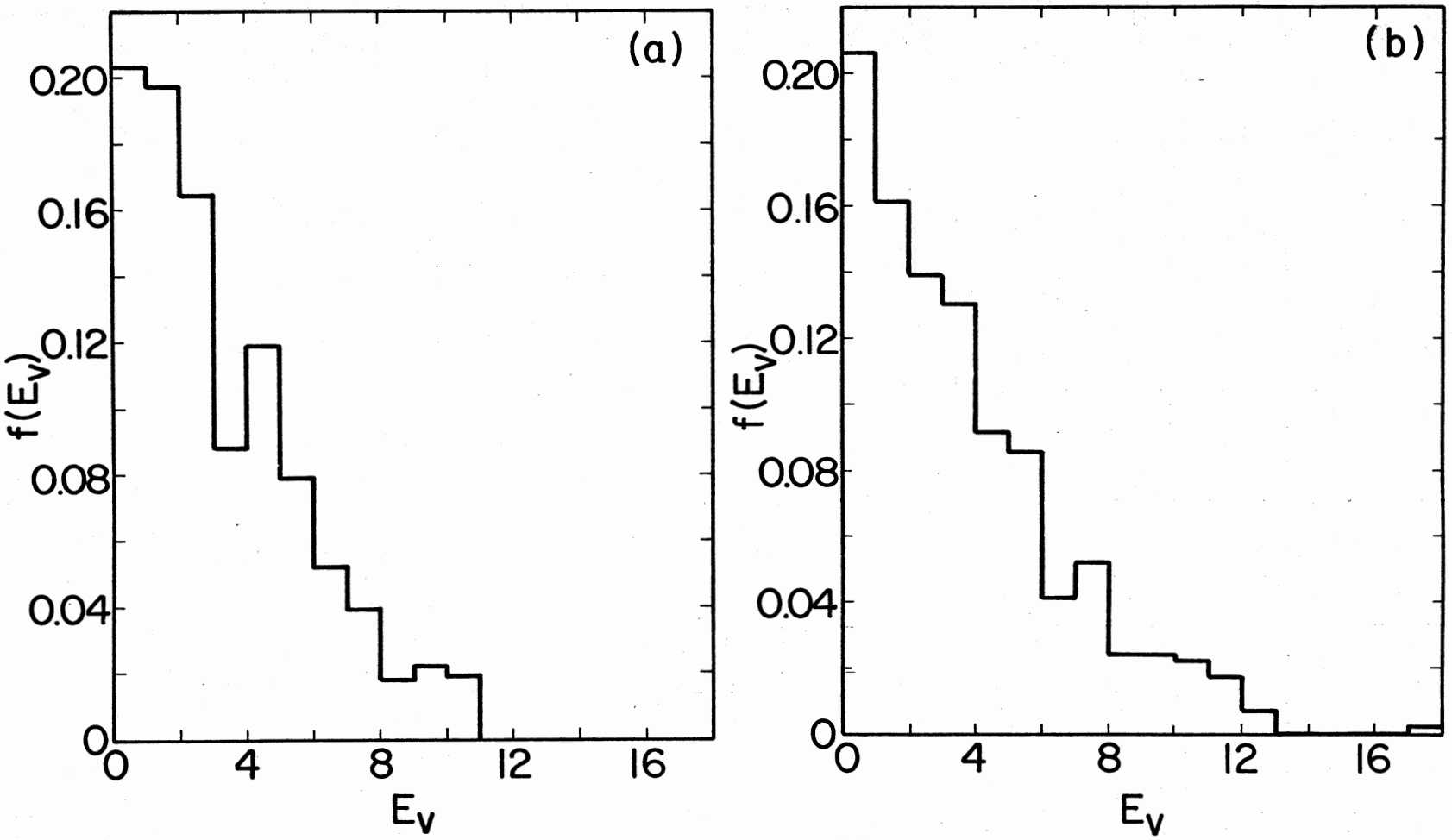

(a) Computed by the CT Procedure

(b) Computed by the CPST Procedure

Figure 29. Product Vibrational Energy Distribution $f(E_v)$ for the (H, H_2) Thermal Exchange Reaction at 900 K, E_v in kcal/mole

reactant region of phase space. Although this will exclude trajectories that never reach S_0 from reactants and for the (H, H_2) system, this is the vast majority. However, one could obtain initial state distributions in the CT formalism of trajectories sampled in the reactant region of phase space by integrating trajectories from reactants to S_0. Then, employing the CPST procedure, one could backintegrate from S_0 to reactants and obtain the reactant state distribution of CPST trajectories sampled on S_0 from a Boltzmann distribution. If the two procedures are equivalent, the reactant state distribution obtained by the two procedures should be the same.

Such a comparison was attempted out of 2250 trajectories examined, the weighted sum of reactive trajectories was 36.7. Of the 500 CPST trajectories examined with initial conditions chosen from a Boltzmann distribution on S_0, 486 backintegrated to reactants. The initial relative speed distribution obtained from the CT and CPST procedures are shown in Figure 30 (a) and (b), respectively. The two distributions do agree on the location of the maximum at V_r = 1.25 vu. However, the CT distribution is skewed to the low velocity side, this could be chosen from choosing V_o as a lower limit for the selection of initial relative velocities1 The relative velocities from which the initial conditions are chosen in the CT procedure actually corresponds to the high velocity tail of the Boltzmann relative speed distribution. An interesting point to notice about the CPST initial relative speed distribution is that there are some trajectories that reach S_0 well below the estimated threshold velocity. It is very difficult to obtain a good estimate of the threshold velocity from the CT procedure. The

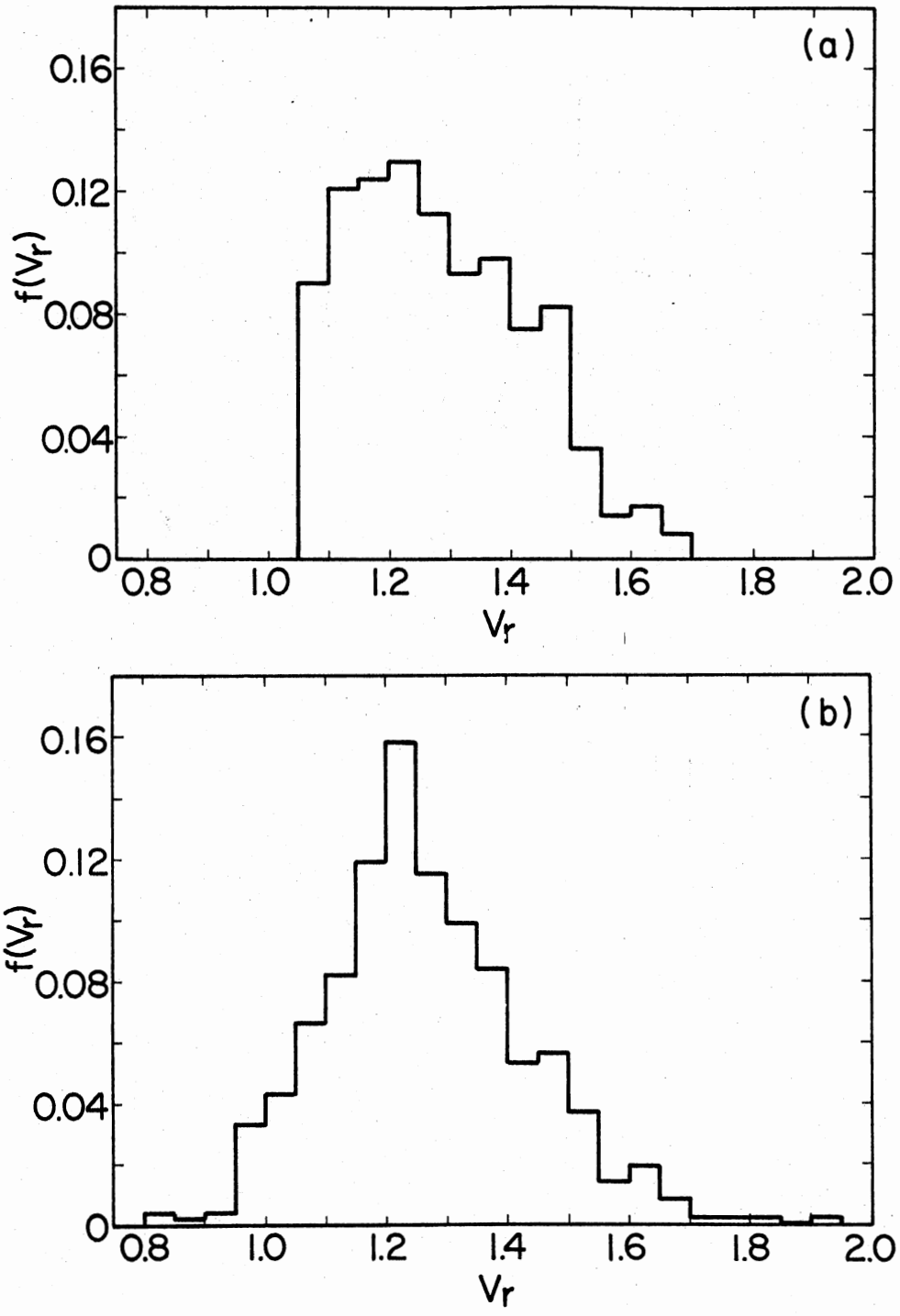

(a) From Trajectories Integrated to S_0 from the Reactant Zone by the CT Procedure
(b) From Trajectories Backintegrated from S_0 to the Reactant Zone by the CPST Procedure

Figure 30. Distribution of Initial Relative Velocities for the (H, H_2) Thermal Exchange Reaction, V_r in Velocity Units

present case is a good example with V_o chosen as 1.014 vu, it is possible the CPST procedure might prove useful in obtaining threshold velocities.

The initial BC internal energy distributions for the (H, H_2) system predicted by the CT and CPST procedures are shown in Figure 31 (a) and (b), respectively. Essentially, there is nothing to compqre the CPST internal energy distribution with, since, the CT results only represent an example of large statistical error. It appears computation of many more trajectories would be required before one could even make qualitative statements about the nature of these distributions.

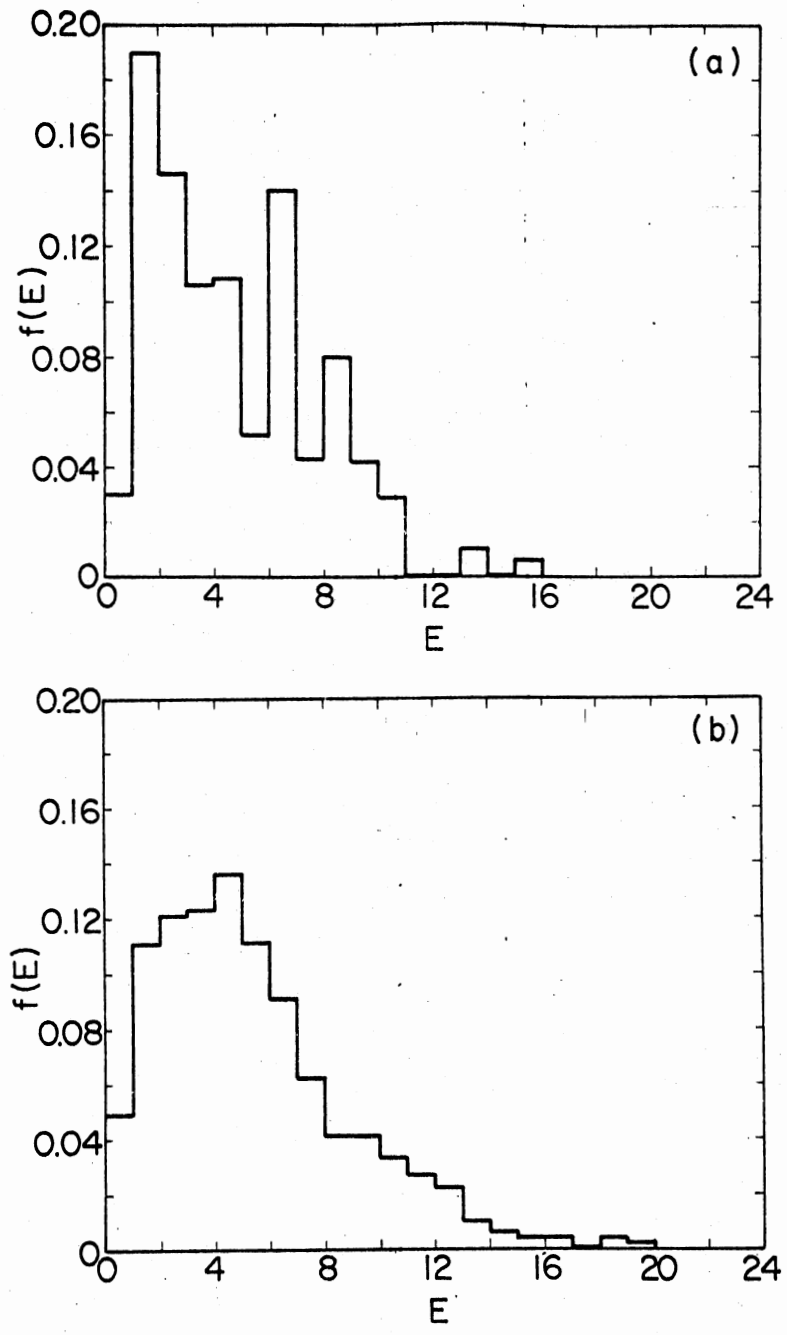

(a) From Trajectories Integrated to S_0 from the Reactant Zone by the CT Procedure

(b) From Trajectories Backintegrated from S_0 to the Reactant Zone by the CPST Procedure

Figure 31. Distribution of Initial BC Internal Energies of Trajectories that Reach S_0 for the (H, H_2) Thermal Exchange Reaction, $E = E_v + E_r$; E has Units of kcal/mole

CHAPTER IV

CONCLUSIONS AND REMARKS

The agreement of the variational and CPST rate coefficients with CT rate coefficients for the (H, H_2) thermal exchange reaction is very good. As far as the CPST rate coefficient is concerned this is not surprising, since, the variational rate coefficient for this case is already a close upper bound of the CT rate coefficient. The CPST correction factor can only improve the agreement. If one is able to find an S_0 that provides a variational rate coefficient that is a close upper bound to the classical rate coefficient, this essentially optimizes the CPST procedure. In practice one usually does not know the classical rate coefficient and has no knowledge of the lower bound. In such a situation a reasonable approach might be to follow a procedure similar to that applied to the (H, I_2) system. Search an (A, B, C) grid for local minima of K′(A, B, C, T); use the set (A, B, C) that provides the lowest local minima in K′(A,B,C,T) to provide an initial guess region for an (A, B, C, D) grid and search the (A, C, D) grid for local minima of K′(A, B, C, D, T) for fixed B. Hopefully, this will be a close upper bound to the true classical rate coefficient.

The Arrhenius parameters computed from the variational and CPST procedures also compare well with CT results. The agreement of the

activation energies for the (H, H_2) system seems to imply that activation energy is not as critically dependent upon the degree of agreement between S_0 and S^o as the individual rate coefficients are. However, in order to obtain a reliable activation energy for the system under study, it appears necessary that the variational rate coefficients be reasonably close to the classical rate coefficients as was demonstrated for the (H, I_2) system. Although there are larger uncertainties in the data (47) (69) upon which the comparisons are based for this system, one should be able to draw some qualitative assessments concerning the variational procedure.

The initial grid search for local minima of K´(A,B,C,T) produced $(E_s)_A < 0$, a poor result for a system treated by classical mechanics with a 0.49 kcal/mole barrier. However, if one minimizes K´(A,B,C,D,T) for the (H, I_2) system, $(E_s)_A$ becomes 0.5 kcal/mole which is equivalent to the barrier height. Although, the experimental and variational frequency factors disagree by a factor of 2.6, this is probably due in large measure to the inadequacy of the potential-energy surface.

The results of the variational study of the (H, H_2) and (H, I_2) thermal exchange reactions appear to serve as an illustration of the hypothesis stated on p. 86. K´(A,B,C,T) was adequate to obtain a reasonable variational rate coefficient for the (H, H_2) system. Since the system potential has a broad saddle point region, it is not too difficult to find an appropriate S that divides the system phase space described by these regions of high potential energy. In addition, there are no low-energy regions of the potential in the proximity of the saddle point as there were for the (H, I_2) system. However, the

(H, I_2) system potential has a low barrier with a small well in the entrance valley. These features both depend upon θ in such a manner that if S is described only by the degrees of freedom r and R, it must traverse the well in the entrance valley. If one does include θ in the description of S, the minimization of K´(A,B,C,D,T) appears to be reasonably successful.

Anderson et al. (42) have made claims that the CPST procedure offers a computational advantage of 10^5-10^6 over the CT procedure if the process under study has steric and/or energy requirements for reaction. The (H, H_2) system certainly falls into this category with 9 kcal/mole barrier to reaction. The CPST procedure has been optimized already at the expense of finding S_0, and the CT rate coefficient at 300 K required 16328 trajectories to obtain a statistical error on the order of 10%. The estimated number of CPST trajectories at 300 K required to obtain a statistical error of 10% is 12-13 which gives a computational advantage on the order of 1300. It appears Anderson's claims are somewhat out of proportion. Of course, if S is not variationally optimized, the CPST procedure may require more computer time than a CT calculation (47).

A SELECTED BIBLIOGRAPHY

(1) Laidler, K. J., Theories of Chemical Reaction Rates, New York: McGraw Hill Book Co., 1969, pp. 1-3, 218.

(2) Tully, J. C., J. Chem. Phys. 60, 3042 (1974).

(3) Tully, J. C. and R. K. Preston, J. Chem. Phys. 55, 562 (1971).

(4) Johnston, H. S., Gas Phase Reaction Rate Theory, New York: Ronald Press, 1966, Chap. 8.

(5) Eyring, H., H. Gershinowitz, and C. E. Sun, J. Chem. Phys. 3, 786 (1935).

(6) Keck, J. C., J. Chem. Phys. 29, 410 (1958).

(7) Rabinowitch, E., Trans. Faraday Soc. 33, 283 (1973).

(8) Rice, O. K., J. Chem. Phys. 9, 258 (1941); 21, 750 (1953).

(9) Careri, G., J. Chem. Phys. 21, 749 (1953).

(10) Wigner, E. P., J. Chem. Phys. 5, 720 (1937).

(11) Light, J. C., J. Chem. Phys. 40, 3221 (1964).

(12) Landau, L. and E. M. Kifshitz, Quantum Mechanics, Reading, Mass.: Addison-Wesly Publishing Co., Inc., 1958.

(13) Pechukas, P. and J. C. Light, J. Chem. Phys. 42, 3281 (1965).

(14) Light, J. C. and J. Lin, J. Chem. Phys. 43, 3209 (1965).

(15) Pechukas, P., J. C. Light, and C. Rankin, J. Chem. Phys. 44, 794 (1966).

(16) Wolf, F., J. Chem. Phys. 44, 1619 (1966).

(17) Lin, J. and J. Light, J. Chem. Phys. 45, 2545 (1966).

(18) Eu, B. C. and J. Ross, J. Chem. Phys. 44, 2467 (1966).

(19) Wigner, E. P. and L. Eisenbud, Phys. Rev. 72, 29 (1947).

(20) Glasstone, S. G., K. J. Laidler, and H. Eyring, Theory of Rate Processes, New York: McGraw Hill Book Co., Inc., 1941.

(21) Miller, W. H., J. Chem. Phys. 65, 2216 (1976).

(22) Keck, J. C., Advan. Chem. Phys. 13, 85 (1967).

(23) Light, J. C., Discuss. Faraday Soc. 44, 14 (1967).

(24) Nikitin, E. E., Theory of Atomic and Molecular Processes in Gases, New York: Oxford U. P., 1974, p. 391.

(25) Bernstein, R. B. and R. D. Levine, J. Chem. Phys. 57, 434 (1972).

(26) Shaul, A. B., R. D. Levine, and R. B. Bernstein, J. Chem. Phys. 57, 5427 (1972).

(27) Levine, R. D. and R. Kosloff, Chem. Phys. Lett. 28, 300 (1974).

(28) Raff, L. M., Colliquim on The Information Theoretic Approach Applied to Chemical Kinetics, 1976.

(29) Levine, R. D. and R. B. Bernstein, Chem. Phys. Lett. 29, 1 (1974).

(30) Levine, R. D. and J. Manz, J. Chem. Phys. 63, 4280 (1975).

(31) Shaul, A. B., Chem. Phys. 1, 244 (1973).

(32) Procaccia, I. and R. D. Levine, J. Chem. Phys. 63, 4261 (1975).

(33) Bernstein, R. B. and R. D. Levine, J. Chem. Phys. 61, 4926 (1974).

(34) Horiuti, J., Bull, Chem. Soc. (Japan) 13, 210 (1938).

(35) Keck, J. C., J. Chem. Phys. 32, 1035 (1960).

(36) Pathria, R. K., Statistical Mechanics, Oxford: Pergamon Press, 1972, pp. 32-36.

(37) Slater, N. B., Theory of Unimolecular Reactions, Ithaca, New York: Cornell University Press, 1959.

(38) Hinshelwood, C. N., The Kinetics of Chemical Change in Gaseous Systems, Oxford: Clarendon Press, 1933.

(39) Mansbach, P. and J. Keck, Phys. Rev. 181, 275 (1969).

(40) Keck, J., Discussions Faraday Soc. 33, 173 (1962).

(41) Anderson, J. B., J. Chem. Phys. 58, 4684 (1973).

(42) Jaffe, R. L., J. M. Henry, and J. B. Anderson, J. Chem. Phys. 59, 1128 (1973).

(43) Morokuma, K., B. C. Eu, and M. Karplus, J. Chem. Phys. 51, 5193 (1969).

(44) Morokuma, K. and M. Karplus, J. Chem. Phys. 55, 63 (1971).

(45) Koeppl, G. W. and M. Karplus, J. Chem. Phys. 55, 4667 (1971).

(46) Porter, R. N. and L. M. Raff. "Modern Theoretical Chemistry", Vol. 3, Dynamics of Molecular Collisions. Ed. Miller, W. H. New York: Plenum, 1975.

(47) Porter, R. N., D. L. Thompson, L. M. Raff and J. M. White, J. Chem. Phys. 62, 2429 (1975).

(48) Mayer, I., J. Chem. Phys. 60, 2564 (1974).

(49) Anderson, J. B. and R. T. V. Kung, J. Chem. Phys. 58, 2477 (1973).

(50) Henry, J. M., J. B. Anderson, and R. L. Jaffe, Chem. Phys. Lett. 20, 138 (1973).

(51) Jaffe, R. I., J. M. Henry, and J. B. Anderson, J. Am. Chem. Soc. 98, 1140 (1976).

(52) Raff, L. M., D. L. Thompson, L. B. Simms, and R. N. Porter, J. Chem. Phys. 56, 5998 (1971).

(53) Anderson, J. B., J. M. Henry, and R. L. Jaffe, J. Chem. Phys. 60, 3725 (1974).

(54) Raff, L. M., L. Stivers, R. N. Porter, D. L. Thompson, and L. B. Sims, J. Chem. Phys. 52, 3449 (1970).

(55) Jaffe, R. L. and J. B. Anderson, J. Chem. Phys. 54, 224 (1971).

(56) Anderson, J. B., J. Chem. Phys. 62, 2446 (1975).

(57) Porter, R. N. and M. Karplus, J. Chem. Phys. 40, 1105 (1964).

(58) Karplus, M., R. N. Porter, and R. D. Sharma, J. Chem. Phys. 43, 3259 (1965).

(59) Porter, R. N., L. M. Raff, and W. H. Miller, J. Chem. Phys. 63, 2214 (1975).

(60) Ralston, A., Mathematics of Computation 16, 431 (1962).

(61) Goldstein, H., Classical Mechanics, Reading, Mass., Addison-Wesley Publishing Co., 1965.

(62) Weatherburn, C. E., An Introduction to Reimannian Geometry and the Tensor Calculus, London, Cambridge University Press, 1938.

(63) Sokolnikoff, I. S., Tensor Analysis, New York, John Wiley and Sons Inc., 1951.

(64) Koeppl, G. W., J. Am. Chem. Soc. 96, 6539 (1974).

(65) Walsh, J. L., J. H. Ahlberg, and E. N. Nilson, J. Math. Mech. 11, 225 (1962).

(66) Sathyamurthy, N. and L. M. Raff, J. Chem. Phys. 63, 464 (1975).

(67) Hildebrand, F. B., Introduction to Numerical Analysis, New York: McGraw-Hill Book Co., Inc., 1956.

(68) Buck, R. Creighton, Advanced Calculus, New York: McGraw-Hill Book Co., Inc., 1956, pp. 10, 49-64.

(69) Sullivan, J. H., J. Chem. Phys. 30, 1292 (1959).

(70) Margenau, Henry and George M. Murphy, The Mathematics of Physics and Chemistry, Robert E. Krieger Publishing Co., Inc., Tenth Reprint, 1976, p. 519.

APPENDIX A

DERIVATION OF $|\vec{\nabla S}|_{\perp}$ IN THE $(W, V, \theta, \phi, \Theta, \Phi)$ COORDINATE SYSTEM

The square of the magnitude of $\vec{\nabla S}$ that is normal to an (n-1) dimensional hypersurface described by S = 0 is given by (62),

$$(\vec{\nabla S}.\vec{\nabla S}) = \frac{\partial S}{\partial x^i}\, g^{ij}\, \frac{\partial S}{\partial x^j} \quad . \tag{A-1}$$

The shorthand notation employed in Eq. (A-1) is an example of the tensor summation convention. That is, one sums over repeated indices. If one includes the proper summation signs, the abbreviated form of Eq. (A-1) appears as,

$$\frac{\partial S}{\partial x^i}\, g^{ij}\, \frac{\partial S}{\partial x^j} = \sum_{i=1}^{n} \frac{\partial S}{\partial x^i} \sum_{j=1}^{n} g^{ij}\, \frac{\partial S}{\partial x^j} \, , \tag{A-2}$$

where the g^{ij} are the components of the conjugate or reciprocal metric tensor given by (63),

$$g^{ij} = G^{ij}/g \, . \tag{A-3}$$

The G^{ij} in Eq. (A-3) is the cofactor of the element g_{ij} of the

determinant of the fundamental metric tensor whose elements are given by,

$$g_{ij} = \frac{\partial x^k}{\partial y^j} \frac{\partial x^k}{\partial y^j} , \qquad \text{(A-4)}$$

where the tensor summation convention has been employed with $x^k(y^i)$ as the old coordinates and y^i as the new ones.

Following the tensor notation the relative cartesian coordinates Q_i are relabeled as $(x^1, x^2, x^3, x^4, x^5, x^6)$ and $(W, V, \theta, \phi, \Theta, \Phi)$ are renamed as $(y^1, y^2, y^3, y^4, y^5, y^6)$. Substituting $r(W, V)$ and $R(W, V)$ into the transformation equations from cartesian to spherical polar, one obtains the $x^i(y^1, y^2, y^3, y^4, y^5, y^6)$. That is,

$$x^1 = \left(\frac{Ay^2 - y^1}{A+B}\right) \text{siny}^3 \, \text{cosy}^4$$

$$x^2 = \left(\frac{Ay^2 - y^1}{A+B}\right) \text{siny}^3 \, \text{siny}^4$$

$$x^3 = \left(\frac{Ay^2 - y^1}{A+B}\right) \text{cosy}^3$$

$$x^4 = \left(\frac{By^2 + y^1}{A+B}\right) \text{siny}^5 \, \text{cosy}^6$$

$$x^5 = \left(\frac{By^2 + y^1}{A+B}\right) \text{siny}^5 \, \text{siny}^6$$

$$x^6 = \left(\frac{By^2 + y^1}{A+B}\right) \text{cosy}^5 \quad . \qquad \text{(A-5)}$$

To construct the fundamental metric tensor, one evaluates its components by employing Eq. (A-4). For example,

$$g_{12} = \frac{\partial x^1_1}{\partial y^1}\frac{\partial x^1_2}{\partial y^2} + \frac{\partial x^2_1}{\partial y^1}\frac{\partial x^2_2}{\partial y^2} + \frac{\partial x^3_1}{\partial x^3}\frac{\partial x^3_2}{\partial y^3} + \frac{\partial x^4_1}{\partial y^4}\frac{\partial x^4_2}{\partial y^4} + \frac{\partial x^5_1}{\partial y^5}\frac{\partial x^5_2}{\partial y^5} +$$

$$\frac{\partial x^6_1}{\partial y^6}\frac{\partial x^6_2}{\partial y^6} = (B-A)/(A+B)^2 \quad . \tag{A-6}$$

Noting that the metric tensor is symmetric, that is;

$$g_{ij} = g_{ji}, \tag{A-7}$$

one can construct the metric tensor by evaluating it's upper diagonal components, the rest following from Eq. (A-7). Continuing in the manner indicated above, employing Eq. (A-4) with the aid of Eq. (A-7), one obtains the fundamental metric tensor:

$$\underset{\sim}{g_Q} = \begin{pmatrix} \frac{2}{(A+B)^2} & \frac{B-A}{(A+B)^2} & 0 & 0 & 0 & 0 \\ \frac{B-A}{(A+B)^2} & \frac{A^2+B^2}{(A+B)^2} & 0 & 0 & 0 & 0 \\ 0 & 0 & \left(\frac{Ay^2-y^1}{A+B}\right)^2 & 0 & 0 & 0 \\ 0 & 0 & 0 & \left(\frac{Ay^2-y^1}{A+B}\right)^2 \sin^3 y^3 & 0 & 0 \\ 0 & 0 & 0 & 0 & \left(\frac{By^2+y^1}{A+B}\right)^2 & 0 \\ 0 & 0 & 0 & 0 & 0 & \left(\frac{By^2+y^1}{A+B}\right)^2 \sin^2 y^5 \end{pmatrix} . \tag{A-8}$$

The determinant of the fundamental metric tensor for this coordinate system is,

$$g_Q = \frac{1}{(A+B)^2} \left(\frac{Ay^2 - y^1}{A+B}\right)^4 \sin^2 y^3 \left(\frac{By^2 + y^1}{A+B}\right)^4 \sin^2 y^5 \ . \qquad \text{(A-9)}$$

Some interesting points may be noted about Eqs. (A-8) and (A-9). It is seen that the (W, V, θ, ϕ, Θ, Φ) coordinate system is nonorthogonal since all off-diagonal of the fundamental metric tensor are zero for orthogonal coordinate systems. The only way this may happen is if B = A. Also, the Jacobian determinant of an admissible transformation is defined as the square root of g_Q (63). If one takes the square root of Eq. (A-9) and writes it in terms of spherical polar coordinates, the result is:

$$J_3 = \frac{1}{A+B} r^2 \sin\theta \, R^2 \sin\Theta \ , \qquad \text{(A-10)}$$

where J_3 is the Jacobian determinant of the transformation from the relative cartesian coordinates to the (W, V, θ, ϕ, Θ, Φ) coordinate system. If one defines J_1 as the Jacobian determinant of the transformation from the relative cartesian to spherical polar coordinates, and J_2 as the Jacobian determinant of the transformation from spherical polar coordinates to the (W, V, θ, ϕ, Θ, Φ) coordinate system, the following expressions are obtained:

$$J_1 = r^2 \sin\theta \, R^2 \sin\Theta$$

$$J_2 = \frac{1}{A+B} \ . \qquad \text{(A-11)}$$

One of the properties of admissible transformations is $J_3 = J_1 J_2$ (63), which yields the same result as Eq. (A-10).

One now has the essentials to obtain the components of the conjugate metric tensor from Eq. (A-3). For example,

$$g^{12} = -g_{21}/(g_{11}g_{22} - g_{12}g_{21}) = A-B \ . \qquad \text{(A-12)}$$

Employing Eq. (A-3) and obtaining some aid from the symmetry property,

$$g^{ij} = g^{ji} \ , \qquad \text{(A-13)}$$

one may construct the conjugate metric tensor. The result is:

$$\underset{\sim}{g_p} = \begin{pmatrix} A^2+B^2 & A-B & 0 & 0 & 0 & 0 \\ A-B & 2 & 0 & 0 & 0 & 0 \\ 0 & 0 & \left(\frac{Ay^2-y^1}{A+B}\right)^{-2} & 0 & 0 & 0 \\ 0 & 0 & 0 & \left(\frac{Ay^2-y^1}{A+B}\right)^{-2} \sin^{-2} y^3 & 0 & 0 \\ 0 & 0 & 0 & 0 & \left(\frac{By^2+y^1}{A+B}\right)^{-2} & 0 \\ 0 & 0 & 0 & 0 & 0 & \left(\frac{By^2+y^1}{A+B}\right)^{-2} \sin^{-2} y^5 \end{pmatrix} . \qquad \text{(A-14)}$$

Obtaining the necessary partial derivatives from Eq. (2-54) and substituting the g^{ij} and the partial derivatives into Eq. (A-2), the expression for $\vec{\nabla S}\cdot\vec{\nabla S}$ is,

$$\frac{\partial S}{\partial y^i} \ g^{ij} \ \frac{\partial S}{\partial y^j} = A^2 + B^2 \ , \qquad \text{(A-15)}$$

APPENDIX B

TABLE XVIII

MOLECULAR UNITS[a]

Physical Quantity	Molecular Unit	CGS Equivalent
length	au	0.529167×10^{-8} cm
mass	amu	$1.6604345 \times 10^{-24}$ g
time	tu	$0.53871469 \times 10^{-14}$ sec
velocity	vu	0.9822769×10^{6} cm/sec
momentum	mom u	$1.631006453 \times 10^{-18}$ g-cm/sec
angular momentum	ang m u	$0.86307479 \times 10^{-26}$ erg-sec
energy	eV	1.60210×10^{-12} erg

[a]Reference 52

APPENDIX C

FORMULATION OF K′(A, B, C, D, T)

Following the general formulation of the flux integral given by Eq. (2-42), one defines S by,

$$S = AR - Br - D\theta - C = 0, \tag{C-1}$$

This defines W from Eq. (2-54) as,

$$W = AR - Br - D\theta \; . \tag{C-2}$$

In addition, the two other transformation equations are defined by,

$$\begin{aligned} V &= R + r \\ U &= \theta, \end{aligned} \tag{C-3}$$

with the inverse transformations

$$\begin{aligned} R &= \frac{BV + W + DU}{A + B} \\ r &= \frac{AV - W - DU}{A + B} \\ \theta &= U \; . \end{aligned} \tag{C-4}$$

One requires the spherical polar momenta expressed in terms of the new momenta P_w, P_v, and P_u to substitute into the Hamiltonian expressed in spherical polar coordinates given by Eq. (2-44) to

obtain the Hamiltonian in terms of the new coordinates and meomenta. This may be accomplished by employing a generating function (61) of the type $F_2(f(q), P)$ where the q's are the old coordinates and the P's are the new momenta. In particular, the f(q) are chosen to be the transformation equations Eqs. (C-2) and (C-3). To obtain the old momenta in terms of the new, F_2 is written as,

$$F_2 = WP_w + VP_v + UP_u + \phi p_\phi + \Theta P_\Theta + \Phi P_\Phi \ , \qquad \text{(C-5)}$$

from which the old momenta may be obtained by,

$$p_i = \partial F_2 / \partial q_i . \qquad \text{(C-6)}$$

The old momenta expressed in terms of the new are therefore,

$$\begin{aligned} P_R &= P_v + AP_w \\ p_r &= P_v - BP_w \\ p_\theta &= P_u - DP_w \ . \end{aligned} \qquad \text{(C-7)}$$

Substituting Eqs. (C-7) and (C-4) into the Hamiltonian, Eq. (2-44) and collecting terms results in the following expression,

$$H = \left(\frac{1}{2\mu} + \frac{1}{2\mu_{A,BC}}\right) P_v^2 + \left(\frac{B^2}{2\mu} + \frac{D^2}{2\mu r^2(U,V,W)} + \frac{A^2}{2\mu_{A,BC}}\right) P_w^2 +$$

$$\frac{1}{2\mu r^2(U,V,W)} P_u^2 + \left(\frac{A}{\mu_{A,BC}} - \frac{B}{\mu}\right) P_v P_w - \frac{D}{\mu r^2(U,V,W)} P_u P_w +$$

$$p_\phi^2/2\mu r^2(U,V,W)\sin^2 U + P_\Theta^2/2\mu_{A,BC}R^2(U,V,W) + P_\Phi^2/2\mu_{A,BC}R^2(U,V,W)\sin^2\Theta$$

$$+ \nu(r(U,V,W),\ R(U,V,W),\ \cos U). \qquad \text{(C-8)}$$

In order to obtain the surface element $d\sigma$ for which S = 0, one must evaluate det $\underset{\sim}{a}_Q(C)$ and det $\underset{\sim}{g}_P(C)$ since,

$$d\sigma(C) = d\sigma_Q(C)\, dV_P(C) = \sqrt{\det \underset{\sim}{a}_Q(C)}\ \sqrt{\det \underset{\sim}{g}_P(C)}\ dV\, dU\, d\phi\, d\Theta\, d\Phi\, dP_w\, dP_v\, dP_u\, dP_\Theta\, dP_\Phi\, dp_\phi, \qquad \text{(C-9)}$$

where $d\sigma_Q(C)$ is the differential surface element defined by S = 0 in the coordinate space, and $dV_P(C)$ is the differential volume element defined by S = 0 in the momentum space.

Since the Jacobian of the transformation from cartesian to $(W,V,U,\phi,\Theta,\Phi,P_w,P_v,P_u,p_\phi,P_\Theta,P_\Phi)$ phase space factors into the product of the momentum and coordinate space Jacobians, the methods of Appendix A (62) (63) may be employed. One may write the components of the metric tensor for the coordinate space transformation on the surface S = 0 as,

$$a_{jk} = \frac{\partial Q^i}{\partial q^j}\ \frac{\partial Q^i}{\partial q^k}\ \Bigg|_{W = C}, \qquad \text{(C-10)}$$

where, in this case the Q^i are the six relative coordinates of the (A, BC) coordinate space (58) and the q^j are the new coordinates. Similarly one may write the components of the metric tensor for the momentum space transformation as,

$$g_{jk} = \frac{\partial p^i}{\partial p^j}\ \frac{\partial p^i}{\partial p^k}\ \Bigg|_{W = C}, \qquad \text{(C-11)}$$

where the P^i are the conjugate momenta of the Q^i, and the p^j are

are the conjugate momenta of the q^j. The resulting metric tensors are given by Eqs. (C-12) and (C-13).

$$\underset{\sim}{a}_Q(C) = \begin{pmatrix} \frac{A^2+B^2}{(A+B)^2} & \frac{D(B-A)}{(A+B)^2} & 0 & 0 & 0 & 0 \\ \frac{D(B-A)}{(A+B)^2} & \frac{2D^2}{(A+B)^2} + r^2(U,V,C) & 0 & 0 & 0 & 0 \\ 0 & 0 & r^2(U,V,C)\sin^2 U & 0 & 0 & 0 \\ 0 & 0 & 0 & R^2(U,V,C) & 0 & 0 \\ 0 & 0 & 0 & 0 & R^2(U,V,C)\sin^2\theta & 0 \\ 0 & 0 & 0 & 0 & 0 & 0 \end{pmatrix} . \tag{C-12}$$

$$\underset{\sim}{g_p}(C) = \begin{bmatrix} A^2+B^2 + \dfrac{D^2}{r^2(U,V,C)} & A-B & \dfrac{-D^2}{r^2(U,V,C)} & 0 & 0 & 0 \\ A-B & 2 & 0 & 0 & 0 & 0 \\ \dfrac{-D^2}{r^2(U,V,C)} & 0 & \dfrac{1}{r^2(U,V,C)} & 0 & 0 & 0 \\ 0 & 0 & 0 & \dfrac{1}{r^2(U,V,C)\sin^2 U} & 0 & 0 \\ 0 & 0 & 0 & 0 & \dfrac{1}{R^2(U,V,C)} & 0 \\ 0 & 0 & 0 & 0 & 0 & \dfrac{1}{R^2(U,V,C)\sin^2\Theta} \end{bmatrix} . \quad \text{(C-13)}$$

Combining the square roots of the determinants of Eqs. (C-12) and (C-13) one obtains,

$$d\sigma(C) = \sqrt{A^2+B^2+D^2/r^2(U,V,C)}\; dV\; dU\; d\phi\; d\Theta\; d\Phi\; dP_w\; dP_v\; dP_u\; dp_\phi\; dP_\Theta\; dP_\Phi \tag{C-14}$$

The velocity normal to the surface S = 0 is defined by Eq. (2-59) as,

$$\vec{v}.\hat{n}_s\Big|_{S=0} = [S,\ H]/|\vec{\nabla S}| \quad . \tag{C-15}$$

Substituting [S, H] and $|\vec{\nabla S}|$ into Eq. (C-15) one obtains

$$\vec{v}.\hat{n}_s(C) = \frac{1}{\sqrt{A^2+B^2+D^2/r^2(U,V,C)}} \left(\left(\frac{B^2}{\mu} + \frac{D^2}{\mu r^2(U,V,C)} + \frac{A^2}{\mu_{A,BC}} \right) P_w \right.$$

$$\left. + \left(\frac{A}{\mu_{A,BC}} - \frac{B}{\mu} \right) P_v - \frac{D}{\mu r^2(U,V,C)} P_u \right) , \tag{C-16}$$

and setting $\vec{v}.\hat{n}_s < 0$ the upper limit to P_w is found to be

$$P_w < \frac{-\left(\frac{A}{\mu_{A,BC}} - \frac{B}{\mu} \right) P_v + \frac{D}{\mu r^2(U,V,C)} P_u}{\left(B^2/\mu + A^2/\mu_{A,BC} + D^2/\mu r^2(U,V,C) \right)} \quad . \tag{C-17}$$

Substituting Eqs. (C-8), (C-14), (C-16) and (C-17) into Eq. (2-42) the expression for the variational rate coefficient is:

$$K'(A, B, C, D, \beta) = \frac{-1}{Q(\beta)} \int_{V'}^{V_{max}} dV \int_0^{\pi} dU \int_0^{2\pi} d\phi \int_0^{\pi} d\Theta \; \chi$$

$$\int_0^{2\pi} d\Phi \; e^{-\beta v(r(U,V,C),\, R(U,V,C),\, \cos U)}$$

$$\chi \int_{-\infty}^{\infty} dP_\Theta \; e^{-\beta P_\Theta^2 / 2\mu_{A,BC} R^2(U,V,C)} \int_{-\infty}^{\infty} dP_\Phi \; \chi$$

$$e^{-\beta P_\phi^2 / 2\mu_{A,BC} R^2(U,V,C) \sin^2\Theta} \int_{-\infty}^{\infty} dp_\phi \; e^{-\beta p_\phi^2 / 2\mu r^2(U,V,C) \sin^2 U}$$

$$\int_{-\infty}^{\infty} dP_u \; e^{-\beta P_u^2 / 2\mu r^2(U,V,C)} \int_{-\infty}^{\infty} dP_v \; e^{-\beta\left(\frac{1}{2\mu} + \frac{1}{2\mu_{A,BC}}\right) P_v^2}$$

$$P_w = \left(-\left(\frac{A}{\mu_{A,BC}} - \frac{B}{\mu}\right) P_v + \frac{D}{\mu r^2(U,V,C)} P_u\right) \Big/ \left(\frac{B^2}{\mu} + \frac{D^2}{\mu r^2(U,V,C)} + \frac{A}{\mu_{A,BC}}\right)$$

$$\int_{-\infty}^{} dP_w \left(\left(\frac{B^2}{\mu} + \frac{D^2}{\mu r^2(U,V,C)} + \frac{A^2}{\mu_{A,BC}}\right) P_w + \left(\frac{A}{\mu_{A,BC}} - \frac{B}{\mu}\right) P_v - \right.$$

$$\left. \frac{D}{\mu r^2(U,V,C)} P_u \right) \; \chi$$

$$\exp\left(-\beta\left(\left(\frac{B^2}{2\mu} + \frac{D^2}{2\mu r^2(U,V,C)} + \frac{A^2}{2\mu_{A,BC}}\right) P_w^2 + \left(\frac{A}{\mu_{A,BC}} - \frac{B}{\mu}\right) P_v P_w - \right.\right.$$

$$\left.\left. \frac{D}{\mu r^2(U,V,C)} P_u P_w \right)\right) . \qquad \text{(C-18)}$$

The upper and lower limits V_{ml} and V' are given by,

$$V_{ml} = ((A + B)r_{ml} + C + DU)/A, \qquad \text{(C-19)}$$

$$V' = \begin{cases} DU/A, \; C = 0, \; D > 0 \\ \dfrac{C + DU}{A}, \; C > 0, \; D > 0 \\ \dfrac{-C - DU}{B}, \; C < 0, \; D > 0, \; U \leq -C/D \\ \dfrac{C + DU}{A}, \; C < 0, \; D > 0, \; U > -C/D \\ -DU/B, \; C = 0, \; D < 0 \\ \dfrac{-C - DU}{B}, \; C < 0, \; D < 0 \\ \dfrac{C + DU}{A}, \; C > 0, \; D < 0, \; U \leq C/(-D) \\ \dfrac{-C - DU}{B}, \; C > 0, \; D < 0, \; U > C/(-D) \; . \end{cases} \qquad \text{(C-20)}$$

After evaluation of the momentum integrals and configuration integrals over ϕ, Θ, and Φ and substitution of,

$$Q(\beta) = \left(\frac{2\pi\mu_{A,BC}}{\beta}\right)^{3/2} \left(\frac{2\pi\mu}{\beta}\right)^{3/2} 4\pi I_2(\beta) \; , \qquad \text{(C-21)}$$

into the result of Eq. (C-18), one obtains:

$$K'(A,\ B,\ C,\ D,\ \beta) = \frac{1}{(A+B)}\sqrt{\frac{2\pi}{\beta}}\ \frac{I_1(A,\ B,\ C,\ D,\ \beta)}{I_2(\beta)}\ , \qquad \text{(C-22)}$$

where I_1 is given by,

$$I_1(A,\ B,\ C,\ D,\ \beta) = \int_0^{\pi} \sin U\ dU \int_{V'}^{V_{ml}} dV\ R^2(U,V,C)\ \chi$$

$$r(U,V,C)\ \sqrt{\frac{r^2(U,V,C)B^2}{\mu} + \frac{D^2}{\mu} + \frac{r^2(U,V,C)A^2}{\mu_{A,BC}}}\quad \chi$$

$$e^{-\beta v(r(U,V,C),\ R(U,V,C),\ \cos U)}. \qquad \text{(C-23)}$$

Substituting $\beta = 1/kT$ and using I_2 of Eq. (2-72) in Eq. (C-22) one obtains Eq. (3-8).

VITA[2]

David Linville Martin

Candidate for the Degree of

Doctor of Philosophy

Thesis: A STUDY OF THE VARIATIONAL THEORY OF REACTION RATES COMPARED TO CLASSICAL TRAJECTORY RESULTS AND STUDIES OF THE COMBINED PHASE-SPACE/TRAJECTORY PROCEDURE FOR THE (H, H_2) AND (H, I_2) SYSTEMS

Major Field: Chemistry

Biographical:

Personal Data: Born in Lawton, Oklahoma, on October 20, 1951.

Education: Graduated from Chattanooga High School, Chattanooga, Oklahoma, in May, 1969; received Bachelor of Science degree in Chemistry from Cameron University, Lawton, Oklahoma, in May, 1973; completed requirements for the Doctor of Philosophy degree at Oklahoma State University, December, 1979.

Professional Experience: Graduate Teaching Assistant, Oklahoma State University, August, 1973-May, 1975; CONOCO Fellow, May, 1975; Graduate Teaching Assistant, August, 1975-May, 1976; National Science Foundation Research Assistant, June, 1976-September, 1979.

Membership in Honorary and Professional Societies: Member of the American Chemical Society; member of Phi Lambda Upsilon, Honorary Chemical Society.